Unintegrated Gluon Distributions at Small-x

Fabio Dominguez

Submitted in partial fulfillment of the
requirements for the degree
of Doctor of Philosophy
in the Graduate School of Arts and Sciences

COLUMBIA UNIVERSITY

2011

ABSTRACT

Unintegrated Gluon Distributions at Small-x

Fabio Dominguez

The study of strong interactions at very high energies has prompted a large interest in the small-x regime of quantum chromodynamics where partons carry a small fraction of the momentum of their parent hadrons. In this regime gluon occupation numbers are believed to be very high leading to saturation of the corresponding parton densities. This thesis is intended to explore the validity of factorization approaches in the small-x regime and establish a relation with partonic interpretations when possible. Two fundamental unintegrated (transverse momentum dependent) gluon distributions are proposed as fundamental building blocks to describe all processes sensitive to the small-x regime which admit a factorized description. Single-particle production processes and two-particle production processes are studied in asymmetric collisions of a dilute probe scattering from a dense target and it is shown that it is possible to recover factorized expression in a particular kinematical limit.

Table of Contents

List of Figures

List of Tables

Acknowledgments

I wish to thank my advisor Professor Alfred Mueller for his guidance, patience and dedication during the last few years. His advice and support have been crucial in these early stages of my academic career and without him this work would not have been possible. Most of all, I wish to thank him for sharing with me part of his wisdom and incredible physical intuition.

I am also indebted to Bowen Xiao, Feng Yuan, Cyrille Marquet, and Stéphane Munier for allowing me the privilege of participating in very fruitful collaborations during the past years. This work would have not reached its final form without their help.

I also wish to thank Aaron Angerami, Bin Wu, Edmond Iancu, Jianwei Qiu, Raju Venugopalan, and Jamal Jalilian-Marian for very helpful discussions and support during the last few years.

Special thanks to my family and my friends who have been there when I have needed them the most.

To my family and friends

Chapter 1

Introduction

The eternal quest of part of the scientific community to determine what is the fundamental structure of matter has led to a widely accepted classification of fundamental particles. Every physicist in the world is taught during his first years of training that all matter is made of fermions (quarks and leptons) which interact through intermediate bosons (photons, gluons, W's, Z's, gravitons). Matter is made of atoms. Atoms are made of protons, neutrons and electrons. Electrons are fundamental particles but protons and neutrons are made of three quarks each. Anyone who has tried to explain this idea to someone outside of the field has probably run into the same question: Has anyone ever seen a quark? The answer to this question is, of course, another question: What do you mean by the word "see"? Leaving semantics aside, a more accurate answer would be that no one has ever detected a free quark but there is plenty of evidence that protons and neutrons are composite particles, and the most successful theory to describe the strong interactions among hadrons assumes that all hadronic states are made of quarks and gluons, and more specifically each proton or neutron must have three "valence" quarks.

How such a simple question has such an elaborate answer is intimately related to the source of many of the difficulties of studying strong interactions. When formulating a quantum field theory describing the dynamics of a certain set of particles, it is

desirable to assign field variables for each observed particle. This strategy worked well for the development of quantum electrodynamics (QED) and later on the complete theory of electroweak interactions but runs into difficulties when strong interactions are considered. Any attempt to formulate a quantum field theory where the fundamental degrees of freedom correspond to observed hadrons runs into problems of self-consistency or is not renormalizable.

Eventually, motivated by developments in hadron spectroscopy and results from deep inelastic lepton-hadron scattering experiments, it was realized that hadrons are composite states and therefore the correct description of strong interactions has to be formulated in terms of the more fundamental quarks and gluons. These fundamental degrees of freedom carry a new kind of charge, referred as the color charge, which leads to the gauge structure of the theory known as quantum chromodynamics (QCD). The puzzle of why isolated quarks and gluons are not observed is addressed by the hypothesis of color confinement, which states that all observed states must be color singlet.

Regardless of all the evidence in favor of hadrons being composite, giving up on the direct relationship between observed particles and the fields of the theory is potentially dangerous for the capability of the theory of producing any testable predictions. In this case, asymptotic states cannot be expanded in a perturbation series in terms of free fields, making the calculation of amplitudes for scattering processes beyond the scope of usual perturbation theory.

The fact that some of the complications of the theory come from the inability to use perturbation theory is not so surprising. If the interactions are inherently strong the corresponding coupling constant is expected to be large, invalidating the use of perturbative methods by means of an expansion in terms of the coupling constant. The strong coupling case is consistent with color confinement, if binding energies are much larger than the quark masses any attempt to break hadrons apart will create additional color charges which rearrange in such a way that color neutrality is

preserved.

To get around this complications, it is important to make use of one of the most important features of strong interactions: asymptotic freedom. Strong interactions are observed to become rather weak when considered at very small distances. This particular observation indicates that there is a regime where a perturbative treatment is well justified and interactions can be accurately described in terms of quarks and gluons. The small distance behavior is only observed in scattering processes when the momentum transfer between the participants is large, in that case it is assumed that only one of the constituents, partons, inside each hadron participate in the hard scattering process. The corresponding partonic cross section is calculable via perturbative methods to any order.

Of course asymptotic freedom does not get rid of non perturbative effects completely, it only says that some part of the process can be calculated perturbatively. Any realistic scattering process still happens between hadronic states and the dynamics determining which particular partons are the ones participating in the hard process is non perturbative. Assuming that perturbative and non perturbative effects do not interfere, the calculation of hadronic cross sections could be thought as a convolution of partonic cross sections with probability distributions of finding a parton in a particular momentum state.

The picture described above is precisely the foundation of the parton model. When considered in the formal framework of QCD several additional features have to be included. This will be discussed in chapters 2 and 3. Most importantly, the formal statement of the model takes the shape of factorization theorems which can be formulated independently of the partonic picture. The probabilistic interpretation of the distributions is not necessary, the definition of the distributions is purely motivated in the ability of factoring out the non perturbative effects.

Having the option of formulating the formalism independently of the partonic picture will prove useful in subsequent chapters when dealing with gluon distributions

and their behavior under gauge transformations. In most cases, the partonic picture will be manifest only in a specific gauge, in some particular cases the partonic picture will not be available in any known gauge. The reason to define distributions with no partonic interpretation will be clear when some particular scattering processes are considered.

The original formulation of the parton model defines the parton distributions as functions of a variable x which, in the appropriate reference frame, can be interpreted as the momentum fraction carried by the parton in the hadron's momentum direction. When QCD considerations are taken into account, the parton distributions acquire an additional dependence in the energy scale characterizing the hard partonic interaction. Even though the distributions represent the non perturbative part of any scattering process, it has been shown that the dependence on the energy scale is determined by perturbative dynamics. More on this in chapter 2. In the same spirit of obtaining important information about parton distributions via perturbative methods, it has been noted that the x dependence in the small-x regime also obeys an evolution equation which can be derived by perturbative considerations.

The main problem when considering evolution of parton distributions at small-x comes form the fact that small-x effects become important in a region where factorization is believed to break down. The problem comes mainly from softer processes becoming increasingly important as gluon distributions grow rapidly when moving to smaller values of x. These difficulties in the formalism will be explained throughout the following chapters and finally summarized in chapter 5.

Despite the complications of the factorization formalism in the small-x region, it is still very instructive to consider gluon distributions at small-x since they give further insight into the dynamics of nonlinear effects. These distributions can be considered either from a purely partonic point of view, leading to the so called Weizsäcker-Williams distribution function, or by trying to recover factorized forms for different cross sections where multiple interactions can be conveniently resummed. Either

of the two approaches makes explicit reference to the transverse momentum of the gluons, leading naturally to a transverse momentum dependent approach to factorization if any factorization at all is recovered. How to reconcile these approaches is first explained in chapter 5 and then put into work for calculating different processes in chapters 6 and 7.

The fact that these different approaches can be reconciled in a consistent way is the main original contribution of this thesis. The existence of several gluon distributions in the small-x regime had already been pointed out some time ago, but it was not well understood why they appeared for different processes and how they could fit in a more general approach. Most of this results are already in published form in Refs. [3; 4; 5]. Here the presentation is mainly focused in the small-x general results in a Color Glass Condensate framework in order to be able to address the small-x evolution of the distributions.

Chapter 2

Quantum Chromodynamics

More than a general review of the whole theory of strong interactions this chapter is intended to emphasize the particular features of QCD which will play an important role in the development of subsequent chapters. For a thorough review of QCD, its foundations and general predictions, the reader is referred to the many available textbooks and reviews such as [6; 7; 8; 9; 10].

In particular, special attention will be given to renormalization issues and how this affects the partonic picture of hard scattering processes as well as multi-particle states and deviations from perturbative treatments in the weakly coupled regime.

2.1 Basics

For a long time now, there has been a common agreement in the high energy physics community that QCD is the correct theory to describe the dynamics of strong interactions. Despite the many technical difficulties in performing accurate calculations, many different experimental tests show a very good agreement with predictions at a qualitative and quantitative level. Among the most important features predicted by QCD are: asymptotic freedom, color degrees of freedom, scaling violations, etc.

Formally speaking, QCD is a particular case of a Yang-Mills theory with gauge

group $SU(N_c)$, and more specifically $N_c = 3$. The additional degree of freedom associated with this gauge group is referred to as color and it plays a main role in the dynamics of the theory. In particular, it is of uttermost importance that the gauge bosons, the gluons, carry color as well as the fermions and therefore can interact among each other.

The QCD Lagrangian is given by

$$\mathcal{L} = -\frac{1}{4} F^a_{\alpha\beta} F^{\alpha\beta}_a + \sum_f \bar{q}_f (i\gamma_\mu D^\mu - m) q_f . \tag{2.1}$$

where $F^a_{\alpha\beta}$ is the field strength tensor derived from the gauge field A^a_α,

$$F^a_{\alpha\beta} = \partial_\alpha A^a_\beta - \partial_\beta A^a_\alpha - g f^{abc} A^b_\alpha A^c_\beta \,, \tag{2.2}$$

all color indices in the adjoint representation of $SU(N_c)$. The fermion spinors q_f are in the fundamental representation and the sum is over all the quark flavors.

The Lagrangian above represents just the classical part of the theory. For the full quantum description of the bosonic degrees of freedom it is necessary to include a gauge-fixing term which would allow to specify the gluon propagator. Moreover, if the gauge-fixing term is of the covariant type then an additional term, the ghost term, is needed to cancel unphysical degrees of freedom. Details about this terms of the Lagrangian will not be provided here. Some details about the gauge choice will be provided when required by the calculations in the subsequent sections.

Some properties of the theory can be inferred directly from analyzing the form of the Lagrangian above. First of all, notice the interactions terms among the different fields. Besides the already familiar fermion-boson vertex, the QCD Lagrangian includes three-gluon and four-gluon vertices. Gluons can interact among themselves and therefore carry color as well, unlike electrodynamics where photons have no charge. This particular feature of the theory makes it conceivable to have a theory with only the gauge fields and no fermions, and therefore makes it possible in some cases to isolate the contributions coming from only the gauge part from the contribution coming from the fermions.

These gluon self-interactions are responsible for most of the distinctive aspects of QCD such as asymptotic freedom and the existence of jets. In the former case, the possibility of gluon splittings allows for an anti-screening effect which manifests in the coupling being effectively larger at larger distances. For the latter case, gluon splitting plays a fundamental role in the creation of large number of particles all coming from the same leading parton.

The second fundamental aspect of the theory that can be directly read from the Lagrangian is gauge invariance. The theory is constructed in such a way that it is invariant under local gauge transformations of the type

$$q(x) \to V(x)q(x), \tag{2.3}$$

$$A_\mu(x) \to V(x)A_\mu(x)V^{-1}(x) + \frac{i}{g}(\partial_\mu V(x))V^{-1}(x), \tag{2.4}$$

with $V(x) \in SU(N_c)$.

Even though this symmetry has to be explicitly broken in order to successfully quantize the bosonic degrees of freedom, the symmetry is still present in the fact that any physical observables should be independent of the specific gauge choice used to construct the gluon propagator. This property is not exclusive of QCD and it is already present in QED where the gauge group is considerably simpler. In terms of the gauge invariance, there is a fundamental difference between non-abelian theories like QCD as compared to abelian theories like QED, and that is that the gauge strength tensor $F^{\mu\nu}$ is not gauge invariant.

This fact has several implications regarding the way processes are pictured in terms of states with a definite number of off-shell particles. For the fermions there is a conserved current which still allows one to define unambiguously the number of fermions in a given state, but for the gluons that ability is lost when $F^{\mu\nu}$ is no longer gauge invariant. A state with only a quark and no gluons can be turned into a state with a quark and many gluons by means of a gauge transformation. This implies that the partonic picture of processes involving hadronic states changes depending on

the gauge choice and therefore one has to pay extra attention to gauge choices when dealing with parton distributions as will be the case in subsequent chapters.

2.2 Running of the coupling and asymptotic freedom

One of the most important properties of the strong interactions, and a feature that must be present in any theory which attempts to successfully describe them, is that of asymptotic freedom. Strong interactions seem to turn off when probed at very short distances. This short-distance behavior is directly related to the high-energy degrees of freedom and therefore an accurate description of this phenomenon has to come from a good understanding of the ultraviolet regime.

The fact that QCD is asymptotically free is not straightforward from the Lagrangian formulation. In order to see explicitly how this property comes about it is mandatory to address the removal of ultraviolet divergences and, in particular, the renormalization procedure applied to the effective fermion-boson vertex. To one-loop order, the beta function can be calculated from the divergent part of the corresponding counterterms [11; 12]. The result is

$$\beta(\alpha_S) = -\frac{\alpha_S^2(11N_c - 2N_f)}{12\pi}, \tag{2.5}$$

where N_f is the number of active fermion flavors.

The most important thing to notice about this result is that for $N_c = 3$ and $N_f < 17$ the beta function is negative. This means that increasing the energy scale lowers the value of the renormalized coupling, which is exactly what you need for an asymptotically free theory. For sufficiently high energies the value of the coupling goes to zero, effectively turning off interactions at very small distances.

Even though specific details of the calculation are not shown here, a few observations can be easily made about the origin of the different contributions to the beta

function. First, the term proportional to the number of fermion flavors comes from the contribution of fermion loops to the gluon propagator. This is the familiar vacuum polarization already present in QED which is often associated with a screening effect by giving the vacuum dielectric properties. On the other hand, the term proportional to the number of colors comes from the contribution of the gluon loops in the gluon propagator and the correction to the vertex due to the triple-gluon vertex.

As was mentioned in the previous section, the fact that non-abelian gauge theories are asymptotically free is a direct consequence of the interactions between gluons. The fact that gluons give an opposite effect as compared to fermions in this case has been argued to be due to the gluons having spin 1 [13]. Even though there is no straightforward intuitive explanation for this phenomenon it is often compared to magnetic polarization. In this picture the familiar QED screening is compared to the dielectric response of the vacuum to the presence of a charge whereas the QCD case resembles the static magnetic case where the fermions show a diamagnetic behavior while the gluons show a paramagnetic behavior which ultimately overcomes the diamagnetic effect to give a total effective anti-screening.

The beta function above shows how the coupling constant changes with the energy scale but does not say anything about its actual value. Given a small value for the coupling at some scale (the renormalization scale) it is possible to calculate the value of the coupling at a different scale, provided the coupling does not get too big so it is still valid to use perturbative techniques. The one-loop result for the beta function can be integrated to obtain an explicit expression in terms of the energy scale with the renormalization scale and the value of the coupling at that point as parameters.

$$\alpha_S(Q^2) = \frac{\alpha_S(\mu^2)}{1 + \alpha_S(\mu^2) b \ln(Q^2/\mu^2)}, \tag{2.6}$$

where μ is the renormalization scale and $b = (11N_c - 2N_f)/12\pi$.

The two parameters above can be replaced for a single dimensionful parameter Λ_{QCD} defined as the scale where the coupling would diverge according to the perturbative expression for the beta function. The coupling does not actually diverge at

that point since perturbation theory loses validity before reaching that energy scale. In terms of this parameter, the coupling to one-loop order takes the form

$$\alpha_S(Q^2) = \frac{1}{b \ln(Q^2/\Lambda_{QCD})}. \tag{2.7}$$

Qualitatively, the order of magnitude of Λ_{QCD} gives the approximate scale where non-perturbative effects become important and therefore perturbation theory breaks down. Experimentally this scale is found to be $\sim$ 200 MeV which is the order of magnitude of the mass of the lightest hadrons. This indicates that we can only trust perturbation theory at energy scales of or higher than 1 GeV.

For the reasons outlined above, the use of perturbative QCD has been limited mostly to the study of hard processes where the exchanged transverse momentum is very large. When that is the case, perturbative methods are used to calculate rates of processes at the partonic level where the degrees of freedom are quarks and gluons. This is in contrast with what is seen in experiments where free quarks and gluons are never observed. Therefore it is necessary to complement the perturbative approach with parton distribution functions and fragmentation functions which take care of the transition from hadronic to partonic degrees of freedom. The physics behind this distribution functions is non-perturbative, and therefore they are not calculable from first principles with the current field theory methods and have to be extracted from data. More about this distribution functions will be discussed in subsequent sections.

2.3 Factorization and distributions

Despite the enormous amount of work that has been devoted in recent years to the study of strongly coupled systems, there is still no reliable systematic way to calculate rates for arbitrary processes in a field theory with a strong coupling. Current theoretical tools rely mostly on perturbative expansions which are valid only as long as there is a small parameter which is typically taken to be the coupling of the interaction.

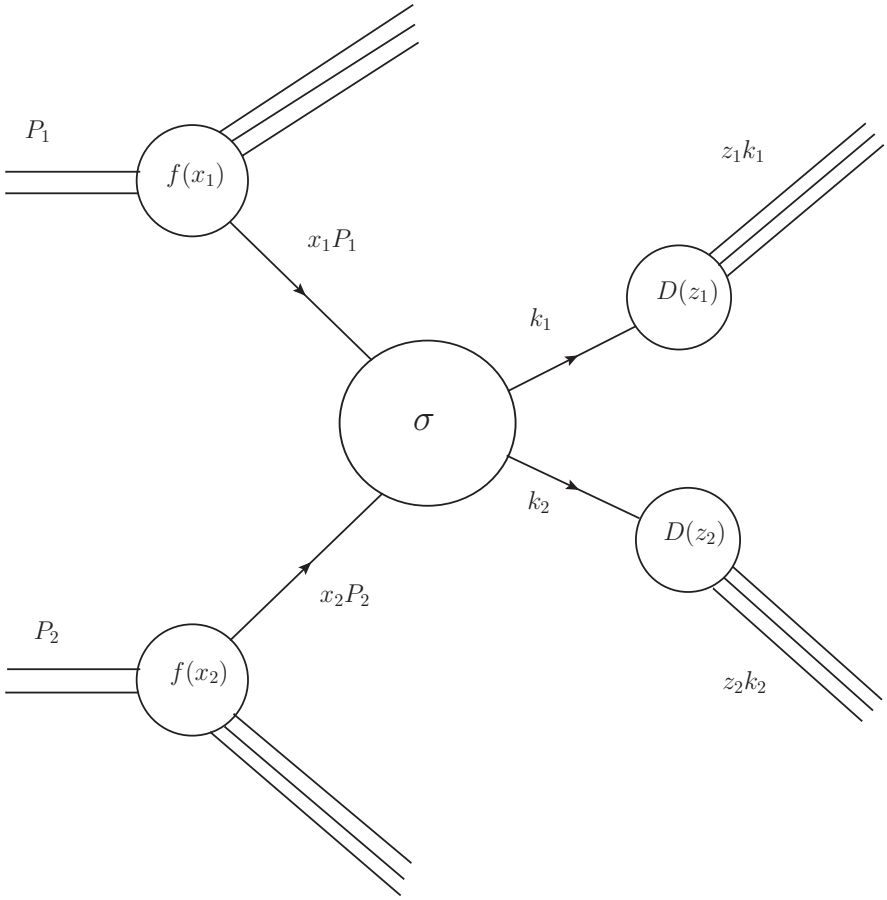

Figure 2.1: Schematic picture of factorization.

As was mention in previous sections, despite the fact that strong interactions are inherently strong, the fact that asymptotic freedom is observed allows the perturbative study of processes where the relevant energy scale of the problem is sufficiently large.

It is important to note that perturbative calculations deal directly with quarks and gluons rather than with the hadronic states present in real experiments. Since these calculations are performed at the partonic level, it becomes important to establish a systematic way to relate partonic processes to hadronic states. As a first step, it was suggested that if it is possible to calculate cross sections at the partonic level all that is left to do in order to find the cross section involving hadronic states is to

convolute the result with the corresponding probability of finding the specific parton involved inside a hadron. Under that setup, processes would be represented as in Fig. 2.1 where f's denote the parton distribution functions (PDF) giving the probability to find a specific parton inside a hadron, σ is the partonic cross section which is perturbatively calculable, and D's denote the fragmentation functions which give the probability of a specific hadron forming from the hadronization of an outgoing parton. The convolution of all these pieces gives the total cross section of the process.

$$\sigma_{tot} = \int dx_1 dx_2 dz_1 dz_2 \; f_{h_1}(x_1) f_{h_2}(x_2) \sigma(x_1 P_1, x_2 P_2; k_1, k_2) D_{h_3}(z_1) D_{h_4}(z_2) \; . \qquad (2.8)$$

The picture described above relies heavily in the assumption of factorization due to the separation of scales. Chapter 3 will be devoted to explain some of the details of this very broad and important subject, here a few comments are provided in order to motivate further discussion in this and subsequent sections. First, it is important to note that this partonic picture is usually better understood in the infinite momentum frame of the hadron and in the light-cone gauge. The choice of light-cone gauge is motivated by some of the nice features present in light-cone quantization (see [14; 15]), among which is the fact that the vacuum of the full-theory is the same as the vacuum of the free theory, therefore allowing for an expansion of any state in terms of non-interacting eigenstates of the free Hamiltonian. The infinite momentum frame is chosen because it allows for a picture of the hadron as a collection of constituents all moving *almost parallel* to each other. Under this setup, partons can be characterized by the hadron's momentum fraction they carry in the longitudinal direction.

Calculating the weights of the different multiparticle states, or equivalently, the probability of finding a parton with a definite momentum fraction, is beyond the scope of perturbation theory. The dynamics of these objects is dominated by branching induced by multiple gluon emissions, which is sensitive to the non-perturbative regime in the collinear limit. When calculated perturbatively, gluon emission from a fast moving parton gives a divergence which comes from integrating over the region of low transverse momentum of the emitted gluon. In order to remove this divergence it is

necessary to introduce a cut-off scale (factorization scale) to separate "soft modes" (in transverse momentum space) from "hard" modes. The soft divergent part is absorbed by the renormalized distribution functions at the given scale while the hard modes dictate the evolution of the distributions with respect to the factorization scale.

The fact that the collinear divergence can be absorbed by the distribution functions is not a trivial statement and requires a more complete proof. Proofs for several cases are available in the literature [6] and some of them will be addressed in Chapter 3. These proofs of factorization actually show that formula (2.8) is just the leading contribution of an expansion in terms of inverse powers of the large energy scale of the problem (necessary to justify the use of perturbation theory).

Now, if these distributions are not calculable from first principles, how can they be used to predict the outcome of any experiment? The answer to this question lies in the idea of universality. These distributions are assumed to be universal in the sense that, for a given hadron, the same distribution should be used for any hard process in which the hadron is involved. In practice, the distributions are measured in deep inelastic scattering experiments and then used to calculate cross sections for hadron-hadron collision experiments. Deep inelastic scattering experiments are ideal to determine the parton distribution functions of a hadron since the probe is color neutral and therefore does not interact strongly.

Instead of presenting a formal treatment of DIS, a few comments will be made concerning relevant kinematics and how parton distributions are extracted from inclusive measurements in DIS. The relevant kinematic variables for this process are the initial 4-momentum of the hadron P^μ and the 4-momentum of the virtual photon q^μ. There are two independent Lorentz scalars for the hadron system which are usually taken to be $Q^2 = -q^2$ and the Bjorken variable

$$x = \frac{Q^2}{2P \cdot q}\,, \tag{2.9}$$

the choice of the latter being motivated by the fact that, up to corrections suppressed by powers of Q^2, it can be identified with the fraction of the total longitudinal mo-

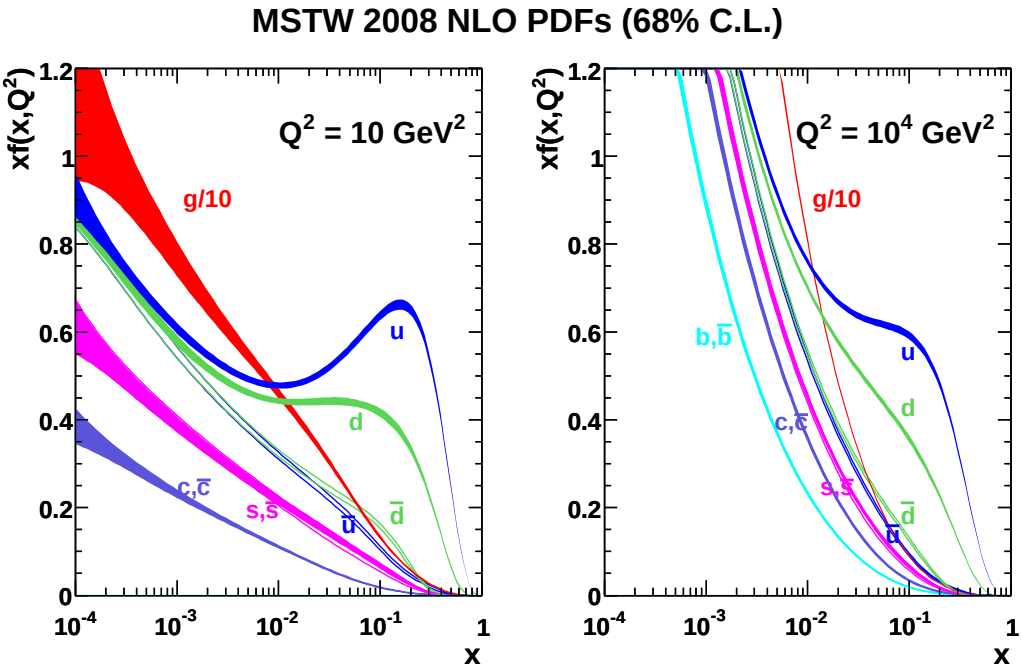

Figure 2.2: Parton distributions at fixed $Q^2 = 10$ GeV^2 and $Q^2 = 10^4$ GeV^2. Taken from [1].

mentum carried by the struck parton. It is sometimes convenient to express quantities in terms of dimensionless variables, in which case Q^2 is replaced by

$$y = \frac{Q^2}{xs} \tag{2.10}$$

with s the usual Mandelstam variable. If factorization holds for this process, the partonic cross section can be calculated to first order using on-shell massless partons independently of the non-perturbative parts of the process. The corresponding hadronization of the struck parton can also be omitted by simply considering the inclusive cross section and therefore summing over all possible hadronic final states.

In the spirit of the parton model, the total cross section is obtained from a convolution of the partonic cross section (calculated perturbatively) with the corresponding parton distribution functions. To first approximation, these parton distributions de-

pend only on the fraction of momentum carried by the parton. Further considerations show that the distributions are also dependent on the factorization scale, which is usually taken by convenience as the hard scale of the process Q^2. Putting these pieces together, it can be easily shown that the inclusive cross section for DIS can be written as

$$\frac{d^2\sigma}{dxdy} = \frac{2\pi\alpha_S^2 s}{Q^4}\left(\sum_f x f_f(x,Q^2)e_f^2\right)\left[1+(1-y)^2\right], \tag{2.11}$$

where $f_f(x,Q^2)$ is the parton distribution function for flavor f and e_f the corresponding electric charge.

It is clear from Eq. (2.11) how to extract the sum of the parton distributions weighted by their electric charge squared (also know as the structure function F_2). In order to access individual distributions for each flavor it is necessary to consider also neutrino deep inelastic scattering. Details on how to extract different parton distributions and the most up to date fits can be found in [2]. Figure 2.2 shows the parton distribution functions as a function of x for $Q^2 = 10$ GeV^2 and $Q^2 = 10^4$ GeV^2.

Figure 2.2 shows that the distribution functions are large at small-x and in particular the gluon distribution becomes dominant. This fact will be central in the rest of the presentation, where only the gluon dynamics will be relevant when dealing with the small-x degrees of freedom.

Even though the original parton model does not account for Q^2 dependence for the parton distribution functions, it was included in Eq. (2.11) since the scale dependence was already anticipated in this section. Figure 2.3 shows this Q^2 dependence of the form factor F_2 for many different fixed values of x.

2.4 Parton evolution

Under particular circumstances, the dependence of the parton distribution functions on its two arguments can be studied by perturbative methods. The result is a set of

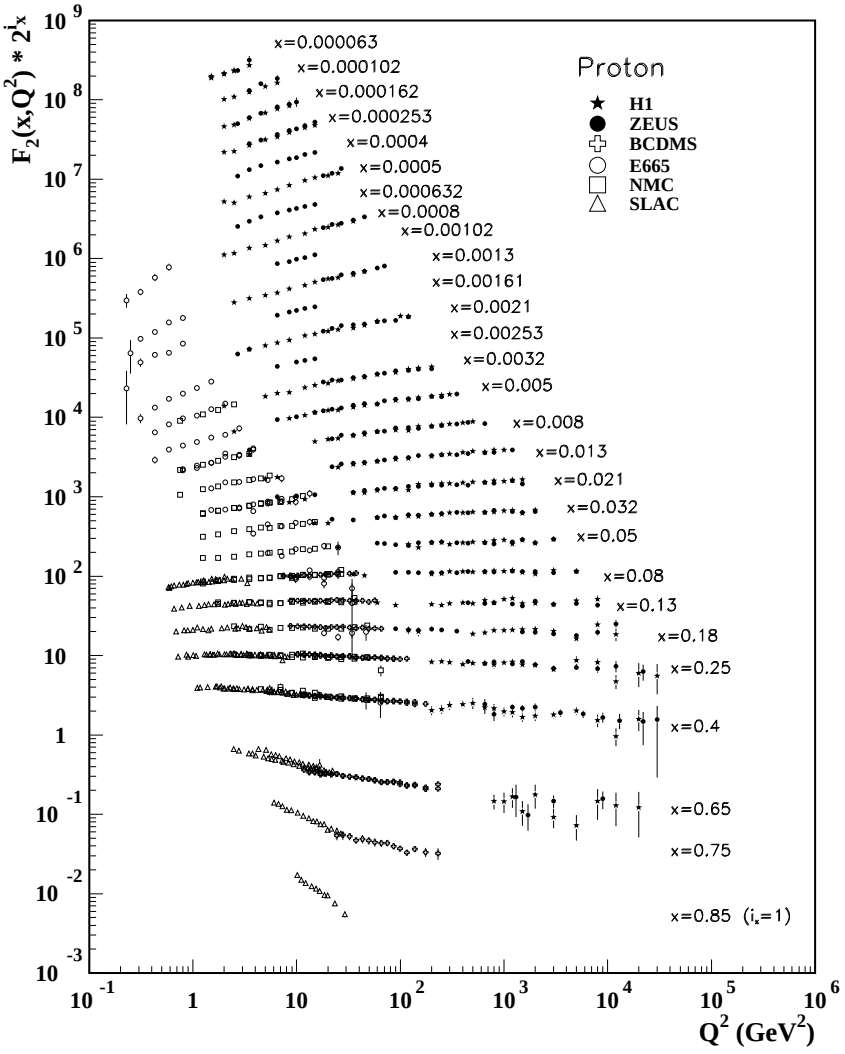

Figure 2.3: Summary of data showing the Q^2 dependence of F_2. Each series of data points for the i_x-th fixed value of x is multiplied by a factor of 2^{i_x}. Taken from [2].

evolution equations which do not determine completely the distributions (since they are inherently non-perturbative) but constrain them to great extent.

2.4.1 DGLAP

It was already observed in the previous section that the parton model can be improved by taking into account corrections that come from considering parton branching in the perturbative limit. The Q^2 dependence of the parton distribution functions can be calculated perturbatively provided that Q^2 is sufficiently large.

Taking into account that the the transverse resolution is set by Q^2, it comes as no surprise that the Q^2 dependence of the distributions is closely related to the already mentioned divergence in the emission amplitude for gluons at low transverse momentum. From this point of view, the distributions $f_i(x, Q^2)$ can be interpreted as the probability of finding parton i where emissions with transverse momentum lower than Q are not resolved. The evolution of the distributions in Q^2 is therefore computed by considering the probability of emitting a parton with transverse momentum close to Q^2.

It is very important to note that even though parton branching is down by powers of the coupling (assumed small due to the large scale Q^2), integration over phase space brings a factor of $\ln(Q^2/\Lambda_{QCD})$ which compensates for the smallness of the coupling. If these contributions are not suppressed then multiple emissions should be resummed. In general the large logarithms are obtained from the region in phase space in which the multiple emissions are strongly ordered in transverse momenta with later emissions having larger momenta. This leads to the usual resummation of large logarithms characteristic of renormalization group equations.

Either following the renormalization group approach or the partonic picture with parton emission having transverse momenta of order Q^2, the evolution equation for the parton distributions, known as the Dokshitzer-Gribov-Lipatov-Altarelli-Parisi

(DGLAP) equation, can be explicitly calculated [16; 17; 18; 19].

$$\frac{d}{d\ln Q} f_i(x,Q) = \frac{\alpha_S(Q^2)}{\pi} \int_x^1 \frac{dz}{z} P_{i/j}(z) f_j(\tfrac{x}{z}, Q), \tag{2.12}$$

where i and j run over all possible parton flavors. The splitting functions $P_{i/j}(z)$ are most easily calculated in light-cone perturbation theory [18]. Clearly, the splitting functions are independent of the quark flavor and are the same for quarks and antiquarks. To first order in the coupling they are given by

$$P_{q/q}(z) = C_F \left[\frac{1+z^2}{(1-z)_+} + \frac{3}{2}\delta(1-z) \right] , \tag{2.13}$$

$$P_{q/g}(z) = \frac{1}{2} \left[z^2 + (1-z)^2 \right] , \tag{2.14}$$

$$P_{g/q}(z) = C_F \left[\frac{1+(1-z)^2}{z} \right] , \tag{2.15}$$

$$P_{g/g}(z) = 2N_c \left[\frac{z}{(1-z)_+} + \frac{1-z}{z} + z(1-z) \right] + \frac{11N_c - 2N_f}{6}\delta(1-z) , \tag{2.16}$$

with $C_F = (N_c^2 - 1)/2N_c$ and the "plus" distribution defined by the property

$$\int_0^1 dz \, \frac{f(z)}{(1-z)_+} = \int_0^1 dz \, \frac{f(z) - f(1)}{1-z} . \tag{2.17}$$

2.4.2 BFKL

The derivation of the DGLAP equation makes use of the collinear divergence in gluon emission to justify the resummation of logarithms in the transverse scale. Similar arguments hold for the other divergence usually present in this kind of processes, the soft divergence. Soft gluon emissions are the driving force of the dynamics at small-x where a proper resummation has to be taken into account due to the large parameter $\ln(1/x)$ compensating the smallness of the coupling in the perturbative regime.

When multiple emission are taken into account it is easy to see that the leading logarithmic contribution comes from the region in phase space where the emitted gluons are strongly ordered in longitudinal momentum with softer emission occurring later in time.

Intuitively, the process of multiple emission can be picture in the following way. Consider the rapidity variable $y = \ln(1/x)$. The probability of emitting one gluon is proportional to the color charge of the system and the rapidity interval available. The larger the rapidity interval is the more gluons would be emitted, and therefore the effective color charge of the system becomes much larger, which consequently increases the probability of further emissions. It can be seen that this phenomenon induces an exponential growth of the number of gluons emitted as a function of the rapidity interval.

A formal study of this dynamics was first done by Balitsky, Fadin, Kuraev, and Lipatov leading to what is now know as the BFKL equation [20; 21; 22; 23]. Being a small-x effect, a more thorough explanation will be given in chapter 4 where a brief review of the derivation is presented along its many consequences and implications.

Chapter 3

Factorization

The subject of factorization in QCD has been widely studied for many decades since it is one of the cornerstones of the predictive power of the theory. Being such an important part of the formalism, it is still a very active field of research with many open interesting problems. Because of these, and many other reasons, a comprehensive review of factorization in QCD is beyond the scope of this work[1].

As was explained in the previous chapter, the concept of factorization comes very naturally in an attempt to be able to take advantage of the full machinery of perturbative methods regardless of the fact that almost any process in QCD is sensitive to large distance phenomena, where the coupling is large and perturbation theory explicitly breaks down. Because of this, factorization is taken for granted without considering its possible downfalls and limitations.

This chapter is intended to review, in a very casual way, what are the assumptions of factorization, for which processes it has been formally proven, and where it breaks down. Also, the formalism of transverse momentum dependent (TMD) factorization is briefly introduced since it is closely related to the main topic of this thesis.

The main reason to consider the TMD formalism is that, even though the study of gluon distributions at small-x is interesting in itself from a theoretical point of view, in

[1]For a full review of the formalism see [6; 24]and references therein.

the development of the study of these distributions special emphasis is made on how to relate them to physical observables and scattering processes. Most of the material of subsequent chapters is focused on the description of the small-x degrees of freedom from an effective field theoretical point of view and how the gluon distributions fit in different processes from this approach. As a consistency check, it will become important to compare to approaches based on factorization as the central idea. This last observation has to be taken with caution since different approaches are not always valid in the same kinematic regions and, therefore, it becomes important to find a common ground where both approaches can be trusted and the comparison makes sense.

3.1 Collinear factorization

The form of factorization that was briefly discussed qualitatively in the previous chapter is usually referred to as collinear factorization. The word collinear is used to emphasize that transverse effects are not taken into account as opposed to the TMD formalism. This is the most established form of factorization and has been successfully used for many decades to both extract parton distributions from data and make testable predictions.

For this factorization to work, it is always assumed an underlying hard scattering process which dominates the dynamics. Consequently, all the energy scales involved are assumed to be large and of the same order. This typically means that the processes which can be addressed this way are inclusive processes where it is necessary to sum over a large class of possible final states, all momentum variables which can not be fixed to be of the same order of the large scale of the problem (usually the center of mass energy of the collision) should be integrated over.

Processes for which collinear factorization is well stablished and proofs to all orders (some with small gaps) are available include DIS, Drell-Yan, e^+e^- annihilation

into hadrons, and single jet production in hadron-hadron scattering. Following the comment made above about the size of the kinematical variables entering the process, a few comments on the validity of this approach for each of the mentioned processes are necessary. For DIS, only the total cross section can be calculated this way since measuring any other particle introduces a transverse momentum scale which can not be fixed to be of the same order as the virtuality of the photon. In Drell-Yan it is required that the virtuality of the virtual boson is of the same order of the center of mass energy and its transverse momentum is also fixed to be of the same order or is integrated over. Similarly for the other processes.

These assumptions are very natural when considered in terms of the parton model, since they allow for a proper separation of time scales justifying the ability to factorize long distance dynamics from short distance dynamics without interference (up to corrections suppressed by the large energy scale). When a high energy scattering process is considered in the center of mass frame, the incoming hadrons are Lorentz contracted and have a very small longitudinal extent, implying that they don't "see" each other before the collision. Their distributions are therefore unaffected by the presence of the other hadron. The assumption that the momentum transfer or virtuality of the intermediate particle is very high ensures that the time scale in which the hard interaction occurs is much shorter than the soft interactions binding the hadrons together, making it reasonable to decouple these two different effects.

This picture can be seen as the interplay of the two effects of having fast moving hadrons, the length contraction in the direction of the collision and the time dilation of the interactions inside the hadron. The first effect combined with the large momentum transfer ensures that the collision occurs between one parton from each hadron only while the second effect implies that at the moment of the hard scattering the partons seem frozen and the inner dynamics of the parent hadrons can be ignored.

All this considerations also imply that the parton distribution functions should be independent of the hard process and therefore universal. This statement plays

a fundamental role in the formalism and without it QCD loses all predictive power for high energy collisions. Since the distributions are determined by inherently non-perturbative phenomena and can not be calculated by standard methods, they have to be extracted from data. It is possible to make sensible predictions only if the distributions extracted from a specific experiment can be used to predict the outcome of a different process, that is only possible if the distributions are universal.

To be more precise, the distributions are not completely independent of the hard process under consideration. As was mentioned in the previous chapter, parton distributions have a (weak) dependence on the energy scale at which the hard scattering occurs, but this dependence can be calculated perturbatively via the DGLAP equation and it is independent of the specific process under consideration, it only depends on the energy scale. In practice, what is done to make testable predictions is to measure the distributions at some particular energy scale, evolve them to the energy scale of the new process to be considered and then use them for the new calculated cross sections.

The fact that separation between perturbative and non perturbative effects can be cast into partonic cross sections and distribution functions allows to consider factorization theorems as the field theoretic realization of the parton model. As such, it becomes necessary to introduce more formal definitions of the parton distribution functions in terms of local operators. The quark distribution can be written in terms of the fermionic field ψ as [24; 25]

$$f_q(x) = \frac{1}{4\pi}\int d\xi^- \; e^{-ixP^+\xi^-}\langle P|\bar{\psi}(0,\xi^-,0_\perp)\gamma^+\mathcal{G}\psi(0,0,0_\perp)|P\rangle, \tag{3.1}$$

for a hadron with large momentum P in the positive z direction. The hadronic state above has a definite momentum and is normalized such that $\langle P'|P\rangle = (2\pi)^3 2P^+\delta(P^+ - P'^+)\delta^{(2)}(P_\perp - P'_\perp)$. The operator $\mathcal{G}$ in between the two field operators is there to guarantee that the definition is gauge invariant and is given by the path ordered

exponential

$$\mathcal{G} = \mathcal{P} \exp\left\{ ig \int_0^{\xi^-} dz^- \; A_c^+(0, z^-, 0_\perp) T^c \right\} \; , \tag{3.2}$$

with the color matrices T^c in the fundamental representation of the gauge group.

As usual, the partonic interpretation is manifest in light-cone gauge where the "gauge link" $\mathcal{G}$ can be dropped and the remaining operator counts the number of quarks with a definite longitudinal momentum.

Analogously, the corresponding definition for the gluon distribution is [24; 25]

$$f_g(x) = \frac{1}{2\pi x P^+} \int d\xi^- \; e^{-ixP^+\xi^-} \langle P | F_a^{+\nu}(0, \xi^-, 0_\perp) \gamma^+ \mathcal{G}_{ab} F_{b\,\nu}^+(0, 0, 0_\perp) | P \rangle, \tag{3.3}$$

where now the gauge link is defined in the adjoint representation and $F^{\mu\nu}$ is the usual field strength tensor. The definitions above will allow to generalize the formalism in a straightforward manner to the case where distributions are allowed to have transverse momentum dependence.

Before the end of this section, it is important to mention two important cases where collinear factorization breaks down and therefore alternative approaches are needed. The first case is when there is another energy scale in the process which is much smaller than the center of mass energy (or whatever kinematical invariant used as the hard scale of the process). In particular processes with particle production at low transverse momentum fall into that category, which motivates the introduction of transverse momentum dependence in the distributions. The next section is devoted to introduce that approach. The second case where collinear factorization loses its validity is when parton densities become too large. In that case, it is not fully justified to consider processes with only one hard interaction and ways of resumming multiple interactions have to be considered. This is particularly troublesome when the small-x regime is considered. Ways of addressing this problem are considered in the next chapter.

3.2 TMD factorization

The main motivation to define and study transverse momentum distributions, and their respective factorization theorems, is to extend the scope of the factorization approach described in the previous section to be able to include processes that, in a partonic picture, would be sensitive to the transverse momentum of the incoming partons. Accounting for transverse momentum dependence implies relaxing the assumption that all energy scales in the problem are of the same order. In particular when the new energy scale is much smaller than the hard scale, this formalism allows one to calculate only the leading term in a series expansion in terms of the ratio of the two energy scales.

In principle, extending the formalism of the previous section to include transverse momentum in the definition should not be too difficult. In terms of the operator definitions all that is needed is to allow for a transverse separation of the two field operators and then perform the Fourier transform on the transverse coordinates [25]. Unfortunately, things are not so simple. The first problem can be seen directly from the form of definitions (3.1) and (3.3), if the fields are allowed to be at different transverse coordinates the gauge link has to include also a transverse part. There is no obvious choice for the path of the gauge link from one point to another and different choices would lead to different definitions, therefore a prescription for the gauge link path is needed. This first observation is potentially problematic since the gauge links are usually seen as a way of resumming contributions from either initial or final state interactions, in the collinear case most of these contributions cancel out but in the TMD case it is likely that these become process dependent, spoiling the universality of the distributions.

Numerous studies have addressed the question of how to determine the appropriate gauge links for different processes with several interesting results [26; 27; 28; 29]. It is now commonly accepted that the gauge links are intimately related with the resummation of gluon emissions collinear to one of the participating partons.

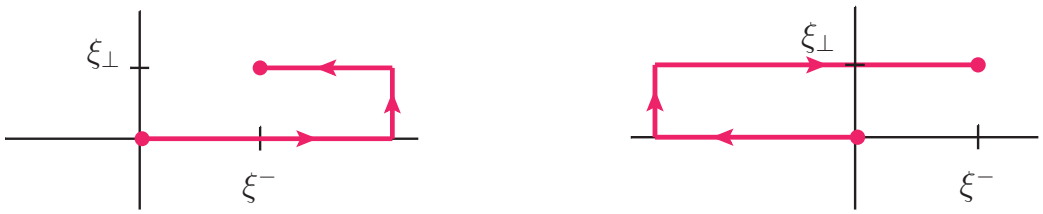

Figure 3.1: Left: path of future pointing gauge link $\mathcal{U}^{[+]}$. Right: path of past pointing gauge link $\mathcal{U}^{[-]}$.

This resummation procedure is quite general and the only differences between different processes is due to the color flow. The simplest example comes from comparing single inclusive deep inelastic scattering (SIDIS) and Drell-Yan processes, when computing the quark distributions for SIDIS it is necessary to consider only final state interactions and therefore the gauge link structure will be "future pointing" with Wilson lines extending in the plus infinite longitudinal direction, while for Drell-Yan the gauge link involved will be "past pointing" with Wilson lines extending to minus infinity in the longitudinal direction. To be more specific, consider the following Wilson lines in the longitudinal and transverse directions:

$$U^n[a,b;x_\perp] = \mathcal{P}\exp\left\{ig\int_a^b dx^-\ A^+(0,x^-,x_\perp)\right\} \tag{3.4}$$

$$U^T[x^-;a_\perp,b_\perp] = \mathcal{P}\exp\left\{ig\int_{a_\perp}^{b_\perp} dx_\perp\cdot A_\perp(0,x^-,x_\perp)\right\}. \tag{3.5}$$

The gauge link involved in the quark distribution for SIDIS is

$$\mathcal{U}^{[+]} = U^n[0,\infty;0_\perp]U^T[\infty;0_\perp,\infty_\perp]U^T[\infty;\infty_\perp,\xi_\perp]U^n[\infty,\xi^-;\xi_\perp]\ , \tag{3.6}$$

and is illustrated in the left side of Fig. 3.1. The transverse gauge links at infinity have been shown to be crucial to maintain the gauge invariance and, even though their contribution will be dropped most of the times by choosing a gauge where the fields are zero at infinity, it is important to keep them in mind when making general considerations. The detailed structured of the transverse link at infinity is chosen in

that particular way for technical reasons [29]. Similarly, the gauge link for the quark distribution in Drell-Yan is

$$\mathcal{U}^{[-]} = U^n[0,-\infty;0_\perp]U^T[-\infty;0_\perp,\infty_\perp]U^T[-\infty;\infty_\perp,\xi_\perp]U^n[-\infty,\xi^-;\xi_\perp]\,, \tag{3.7}$$

and is illustrated in the right side of Fig. 3.1.

For the gluon distributions it is convenient to write the gauge links in the fundamental representation instead of the adjoint representation used in Eq. (3.3) for the collinear case. First note that any gauge link in the adjoint representation can be written in terms of the fundamental representation version using the identity

$$F_a(\xi)\mathcal{G}_{ab}F_b(0) = \mathrm{Tr}\left[F_a(\xi)T^a\mathcal{G}F_b(0)T^b\mathcal{G}^\dagger\right], \tag{3.8}$$

but in the fundamental representation more general gauge links can be defined by allowing different paths for the fundamental gauge links connecting the two points on either side.

Since the gauge links are related to either initial or final state interactions between the incoming hadron under consideration and other participants in the hard interactions, it is natural to include in the gauge link Wilson lines for each of the other participants, future pointing for outgoing partons and past pointing for incoming partons. Depending on the identity of the parton such Wilson line would be either in the fundamental (for quarks and antiquarks) or the adjoint representation (for gluons). The procedure of how to combine all these pieces into one gauge link structure is thoroughly explained in [28]. In particular, the two-to-two processes considered in the appendix of [28] will be crucial to the study of two-particle measurements of chapter 7.

It is important to note that it has been shown that this approach does not work in general for hadron-hadron collisions where it has been explicitly shown that TMD factorization breaks down [30; 31]. The problem comes from the fact that the soft gluon interactions can be resummed into gauge links as long as only one hadron is considered at a time. Gluon emissions from different participants could interfere

in complicated ways that can not be cast into a factorized version. The approach described above to determine the appropriate gauge link for a process works only when the transverse momentum of only one of the participants in the scattering process is relevant. For later chapters, when asymmetric collisions of a dilute probe with a dense nuclear target are considered, this approach remains valid.

Some approaches to include evolution in the x variable for these distributions have been made in a rather different framework. In the language of small-x physics, unintegrated gluon distributions were first considered as a way of describing heavy quark production processes [32]. There it was shown that in the two-gluon approximation it is possible to obtain factorized formulas using transverse momentum dependent distributions which satisfy the BFKL evolution equation. Even though this approach successfully resums multiple gluon emissions, it ignores non linear effects which play an important role in the dynamics in the small-x regime. How to include this effects is the main objective of the rest of this document.

As a final comment on TMD factorization, it is important to note that there are extra complications with establishing the validity of this formalism. Among them are the presence of soft factors and the rapidity divergences of the light-light gauge links. These issues will not be addressed here. The most up to date developments in this field can be found in [6].

Chapter 4

Small-x Physics

As the main framework of the material presented in this thesis, the subject of small-x physics deserves a chapter on its own. Here the main motivations for looking at this particular regime and what are the techniques that have been developed to understand its dynamics will be explained to some detail. Particular attention will be paid to results that will be central in the presentation of subsequent chapters but most of the details are left out and can be found in any of the many good reviews on the subject [33; 34; 35; 36; 37].

4.1 Why is small-x physics relevant?

The high energies reached at the current accelerator collider experiments have played a very important role in the development of new techniques to describe the dynamics of strong interactions. In particular, the description of the dynamics of partons with small Bjorken x has become increasingly important as this regime is now kinematically accessible and considerably affects particle production mechanisms in hadron collisions. The high energy limit of hadronic interactions was poorly understood from the usual perturbative QCD approach commonly used for processes with a large momentum transfer. The reason is that factorization breaking contributions become

more relevant as they can be enhanced by factors of the total energy without raising the momentum exchange of the partonic interaction.

These previous considerations lead one to think that perturbative methods are not suitable for the high energy limit of hadronic interactions and therefore there is little that can be done with standard methods. The solution to this predicament comes from the fact that parton densities grow at low values of x creating a high density system. Under these conditions parton distributions "saturate" generating a semi-hard scale characterizing the transition between the saturated and non-saturated regimes [38; 39]. The presence of this semi-hard scale justifies a weak coupling approach, but the large number of partons implies that multiple interactions are important and therefore care should be taken when using perturbative approaches. The resummation of contributions coming from either multiple emissions or multiple scatterings with a target becomes a central piece of the formalism and, as will be seen in subsequent sections, has many interesting consequences.

It was already mentioned in Section 2.4 that when small-x evolution is taken into account via the BFKL formalism multiple emissions are expected and the number of gluons grows exponentially as a function of rapidity. This result, as will be explained below in this chapter, raises very interesting issues that lead to think that further developments and non-linear dynamics are needed to get a full description of the small-x regime. Among those issues is the fact that, since rapidity scales as the logarithm of the center of mass energy of the collision process, the total cross section would grow as a power of energy, violating unitarity bounds [40]. Again, the resolution to this problem is provided by saturation, which predicts that when the density of color charges reaches a critical value recombination effects become important and unitarize the corresponding cross section.

All these high density effects play an important role in the description of the early stages of heavy ion collisions and therefore are crucial in an accurate description of the creation of the quark-gluon plasma observed at RHIC and LHC. A complete

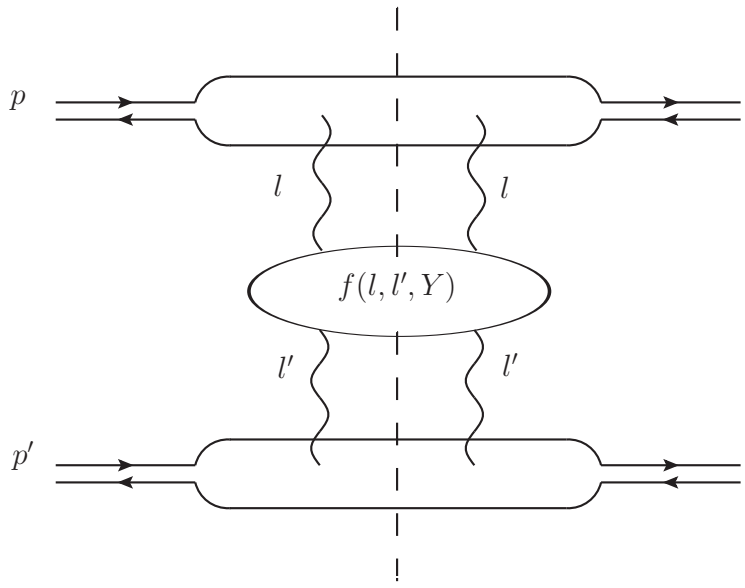

Figure 4.1: Scattering of two onia with evolution in the two gluon interaction.

understanding of the high density systems entering a heavy ion collision would allow one to separate hot matter effects from initial state effects and therefore allow for a better understanding of processes like deconfinement and thermalization.

4.2 BFKL

The formulation of the BFKL equation is considered as one of the most important steps in the development of small-x physics. Despite the possible problems it may have at very high energies, it remains a very good approximation with many phenomenological applications. This section is devoted to explaining its formulation, in momentum space as well as in transverse coordinate space, features of its solutions, and possible problems.

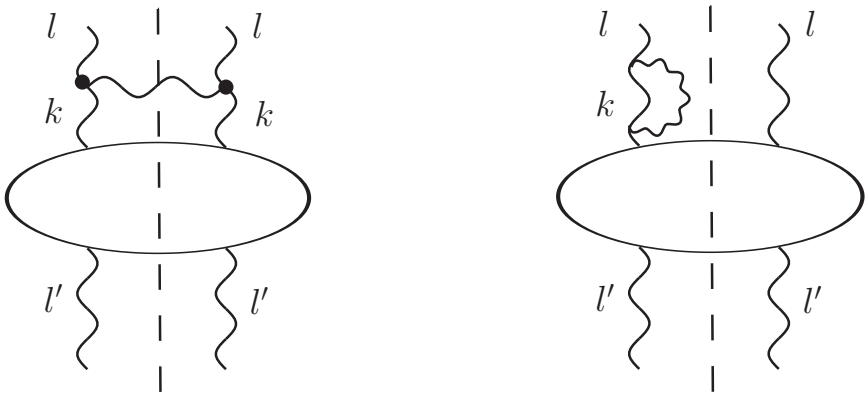

Figure 4.2: Left: real evolution correction. Right: example of a virtual evolution correction.

4.2.1 Formulation in momentum space

One of the original derivations of the BFKL equation [23] was performed in the framework of a collision of two onia (heavy bound quark-antiquark pairs). The ingredients to calculate the total cross section for such a process are the onia light-cone wave functions and the imaginary part of the forward onium-onium scattering amplitude. The momentum space version of this process is depicted in Figure 4.1 where $f(l, l', Y)$ is the forward amplitude in momentum space, l and l' transverse momenta, and Y is the rapidity variable which is proportional to the logarithm of the center of mass energy.

The evolution in rapidity is obtained by considering emission of (real and virtual) softer gluons. Examples of both kinds of contributions are shown in Figure 4.2 where the thick dots in the real contribution stand for the Lipatov vertex which sums all the possible ways to attach the emitted gluon [23; 22]. Putting the pieces together, the BFKL equation takes the form

$$\frac{\partial f(l, l', Y)}{\partial Y} = \frac{\alpha_S N_c}{\pi^2} \int \frac{d^2k}{(k-l)^2} \left[f(k, l', Y) - \frac{l^2 f(l, l', Y)}{k^2 + (k-l)^2} \right] . \tag{4.1}$$

The first term inside the square bracket correspond to the real contribution while the

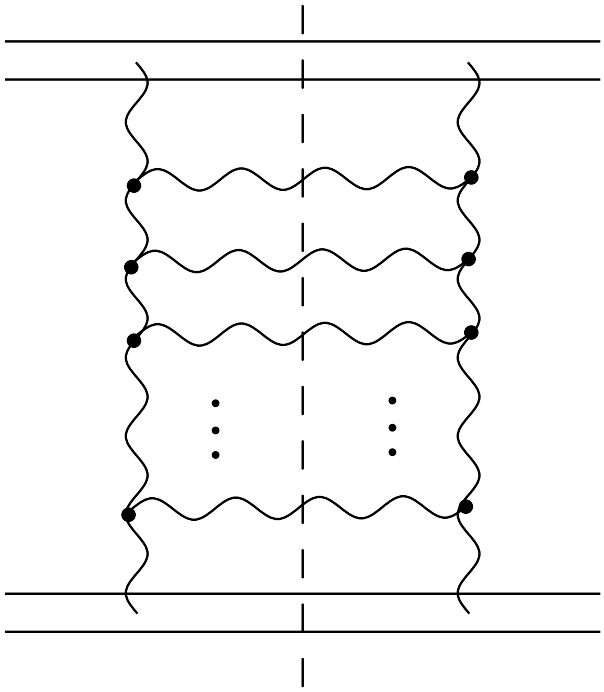

Figure 4.3: BFKL ladder after multiple iterations.

second term accounts for the virtual pieces.

Equation (4.1) above can be rewritten as an integral equation which could be solved by iteration. Under this approach, a term with a fixed number on gluon emission is represented by the ladder diagram of Figure 4.3 where again the thick vertices both sides of the cut represent the Lipatov vertex and the t-channel gluon lines should be interpret as Reggeized gluon propagators [23; 22].

4.2.2 Formulation in transverse coordinate space

The derivation of the BFKL equation in transverse coordinate space is easier to understand in terms of the dipole model introduced by Mueller [41], which is formulated in the large-N_c limit. Under this framework, emission of soft gluons is taken as part of the onia wave functions which are now dependent on the rapidity variable. In the large-N_c limit these emitted gluons are replaced by quark-antiquark pairs and

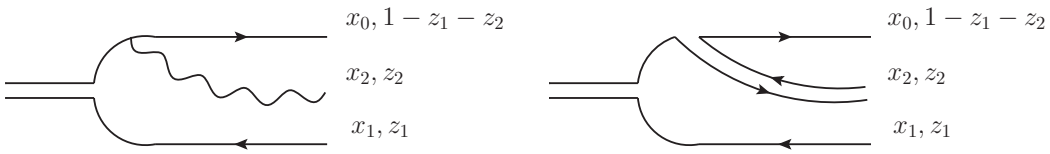

Figure 4.4: Dipole splitting in large N_c limit. Transverse coordinates and longitudinal momentum fractions are explicitly shown.

therefore each emission is considered as the original color dipole splitting into two new dipoles (see Figure 4.4).

This dipole splitting is easily calculated in light-cone perturbation theory [15]. Adding the contributions from emission from the quark and emission from the anti-quark, the amplitude for the splitting is

$$-\frac{igT^a}{\pi}\left(\frac{x_2-x_0}{(x_2-x_0)^2}-\frac{x_2-x_1}{(x_2-x_1)^2}\right)\cdot\epsilon^\lambda\ , \tag{4.2}$$

where T^a is the color matrix in the fundamental representation and ϵ^λ is the transverse part of the polarization vector of the emitted gluon. After squaring this amplitude, summing over the gluon polarization and color, and including the appropriate phase space factors, the probability for soft emission in transverse coordinate space representation is given by

$$dP=\frac{\alpha_s C_F}{\pi^2}\frac{(x_0-x_1)^2}{(x_0-x_2)^2(x_1-x_2)^2}\,d^2x_2\,dy_2\ , \tag{4.3}$$

with $dy_2 = dz_2/z_2$. The quantity shown in Equation (4.3) is also known as the dipole kernel and will appear every time that soft gluon emissions are considered from a color singlet configuration in a transverse coordinate representation.

Since the evolution is put in the wave function of the onia, the relevant quantity to study its evolution is the density of dipoles in the onium state. Defining $n(x_0 - x_1, x, Y)$ as the number density of dipoles of size x in an onium state of size $x_0 - x_1$

at rapidity Y, the corresponding evolution equation reads then

$$\frac{\partial}{\partial Y} n(x_0 - x_1, x, Y) = \frac{\alpha_S C_F}{\pi^2} \int d^2 x_2 \, \frac{(x_0 - x_1)^2}{(x_0 - x_2)^2 (x_1 - x_2)^2} \times \left[n(x_0 - x_2, x, Y) + n(x_2 - x_1, x, Y) - n(x_0 - x_1, x, Y) \right] . \tag{4.4}$$

The different pieces of this equation are easy to understand. Since the evolution is caused by soft gluon emission it is natural to include the dipole kernel of Eq. (4.3). The first two terms in the bracket correspond to the densities on the two new color dipoles while the last term is the virtual correction which accounts for the loss of the initial dipole after emission.

A few comments are necessary to explain the validity of the physical picture explained above. First, it is important to note that the leading logarithmic approximation plays a fundamental role. The fact that the longitudinal momentum of the emitted gluon is much softer than the original quark and antiquark is what allows to ignore recoil effects and keep the transverse coordinates of the original dipole unchanged. Second, even though the large-N_c limit is crucial to formulate the evolution equation only in terms of dipole densities, the result is exact within the leading logarithmic approximation, in other words, the finite N_c corrections are not enhanced by large logarithms.

Eq. (4.4) is known as the coordinate version of the BFKL equation. The connection with the momentum space version of BFKL is by no means straightforward mainly because the objects involved in the description are not the same. However, when observable quantities such as the total cross section for the scattering of two onia are considered both approaches yield the same results. Different methods to show the equivalence of the two approaches can be found in [42; 43]. For the purposes of this document, only the coordinate version will be considered since resummation of multiple scatterings, which were already mention to play an important role in the small-x regime, are much easier to deal with in coordinate representation.

Instead of the setup of two onia states scattering from each other, the situation that will be recurrent in subsequent sections is the scattering of a dipole in a nuclear target. The forward scattering amplitude of a dipole with a quark with transverse coordinate x_0, an antiquark with transverse coordinate x_1, evaluated at rapidity Y, $N(x_0, x_1, Y)$ can be obtained by convoluting the dipole density n with the amplitude of scattering of a dipole from a nucleon integrated over the nuclear length (in the leading twist case). The evolution of this dipole scattering amplitude is put all in the dipole wave function, and therefore the amplitude $N(x_0, x_1, Y)$ also satisfies the BFKL equation.

$$\frac{\partial}{\partial Y} N(x_0, x_1, Y) = \frac{\alpha_S C_F}{\pi^2} \int d^2x_2 \, \frac{(x_0 - x_1)^2}{(x_0 - x_2)^2 (x_1 - x_2)^2} \times \left[N(x_0, x_2, Y) + N(x_2, x_1, Y) - N(x_0, x_1, Y) \right] . \tag{4.5}$$

4.2.3 Solution of the BFKL equation

The subject of how to solve the BFKL equation in its different versions have been widely address in the literature [44; 23; 22; 42; 43]. Here, only the final results are presented in order to be able to observe characteristic features of the BFKL evolution.

The standard procedure to solve this equation is to take advantage of the scale invariance of the kernel to find its eigenfunctions and eigenvalues. In terms of these, the solution of Eq. (4.4) can be written explicitly as

$$n(x_0 - x_1, x, Y) = 2 \int_{-\infty}^{\infty} \frac{d\nu}{2\pi} \left(\frac{|x_0 - x_1|}{x} \right)^{1+2i\nu} e^{\frac{2\alpha_S N_c}{\pi} \chi(\nu) Y}, \tag{4.6}$$

where $\chi(\nu) = \psi(1) - \frac{1}{2}\psi(\frac{1}{2} + i\nu) - \frac{1}{2}\psi(\frac{1}{2} - i\nu)$ and $\psi(x) = \frac{d}{dx} \ln \Gamma(x)$. The integration above can be perform around the saddle point in $\nu = 0$ yielding the result

$$n(x_0 - x_1, x, Y) = \frac{|x_0 - x_1|}{2x} \frac{e^{(\alpha_P - 1)Y}}{\sqrt{\frac{7}{2} \alpha_S N_c \zeta(3) Y}} \exp \left[- \frac{\pi \ln^2 \left(\frac{|x_0 - x_1|}{x} \right)}{14 \alpha_S N_c \zeta(3) Y} \right] , \tag{4.7}$$

with $\alpha_P - 1 = \frac{4\alpha_S N_c}{\pi} \ln 2$.

The most important feature of this solution is the exponential growth with rapidity. When expressed in terms of the center of mass energy of a collision process it implies that total cross sections grow as $s^{\alpha_P - 1}$. This asymptotic behavior at large energies is characteristic of the hard Pomeron from Regge theory. The problem with this behavior is that it violates the Froissart bound [40] and therefore is inconsistent with the unitarity of the theory.

4.2.4 Unitarization: the Balitsky-Kovchegov equation

The main reason why BFKL stops being a good approximation at very high energies is that it does not account for the nonlinear effects which are a fundamental part of non-abelian theories. In the physical picture of multiple gluon emission or dipole splitting, the nonlinear effects take the form of gluon (or dipole) recombination. If soft gluon emission is enhanced by a large logarithm of the energy, then gluon recombination is enhanced by a factor of density, when the density becomes of the order of 1 over the coupling then recombination effects have to be resummed as well.

A first attempt to include this nonlinear effects in the BFKL formalism, without making fundamental changes to the framework, was first proposed independently by Balitsky [45; 46] and Kovchegov [47; 48]. Take as a starting point the coordinate space version of BFKL in terms of the dipole-nucleus scattering amplitude Eq. (4.5). There, the first two terms correspond to the real emission and each term accounts for the case where only one of the resulting dipoles interacts with the nucleus, while the last term corresponds to the virtual correction where the original dipole is the one interacting with the nucleus. The natural thing to do to account for nonlinear effects would be to include a term where both dipoles can interact with the nucleus. The

resulting equation would be

$$\frac{\partial}{\partial Y}N(x_0,x_1,Y) = \frac{\alpha_S C_F}{\pi^2}\int d^2x_2\,\frac{(x_0-x_1)^2}{(x_0-x_2)^2(x_1-x_2)^2}\,[N(x_0,x_2,Y) + N(x_2,x_1,Y) - N(x_0,x_1,Y) - N(x_0,x_2,Y)N(x_2,x_1,Y)]\ . \tag{4.8}$$

This equation is known as the Balitsky-Kovchegov (BK) equation. It can be derived by formal methods with the use of a mean field approximation that allows to separate the scatterings of the two dipoles in the nonlinear term.

Despite its apparent simplicity, the BK equation solves most of the troublesome issues present in the solutions of the BFKL equation. Several thorough studies, both analytical and numerical, of this equation have been performed [49; 50; 51; 52; 53; 54; 55; 56] since its original proposal and it has become one of the most commonly used tools for phenomenological studies of small-x phenomena.

The explanation above in terms of dipole-nucleus scattering does not refer explicitly to recombination of gluons or dipoles as was suggested in the beginning of this section as the source of nonlinear effects. To make explicit the relation with recombination it is necessary to consider the picture of BFKL in terms of density of dipoles instead an onium state, there the nonlinear term has the interpretation of the probability of creating a dipole of the original size provided there were two dipoles of the appropriate size inside the onium state. In terms of the ladder diagrams, as the one in Figure 4.3, the nonlinear term allows merging of ladders, which was not an option in the original form of BFKL.

The BK equation will appear again later when a complete analysis of nonlinear evolution is presented. The presentation of the features of solutions to the BK equations is postponed until then.

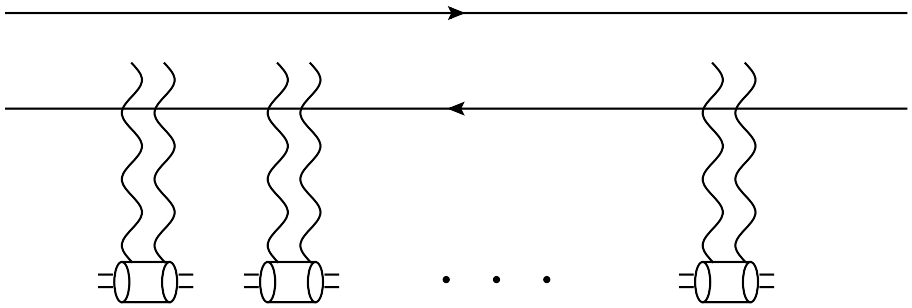

Figure 4.5: Multiple scattering of a dipole on independent nucleons via two-gluon exchange.

4.3 Saturation

At the end of the previous section it was noted that there is a close relation between the effects of gluon recombination and resummation of multiple scatterings. This will be a recurrent topic for the rest of this document as it is often useful to consider different physical pictures of the same processes which are related by a change of gauge or a change of reference frame. In the material presented so far, the phenomenon of saturation has been mentioned in the context of gluon recombination and advertised as the consequence of nonlinear effects when parton (gluon) densities become large enough. Here saturation will be presented as an inherent property of the resummation of multiple scattering even when small-x evolution is not taken into account.

The starting point for this analysis is the forward dipole-nucleus scattering amplitude mentioned in section 4.2.2. This amplitude is of uttermost importance when nuclear DIS is considered, as the process can be described as the convolution of the probability of the virtual photon splitting into a quark-antiquark pair with the respective dipole nucleus amplitude. Also, in the spirit of the large-N_c dipole model, processes involving gluons are often represented in terms of dipole splittings where the dipole-nucleus amplitude plays a central role in describing scattering processes.

In covariant gauge and assuming that nucleons inside the nucleus are dilutely

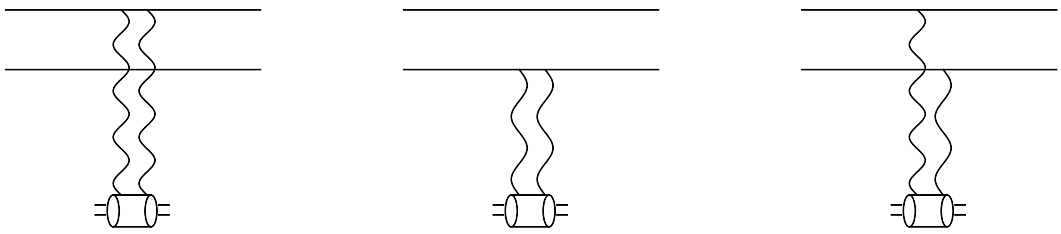

Figure 4.6: Three diagrams involved in dipole-nucleon scattering in the two-gluon approximation.

distributed, the multiple scattering of the dipole on the nucleus can be seen as a succession of dipole-nucleon independent interactions (see Fig. 4.5). Being the amplitude in question a forward amplitude, it is necessary to consider singlet interactions with each nucleon such that it remains color neutral. To lowest order, this condition translates in the dipole-nucleon interaction being mediated by two-gluon exchanges. In the case of a large nucleus, the two-gluon approximation is justified by considering the multiple scattering series as an expansion in the parameter $\alpha_S^2 A^{1/3}$ which can be of order one for a sufficiently large nucleus. The fact that this two-gluon interactions are indeed ordered as Fig. **??** suggests and there are no contributions where gluons from different nucleons cross is not a trivial matter. To show that that is indeed the case, it is necessary to make use of the fact that this setup assumes eikonal scattering due to the very high energy of the probe. Details of the calculation showing that diagrams which are not ordered can be safely neglected can be found in Ref. [57] and will not be presented here.

The dipole-nucleon interaction has to include the three diagrams of Fig. 4.6 which are conveniently grouped this way in order to cancel the infrared divergence of the single diagrams. The resulting dipole-nucleon cross section is shown [57; 58] to be proportional to the gluon distribution of the nucleon, which to a lowest order approximation is independent of x.

$$\frac{\sigma^{q\bar{q}N}}{2} = \frac{\alpha_S \pi^2}{2N_c} x_\perp^2 x G_N(x, 1/x_\perp^2), \tag{4.9}$$

where the gluon distribution is taken as [58]

$$xG_N(x,Q^2) = \frac{\alpha_S C_F}{\pi} \ln \frac{Q^2}{\Lambda^2}. \tag{4.10}$$

Given the ordering mentioned above, it is easy to see that multiple independent interactions exponentiate for the calculation of the S-matrix. The probability for one scattering is obtained after multiplying the cross section above with ρ the density of nucleons in the nucleus and the longitudinal distance seen by the probe at an impact parameter b given by the nuclear profile function $T(b)$. The corresponding result for the S matrix as a function of the dipole separation and the impact parameter is

$$\begin{aligned} S(x_\perp, b) &= e^{-\frac{\rho T(b)\sigma^{q\bar{q}N}}{2}} \\ &= \exp\left\{-\frac{\pi\alpha_S^2 C_F \rho T(b)}{N_c} x_\perp^2 \ln(1/x_\perp\Lambda)\right\}, \end{aligned} \tag{4.11}$$

or, in terms of the scattering amplitude $N(x_\perp, b)$, we get the Glauber-type formula [58; 59]

$$N(x_\perp, b) = 1 - \exp\left\{-\frac{\pi\alpha_S^2 C_F \rho T(b)}{N_c} x_\perp^2 \ln(1/x_\perp\Lambda)\right\}. \tag{4.12}$$

The quark saturation scale $\bar{Q}_s$ is defined such that the transition from the linear regime where N is small and grows as $x_\perp^2$ to the saturated regime where $N \sim 1$ occurs at $x_\perp \sim 1/\bar{Q}_s$. Sometimes it is convenient to define the quark saturation scale without the logarithmic dependence $\bar{Q}_{s0}$ in which case the dipole amplitude can be written in the convenient compact form

$$N(x_\perp) = 1 - e^{-\frac{\bar{Q}_{s0}^2}{4} x_\perp^2 \ln(1/x_\perp\Lambda)}. \tag{4.13}$$

4.4 Color Glass Condensate

The quasi-classical approach described in the previous section has the advantage of having a direct physical picture where it is easy to guess which diagrams contribute and have to be included in the resummation. In order to include small-x evolution in this approach it is necessary to consider gluon emissions in the projectile dipole

and then consider the separate interactions with the nucleus of the resulting partonic system. Several high-energy processes have been studied under this setup with very interesting results. This procedure has the limitation that it somehow obscures the inner dynamics of the partons in the nucleus by putting all the evolution in the incoming probe and does not allow for a clear picture for the effects of high parton densities.

To make manifest the partonic structure of the nucleus and relate saturation phenomena to this particular dynamics, it is necessary to change reference frames and use light-cone gauge. The multiple scattering picture of the previous section is set in a reference frame where the nucleus is at rest and the energy dependence is all carried by the incoming probe. For that setup, the choice of a covariant gauge is convenient as it allows for the mentioned ordering of the two-gluon interactions. If instead, the infinite momentum frame of the nucleus and light-cone gauge are used, the partonic picture of the nucleus becomes manifest and the energy dependence is all put in the partonic distributions of the nucleus.

This is the starting point for the effective theory which is currently the most accepted approach to describe small-x degrees of freedom, the Color Glass Condensate (CGC) [60; 61; 62; 63; 64; 65; 66; 67; 68; 69; 70]. Several review papers have been written with detailed explanations of the formalism [33; 34; 35; 36; 37]. This chapter is intended to highlight the aspects of the theory that will be central for the presentation of the results of chapters 7 and 8 where this formalism plays a crucial role.

Since at small-x the gluon distributions are much bigger than the quark distributions, the emphasis of CGC is in the dynamics of the gluonic degrees of freedom. The foundations of the theory lay in the following observation: for a fast moving nucleus, partons with large fractions of the total momentum can be seen as static and therefore treated as sources for the dynamics of the gluons at smaller momentum fractions which, thanks to the large occupation numbers, can be treated semi-classically [60; 61]. Treating the gluonic degrees of freedom classically means solving the classi-

cal Yang-Mills equations of motion with an external source (determined by the fast moving partons),

$$(D_\nu F^{\mu\nu})_a(x) = J^\mu_a(x). \tag{4.14}$$

This can not be done perturbatively, since the gauge field is assumed to be large due to the large number of gluons, and an exact solution is therefore needed.

4.4.1 Classical gluon field

Anticipating the kinematical setup that will be used in subsequent chapters, the presentation here does not follow the usual approach with a fast moving nucleus in the light-cone plus direction as it is usually done. Instead, the nucleus is assumed to be moving in the negative z direction which correspond to motion along the light-cone minus direction. The large component of the nucleus momentum is therefore P^-. The light-cone gauge in which the partonic picture is manifest is therefore the $A^- = 0$ gauge. The general derivation is the same as in [33; 34] interchanging the plus and minus components.

Since the nucleus is moving in the minus direction, the source current is taken to have only a minus component

$$J^\mu_a(x) = \delta^{\mu-}\rho_a(x^+, x_\perp), \tag{4.15}$$

with ρ_a the source color charge density, which is independent of x^- due to current conservation.

Finding a solution in the desired gauge is not straightforward. On the other hand, things are simpler in covariant gauge where a simple solution is available for the current given above. It is easy to check that

$$\tilde{A}^\mu_a(x) = \delta^{\mu-}\alpha_a(x^+, x_\perp), \quad \text{with} \quad -\nabla^2_\perp \alpha_a(\vec{x}) = \rho_a(\vec{x}), \tag{4.16}$$

is a solution of the Yang-Mills equations. Even though this solution is not in a gauge that allows for a direct partonic interpretation, it is very useful for many

computations and will reappear later when scattering processes with a high-energy probe are considered. This solution can be transformed to the desired light-cone gauge of the nucleus by a simple transformation. The resulting field is

$$A_a^+(x) = A_a^-(x) = 0 \qquad A_a^i(x) = \frac{i}{g}\left[\partial_i U(x^+, x_\perp)\right] U^\dagger(x^+, x_\perp), \tag{4.17}$$

with U an element of the gauge group determined by the gauge condition $A^- = 0$,

$$U(x^+, x_\perp) = \mathcal{P}\exp\left\{ig\int_{x+}^{\infty} dz^+\ \alpha_a(z^+, x_\perp)\right\}. \tag{4.18}$$

The limits on the integral over z^+ are conveniently chosen such that the field vanishes at infinity. This path ordered Wilson line in the fundamental representation will appear again several times in different contexts, here it is a gauge transformation but later it will be used to describe multiple interactions on a fast moving quark.

From (4.17) it is straightforward to calculate the gauge strength tensor, which only nontrivial components are

$$F_a^{-i}(x^+, x_\perp) = -U(x^+, x_\perp)\ \partial_i\alpha_a(x^+, x_\perp)\ U^\dagger(x^+, x_\perp) = -\tilde{U}_{ab}^\dagger(x^+, x_\perp)\ \partial_i\alpha_b(x^+, x_\perp) \tag{4.19}$$

where $\tilde{U}_{ab}$ is the Wilson line in the adjoint representation. This calculation of the fields will be used in the next chapter to calculate explicitly the density of gluons.

From the derivation above it is clear that the fields associated with the small-x degrees of freedom are completely determined by the fast moving sources described by the density ρ_a. In order to calculate observables from this theory a weighted average has to be taken over the possible values of the color charge densities. This average is performed via a functional integration with a properly normalized weight function which is in principle not known (more details in the next subsection). The physics that determines the specific form of this weight function is non perturbative but, as will be seen later, its evolution with rapidity can be calculated by perturbative methods.

4.4.2 Functional formulation

Once established how to compute the gauge field from the source color charge density all that is left to determine physical observables is a way to describe appropriately the color charge source and account for possible fluctuations. It was already mentioned that the approach to follow is to take a functional average over all possible source configurations with a properly normalized weight function. More explicitly, for an operator $\mathcal{O}(A)$ which is a function of the gauge field, its average over the color sources is written as

$$\langle \mathcal{O} \rangle_Y = \int \mathcal{D}\rho \, W_Y[\rho] \mathcal{O}[\rho] \, , \tag{4.20}$$

where $\mathcal{O}$ is a function of the source color charge density through the construction of the previous subsection. The subindex Y in the average and in the weight function is there to emphasize that, in this framework, the rapidity evolution is all put in the nucleus and therefore the weight function is rapidity dependent.

The interpretation given to this rapidity dependence in terms of the physical picture in which the small-x degrees of freedom behave classically with the large-x components serving as color sources is the following: the rapidity variable is related to the lowest longitudinal momentum fraction x_A probed in a given scattering via $Y = \ln(1/x_A)$, this lowest longitudinal momentum fraction determines the separation between what is considered large and small x and therefore determines what should be included as part of the color sources. If this separation of sources and dynamical fields is not taken at the appropriate value, quantum fluctuations are enhanced by large logarithms and therefore the quasi-classical approximation is no longer justified.

4.4.3 Eikonal scattering in terms of Wilson lines

In order to be able to compare with previous approaches, the CGC formalism has to provide a way of calculating amplitude for multiple scatterings of partons in a nucleus. In the spirit of the previous subsections, the way to proceed is to express

the scattering S-matrix in terms of the gauge field of the nucleus and then perform the CGC average over field configurations.

Given that the central focus of this discussion is on high energy probes, it is common to use the eikonal approximation where the transverse coordinates remain frozen during the scattering. This approximation leads to great simplifications and is the main reason why the multiple scattering analysis is often performed in transverse coordinate space instead of momentum space.

Consider a quark undergoing multiple scatterings with some static scattering centers as depicted in Fig. **??**. Each gluon insertion accounts for a factor of the form $\bar{u}(p')igA_a^\mu(x)T^a\gamma_\mu u(p)$. Considering that the fast moving quark is a right mover and therefore p^+ is much larger than all the other momentum components, it is easy to see that in the eikonal approximation only the A^- component of the field will contribute to the scattering. In the eikonal approximation the transverse coordinates are the same for all the scattering centers, but the longitudinal coordinate should be integrated over. The ordering of the scattering centers implies that the series organized in terms of the number of scatterings can be resummed into a path ordered exponential of the form [71]

$$U(x_\perp) = \mathcal{P}\exp\left\{ig\int dx^+\ A_a^-(x^+, x_\perp)T^a\right\}. \tag{4.21}$$

The integration limits in the x^+ integration can be safely taken to $\pm\infty$ as long as it is understood that the gauge field goes to zero rapidly outside of the nucleus (which is true in a covariant gauge).

The explanation above is intended more as an illustration than a derivation and therefore some important aspects were omitted. A few words of caution should be mentioned for completeness sake. First, the argument is valid in a covariant gauge where it is possible to pick up the leading contribution from the eikonal vertex, the same can not be said of the light-cone gauge of the target where the minus component of the field is set to zero. Second, the x^- dependence was completely ignored in the argument which is a valid approximation as long as the coherence time of the probe

is much longer than the length of the target. This approximation has as a direct consequence that the momentum transfer induced by the scattering is only transverse and the longitudinal component of the quark momentum is conserved.

If instead of a quark the incoming particle is an antiquark, the result would be the complex conjugate of the same Wilson line in (4.21). It can also be shown that the same argument applies when the incoming particle is a gluon instead of a quark with the only difference that the color matrices are now in the adjoint representation leading to an adjoint representation Wilson line [71].

This formalism allows one to calculate the dipole-nucleus amplitude of section 4.3. The scattering of the quark gives a Wilson line in the fundamental representation while the scattering of the antiquark gives a conjugate Wilson line (ordered in the inverse direction). The singlet part of the pair dominates, so it is common to write the scattering matrix for the dipole-nucleus scattering as

$$S(x_0, x_1) = \frac{1}{N_c}\langle \mathrm{Tr} U(x_0) U^\dagger(x_1)\rangle. \tag{4.22}$$

In the following subsection an example of how to calculate this amplitude with a particular model for the weight function will be explicitly shown.

4.4.4 Recovering the two-gluon approximation

For practical purposes, knowing how to calculate correlators for an arbitrary number of sources is equivalent to knowing the explicit form of the weight function. From these correlators it is possible to derive expressions for the corresponding same light-cone time correlators of an arbitrary number of gauge fields, which is all that is needed to compute averages of operators which are smooth functions of the gauge field.

The simplest non trivial choice for the correlators is such that two-point correlations are local and any higher point connected correlator is exactly zero. The locality of the two-point correlator implies

$$\langle \rho_a(x^+, x_\perp)\rho_b(y^+, y_\perp)\rangle = \delta_{ab}\delta(x^+ - y^+)\delta^{(2)}(x_\perp - y_\perp)\mu^2(x^+)\ , \tag{4.23}$$

where the function μ^2 characterizes the color charge density and is assumed independent of the transverse coordinates for simplicity.

The choice for local correlators in the longitudinal direction can be justified on the basis of assuming that color charges corresponding to different nucleons are not correlated. Strictly speaking this does not imply a delta function in the longitudinal direction, moreover, in order to avoid troublesome singularities it is necessary to consider the longitudinal structure of this correlators over some small region for some particular calculations. For the level of detail required in the following calculations the delta function approximation works fine.

The structure described above, where the only non trivial correlators are given by Eq. (4.23) can be easily reproduced with a Gaussian weight function of the form

$$W[\rho] = \exp\left\{ -\int d^2x\, d^2y\, dz^+ \frac{\rho_a(z^+, x_\perp)\rho_a(z^+, y_\perp)}{2\mu^2(z^+)} \right\}. \tag{4.24}$$

This particular choice of weight function is commonly known as the McLerran-Venugopalan model [60; 61] and is often used as an initial condition for the rapidity evolution.

Note that in the definition of the correlators, as well as the weight function above, the rapidity dependence has been omitted. The reason for this omission is that this particular structure is not respected by the evolution, the Gaussian weight develops other components and new non trivial correlators appear. As a phenomenological tool, one can allow for rapidity dependence within the Gaussian approach by making the function μ^2 rapidity dependent with its evolution dictated by the evolution equation of the two-point correlation (which will be shown to be equivalent to the BK equation in the large-N_c limit). Recent analytical studies have shown that this approach misses contributions to the evolution of the operators which are not N_c suppressed [72]. In order to quantify how good is this Gaussian approximation further numerical studies are needed and are currently under way.

As it is suggested in the title of this subsection, this model reproduces the results obtained by considering multiple scatterings in the two-gluon approximation

as explained in section 4.3. To see this consider the dipole-nucleus S-matrix of Eq. (4.22). The way to proceed to evaluate this correlator is to expand the Wilson lines and evaluate the correlators of multiple fields via Wick's theorem. In order to follow this procedure it is important to consider the two-point correlator in terms of the gauge field instead of the color charge density. Taking into account that the field that appears in the exponent of the Wilson lines is given in covariant gauge as defined in (4.16), the correlator of two such fields is given by

$$g_S^2\langle A_c^-(x^+,x_\perp)A_d^-(y^+,y_\perp)\rangle = \delta_{cd}\delta(x^+-y^+)\mu^2(x^+)L_{xy}, \tag{4.25}$$

with L given in terms of the two-dimensional massless propagator G_0,

$$L_{xy} = g_S^4\int d^2z\; G_0(x_\perp - z_\perp)G_0(y_\perp - z_\perp), \qquad G_0(x_\perp) = \int \frac{d^2k}{(2\pi)^2}\frac{e^{ik\cdot x_\perp}}{k^2}. \tag{4.26}$$

There are two different kinds of pairings of the field that should be considered. First, consider correlators between two fields from the same Wilson line. One of such correlators at a transverse coordinate $x_\perp$ gives a contribution of $-C_F\mu^2 L_{xx}/2$ where $\mu^2 = \int dz^+\;\mu^2(z^+)$. It has a color singlet structure and therefore can be factored out of the calculation of any specific term in the expansion. When multiple occurrences of this kind of correlator are considered, it is easy to notice that the path-ordering of the Wilson line together with the locality in the longitudinal coordinate of the correlators imply that these contributions exponentiate.

Now consider correlators between fields from different Wilson lines. Again the path-ordering of the Wilson line together with the longitudinal locality of the correlators allow to simplify greatly the calculation since they imply that each of these correlators are in a color singlet structure each contributing a factor of $C_F\mu^2 L_{xy}$. These contributions also exponentiate nicely giving the following result for the S-matrix,

$$S(x_\perp,y_\perp) = e^{-\frac{C_F}{2}\Gamma(x_\perp - y_\perp)}, \tag{4.27}$$

where $\Gamma(x_\perp - y_\perp) = \mu^2(L_{xx} + L_{yy} - 2L_{xy})$. This result is already reminiscent of Eq. (4.11). To notice that indeed the result is the same, the function Γ has to be

evaluated. This can be done with the help of (4.26) where a cut-off scale is necessary to regulate the transverse two-dimensional propagator, the result agrees completely with (4.11) (see details of this derivation in [73]).

4.4.5 Quantum evolution

In this framework, the inclusion of quantum evolution is done through the dependence on rapidity of the weight function used in the functional definition of the effective theory. Since the theory is based in the assumption that the gauge field can be treated classically by solving the classical Yang-Mills equations of motion, the effect of quantum fluctuations is accounted for by renormalizing the source term whenever the quantum corrections become important. These quantum fluctuations take the form of gluon emissions form the original sources, creating new color charges that affect the dynamics of the gauge fields at the relevant scale.

Seen this way, it seems that this new procedure is analogous to BFKL evolution where multiple soft emissions were already taken into account, the difference lays in the fact that in these formalism the nonlinear effects are included in a natural way by just including a few more diagrams for the evolution of the weight function. These new diagrams account for the nonlinearities arising from the gauge field being a nonlinear function of the sources and from the propagation of the newly radiated gluon in the background field, therefore allowing gluon recombination and merging of BFKL ladders.

A one loop calculation is enough to include the leading logarithmic effects and the high density effects. The details of the calculation are quite technical and will be skipped in this presentation. The resulting evolution equation takes the form of a renormalization group equation for the weight function $W_Y[\rho]$ and it is usually referred in the literature as the Jalilian-Marian–Iancu–McLerran–Weigert–Leonidov–Kovner (JIMWLK) equation. It can be written in the following compact form [68;

70],

$$\frac{\partial W_Y[\rho]}{\partial Y} = \frac{1}{2}\int d^2x_\perp d^2y_\perp \, \frac{\delta}{\delta\rho_a(x_\perp)}\xi_{ab}(x_\perp, y_\perp)[\rho]\frac{\delta}{\delta\rho_b(y_\perp)}W_Y[\rho], \tag{4.28}$$

where ξ is related to the charge-charge correlator induced by including in the source term the fluctuations at a rapidity Y. The explicit form of ξ is not very illuminating and not particularly useful for specific calculations. Therefore, it is common to express Eq. (4.28) in terms of the covariant field α of Eq. (4.16) where the kernel takes a simpler form in terms of Wilson lines,

$$\frac{\partial W_Y[\alpha]}{\partial Y} = \frac{1}{2}\int d^2x_\perp d^2y_\perp \, \frac{\delta}{\delta\alpha_a(x_\perp)}\eta_{ab}(x_\perp, y_\perp)[\alpha]\frac{\delta}{\delta\alpha_b(y_\perp)}W_Y[\alpha], \tag{4.29}$$

with

$$\eta_{ab}(x_\perp, y_\perp) = \frac{1}{\pi}\int \frac{d^2z_\perp}{(2\pi)^2}\,\frac{(x_\perp - z_\perp)\cdot(y_\perp - z_\perp)}{(x_\perp - z_\perp)^2(y_\perp - z_\perp)^2} \times \left[1 + \tilde{U}^\dagger(x_\perp)\tilde{U}(y_\perp) - \tilde{U}^\dagger(x_\perp)\tilde{U}(z_\perp) - \tilde{U}^\dagger(z_\perp)\tilde{U}(y_\perp)\right]_{ab}, \tag{4.30}$$

where the $\tilde{U}$'s are Wilson lines in the adjoint representation.

The equation above, in its different versions, contains all the information needed to compute the small-x evolution of any observable of the effective theory. In order to make useful predictions, it is necessary to derive specific evolution equation for the observables of interest. It is easy to see from Eq. (4.29) that such evolution equation takes the form

$$\frac{\partial\langle\mathcal{O}\rangle_Y}{\partial Y} = \frac{1}{2}\int d^2x_\perp d^2y_\perp \, \left\langle \frac{\delta}{\delta\alpha_a(x_\perp)}\eta_{ab}(x_\perp, y_\perp)[\alpha]\frac{\delta}{\delta\alpha_b(y_\perp)}\mathcal{O}[\alpha]\right\rangle_Y. \tag{4.31}$$

In particular, it can be applied to the trace of two Wilson lines to reproduce the BK equation of section 4.2.4. For this case, it has been proven that the JIMWLK equation reduces to [70]

$$\frac{\partial}{\partial Y}\left\langle \mathrm{Tr}\left[U(x_\perp)U^\dagger(y_\perp)\right]\right\rangle_Y = -\frac{\alpha_S N_c}{2\pi^2}\int d^2z_\perp \, \frac{(x_\perp - y_\perp)^2}{(x_\perp - z_\perp)^2(y_\perp - z_\perp)^2} \times \left\{\left\langle \mathrm{Tr}\left[U(x_\perp)U^\dagger(y_\perp)\right]\right\rangle_Y - \frac{1}{N_c}\left\langle \mathrm{Tr}\left[U(x_\perp)U^\dagger(z_\perp)\right]\mathrm{Tr}\left[U(z_\perp)U^\dagger(y_\perp)\right]\right\rangle_Y\right\}. \tag{4.32}$$

This equation has the problem that it is not a closed equation but rather the first step of an infinity hierarchy of equations, each one relating the evolution of a correlator to a correlator with more Wilson lines. The pioneering works of Balitsky and Kovchegov assumed a mean field approximation in a large nucleus in the large-N_c limit to be able to separate the correlator appearing in the second term. Under those conditions, and using the notation of Eq. (4.22), Eq. (4.32) takes the form

$$\frac{\partial}{\partial Y} S(x_\perp, y_\perp)_Y = -\frac{\alpha_S N_c}{2\pi^2} \int d^2 z_\perp \, \frac{(x_\perp - y_\perp)^2}{(x_\perp - z_\perp)^2 (y_\perp - z_\perp)^2} \times \left[S(x_\perp, y_\perp)_Y - S(x_\perp, z_\perp)_Y S(z_\perp, y_\perp)_Y \right], \tag{4.33}$$

which clearly agrees with Eq. (4.8) in the large-N_c limit.

Chapter 5

Basic Gluon Distributions at Small-x

After the necessary tools have been introduced in previous chapters, it is time to start addressing the main issue of this thesis: gluon distributions at small-x. So far, it has only been stated that the small-x regime is dominated by gluons since soft emission is enhanced by large logarithms and that, at some point, that growth has to slow down via saturation mechanisms in order to satisfy unitarity constraints. This chapter is intended to shed some light on how these previous observations can be quantified and how more insight can be obtained from the small-x dynamics described in chapter 4.

From all the integrated parton distributions used in perturbative QCD via collinear factorization, the gluon distribution is the least constrained by current data, specially at low-x. This is mostly due to the fact that gluons only interact via strong interactions and therefore leptonic probes can only give indirect measurements via scaling violations, which are know to be small due to the fact that the dependence on the transverse momentum scale is only logarithmic. The fact that the situation is worse at low-x is also largely due to the small-x region being only available at very high energies, where the applicability of collinear factorization is somewhat restricted because of the large effect of multiple interactions with the absence of a single large

momentum transfer.

As will be explained in the next section, it becomes natural to consider unintegrated gluon distributions in the small-x regime. Because of this, the rest of the chapter is devoted to introduce such transverse momentum dependent distributions and relate them to the formalism of chapter 3. In particular two different definitions of unintegrated gluon distributions will be considered, the Weizsäcker-Williams distribution and the Fourier transform of the dipole scattering amplitude. The initial motivation to consider these two particular cases will be explained at length in the following sections and the reason why it is sufficient to consider only these two distributions will be addressed in chapter 7.

5.1 Integrated vs unintegrated

It is very important for the development of the rest of the chapter, as well as subsequent chapters, to review the ideas behind the choice of unintegrated distributions over integrated distributions in an attempt to describe gluon dynamics at small-x. This section is therefore intended to summarize those ideas that have been presented in previous chapters leading to that conclusion. Among them are: increasing contributions from soft processes not accounted for in collinear factorization, multiple scattering becoming important as gluon densities grow, and the dynamic generation of a semi-hard intrinsic transverse momentum scale which requires transverse momentum of partons to be taken into account.

It is important to note that the effects mentioned above are not independent. In fact they are all intimately related and, in some cases, can be easily related to one another by a change of reference frame. This was already observed in chapter 4 where it was seen that nonlinear effects can manifest in the form of gluon recombinations or in the form of coherent multiple scatterings.

The high energy limit of strong interactions has been know to be problematic

from a factorization point of view for a long time. Before the development of modern techniques associated with the description of the small-x degrees of freedom, very high energy (diffractive) scattering had been studied through Regge theory to some extent, but it was thought that a perturbative treatment of that regime was out of the question. Nevertheless, the development of BFKL helped to clarify the situation since it showed that the power-like behavior of total cross sections for some of the processes could be explained by resummation of soft emissions. In that sense, it is natural to relate this phenomenon to the presence of high densities of partons, and in particular gluons. From that point of view, the breakdown of factorization is due to the presence of many partons from which the probe can scatter, increasing the probability of multiple scatterings without a single large momentum transfer of the order of the center of mass energy. In other words, coherence effects become increasingly important to the point that the incoherent picture in which factorization is based on loses its validity.

The picture of collinear factorization is not completely lost at very high energies and usually it is still considered as a consistency check for the appropriate kinematical limits. When considering the transverse momentum distribution of a produced particle, it is important that when this transverse momentum is taken very large (of the same order of the center of mass energy) the collinearly factorized expressions are recovered. What is being emphasized in the description above is that processes where that factorized description runs into trouble are now dominant and therefore it is needed to consider alternative approaches.

All the previous considerations already suggest that TMD factorization can have better luck than collinear factorization in an attempt to describe processes at small-x. The momentum picture of BFKL is clearly expressed in terms of gluons in the target having a definite transverse momentum. Also, the multiple scattering picture was shown to be directly related with saturation where the boundary between different regimes is given by a transverse momentum scale. Moreover, the gauge link structure

which seemed so fundamental in the definitions of the TMD distributions has the same form of the Wilson lines encountered in the description of multiple scatterings in the eikonal approximation, suggesting that what was seen as the resummation of collinear gluons in a particular approach can be cast into the multiple scattering picture at high densities proper of the small-x regime.

5.2 Weizsäcker-Williams distribution

The first unintegrated gluon distribution to be introduced here is the one known in the literature [74] as the Weizsäcker-Williams distribution. The name comes from the fact that it can be calculated from a correlator of two non-Abelian Weizsäcker-Williams fields of the hadron (nucleus) in the quasi-classical case. Its definition is motivated by an attempt to propose an unintegrated distribution that actually counts explicitly the number of gluons in a given momentum state in some physical gauge.

An important comment should be made here regarding gauge invariance of the quantities of interest. As was already mentioned in chapter 3, gauge invariance is a desirable property for any distribution intended to be used in the calculation of a physical observable. Nevertheless, the partonic picture of a physical state is gauge dependent and the occupation number of gluonic states changes when a gauge transformation is performed. What it is being attempted by the definition of the Weizsäcker-Williams distribution is to find a distribution which is gauge invariant but allows for a partonic interpretation only when a convenient gauge is chosen. In other words, results from calculations and the actual value of the distribution does not change when the gauge is changed, but that value is taken literally as the number of gluons in a specific state only for a particular gauge choice.

It has already been argued several times in previous chapters that one of the advantages of light-cone gauge is that it allows for a straightforward representation of hadronic states in terms of a partonic basis. Because of this property, it is natural to

chose the light-cone gauge as the particular gauge in which the Weizsäcker-Williams distribution can be interpreted as the number density of gluons.

In chapter 3 it was already seen that a definition of a transverse momentum dependent distribution attempting to count explicitly the number of gluon runs into problems regarding gauge invariance. The way to solve this issue was to introduce gauge links connecting the two point where the bilocal product of field operators was evaluated. In order to recover the partonic picture it is necessary that the gauge link cancel out in the particular gauge chosen for this interpretation. In the light-cone gauge this is achieved by choosing the gauge link path along the light-cone, therefore giving a trivial contribution due to the gauge fixing condition. In order to ensure gauge invariance, the gauge link must also have a transverse part which is taken at infinity in the longitudinal direction where the field can also be taken to be zero by means of additional gauge freedom.

The gauge link structure described above has been addressed in the literature before [25; 75] in different contexts. In particular, the corresponding definition of the WW gluon distribution function takes the form

$$xG^{(1)}(x,k_\perp) = \int \frac{d\xi^- d^2\xi_\perp}{(2\pi)^3 P^+} e^{ixP^+\xi^- - ik_\perp\cdot\xi_\perp} \langle P|F^{+i}(\xi^-,\xi_\perp)\mathcal{L}_\xi^\dagger \mathcal{L}_0 F^{+i}(0)|P\rangle \ , \tag{5.1}$$

where $F^{\mu\nu}$ is the gauge field strength tensor and

$$\mathcal{L}_\xi^\dagger = \mathcal{P}\exp\left\{-ig\int_{\xi^-}^{\infty} d\zeta^- A^+(\zeta,\xi_\perp)\right\}\mathcal{P}\exp\left\{-ig\int_{\xi_\perp}^{\infty} d\zeta_\perp\cdot A_\perp(\zeta^-=\infty,\zeta_\perp)\right\} \tag{5.2}$$

is the gauge link in the adjoint representation. In the above definition, we assume that the hadron is moving along the $+\hat{z}$ direction. This gluon distribution can also be defined in the fundamental representation [28],

$$xG^{(1)}(x,k_\perp) = 2\int \frac{d\xi^- d\xi_\perp}{(2\pi)^3 P^+} e^{ixP^+\xi^- - ik_\perp\cdot\xi_\perp} \langle P|\mathrm{Tr}\left[F^{+i}(\xi^-,\xi_\perp)\mathcal{U}^{[+]\dagger}F^{+i}(0)\mathcal{U}^{[+]}\right]|P\rangle \ , \tag{5.3}$$

where the gauge link $\mathcal{U}^{[+]}$ was defined in Eq. (3.6).

In Eqs. (5.1) and (5.3) it is evident that by choosing the light-cone gauge with certain boundary condition for the gauge potential ($A_\perp(\zeta^- = \infty) = 0$ for the specific case above), the gauge link contribution can be dropped leading to the standard number density interpretation.

The definitions above are written in terms of the language introduced in chapter 3 for the formal definition of the TMD distributions where the expectation value of the relevant operators is computed with a hadronic state with a relativistic normalization. When this distribution is considered in the small-x regime using the CGC framework of chapter 4 this expectation value should be substituted by the averaging over field configurations introduced in section 4.4, taking into account the proper normalization factors.

The computation of the distribution in the CGC framework would need an explicit form of the nuclear weight function. The standard method to do this is to perform the calculation using the McLerran-Venugopalan model and then consider quantum evolution via JIMWLK. The first part of this program is a known result [61], while the second has not been thoroughly studied and only preliminary results are available and will be presented in chapter 8. Here the MV model evaluation is reviewed.

When the gauge link contribution is dropped, the relevant correlator to calculate involves only two gauge strength tensors evaluated a two different points. Switching to the setup from section 4.4.1, where the nucleus is a left mover, the correlator takes the form $\langle F_a^{-i}(x^+, x_\perp) F_a^{-i}(y^+, y_\perp)\rangle$ with the gauge strength tensor given by Eq. (4.19). In the spirit of the MV procedure to evaluate correlators outlined in section 4.4.4, it is necessary to consider all possible pairings of fields (the covariant field α_a in this case). It is easy to see that the path-ordering of the Wilson lines in Eq. (4.19), rotational invariance and the locality in the longitudinal coordinate of the two-point

correlators imply that the correlator above can be written as

$$\begin{aligned}\langle F_a^{-i}(x^+,x_\perp)F_a^{-i}(y^+,y_\perp)\rangle &= \left\langle \partial_i\alpha_b(x^+,x_\perp)\partial_i\alpha_c(y^+,y_\perp)\right\rangle \left\langle \tilde{U}^\dagger_{ab}(x^+,x_\perp)\tilde{U}_{ca}(y^+,y_\perp)\right\rangle \\ &= \frac{1}{g_S^2}\delta(x^+-y^+)\mu^2(x^+)\left(\nabla_\perp^2 L_{xy}\right)\left\langle \mathrm{Tr}\tilde{U}^\dagger(x^+,x_\perp)\tilde{U}(x^+,y_\perp)\right\rangle .\end{aligned} \tag{5.4}$$

The correlator involving the Wilson lines above is evaluated in the exact same way that it was done in section 4.4.4 with a few modifications. Since the Wilson lines here are in the adjoint representation, as opposed to the Wilson lines in the fundamental representation considered before, two changes have to be made. One, the Casimir C_F appearing in formula (4.27) should be replaced by the corresponding Casimir of the adjoint representation N_c. Two, the factor of N_c in the denominator of (4.22) is the number of quark colors and therefore should be replaced by the number of gluon colors N_c^2-1. Besides the changes induced by the change in representation, it should also be taken into account that the Wilson lines above start at x^+ in the longitudinal coordinate, therefore the definition of the function Γ appearing in (4.27) should be replaced by

$$\Gamma(x^+,x_\perp-y_\perp)=\left(\int_{x^+}^\infty dz^+\ \mu^2(z^+)\right)(L_{xx}+L_{yy}-2L_{xy}). \tag{5.5}$$

Putting all these pieces together, the correlator of two field strength tensors takes the form

$$\langle F_a^{-i}(x^+,x_\perp)F_a^{-i}(y^+,y_\perp)\rangle = \frac{1}{g_S^2}\delta(x^+-y^+)\mu^2(x^+)\left(-\nabla_\perp^2 L_{xy}\right)(N_c^2-1)e^{-\frac{N_c}{2}\Gamma(x^+,x_\perp-y_\perp)}. \tag{5.6}$$

Using this result in the properly CGC normalized expression for the WW distribution,

$$\begin{aligned}xG^{(1)}(x,k_\perp) &= 4\int\frac{dx^+d^2x_\perp dy^+d^2y_\perp}{(2\pi)^3}e^{ixP^-(x^+-y^+)-ik_\perp\cdot(x_\perp-y_\perp)}\langle F_a^{-i}(x^+,x_\perp)F_a^{-i}(y^+,y_\perp)\rangle \\ &= \frac{S_\perp}{2\pi^2\alpha_S}(N_c^2-1)\int dx^+\frac{d^2r_\perp}{(2\pi)^2}e^{-ik_\perp\cdot r_\perp}\mu^2(x^+)\left(-\nabla_\perp^2L_{xy}\right)e^{-\frac{N_c}{2}\Gamma(x^+,r_\perp)} \\ &= \frac{S_\perp}{4\pi^2\alpha_S}\frac{N_c^2-1}{N_c}\int\frac{d^2r_\perp}{(2\pi)^2}e^{-ik_\perp\cdot r_\perp}\frac{\nabla_\perp^2\Gamma(r_\perp)}{\Gamma(r_\perp)}\left(1-e^{-\frac{N_c}{2}\Gamma(r_\perp)}\right),\end{aligned} \tag{5.7}$$

where $S_\perp$ is the transverse area of the nucleus which appears explicitly since it was assumed, for simplicity, that the nuclear density is uniform in the transverse plane. Also, in the last line the function Γ is the previous version of section 4.4.4 without longitudinal dependence. Using the explicit evaluation of Γ and keeping only the leading logarithmic part, this distribution can be written in terms of the gluon saturation scale Q_{s0} (which differs from the quark saturation scale only by a Casimir operator $Q_{s0}^2 = \frac{N_c}{C_F}\bar{Q}_{s0}^2$),

$$xG^{(1)}(x,k_\perp) = \frac{S_\perp}{\pi^2\alpha_S}\frac{N_c^2-1}{N_c}\int\frac{d^2r_\perp}{(2\pi)^2}e^{-ik_\perp\cdot r_\perp}\frac{1}{r_\perp^2}\left(1-e^{-\frac{Q_{s0}^2}{4}r_\perp^2\ln(1/r_\perp\Lambda)}\right). \tag{5.8}$$

A very important consequence of the result above is that it shows the distinction between the dilute regime and the saturation regime. At large values of transverse momentum, $k_\perp \gg Q_s$, the Fourier transform is dominated by small values of $r_\perp$ and therefore the exponential can be expanded to first order. Then $xG^{(1)}(x,k_\perp) \propto \frac{Q_{s0}}{k_\perp^2}$. On the other hand, for small values of the transverse momentum, $k_\perp \ll Q_s$, the Fourier transform is dominated by large values of $r_\perp$ where the exponential can be neglected (and therefore acts overall as a cut-off). In this regime $xG^{(1)}(x,k_\perp) \propto \ln\frac{Q_s^2}{k_\perp^2}$, showing that for small values of the transverse momentum the distribution saturates leading to a much smaller growth in the occupation numbers of the corresponding states.

In the derivation above, the Wilson lines in the adjoint representation were part of the gauge strength tensor, where they were playing the role of a gauge transformation to the desired gauge where the partonic picture is manifest. On section 4.4.3 it was argued that, in covariant gauge, Wilson lines in the adjoint representation are an appropriate way of computing multiple scatterings of gluons in a nuclear target. In the particular case above, the Wilson lines are not defined over the full range of the longitudinal coordinate, they start somewhere inside the nucleus and extend all the way to infinity. If these Wilson lines were to be interpreted as gluons undergoing multiple scatterings they would have to be created somewhere inside the nucleus, which seems unlikely given that there are no other high energy particles transversing the

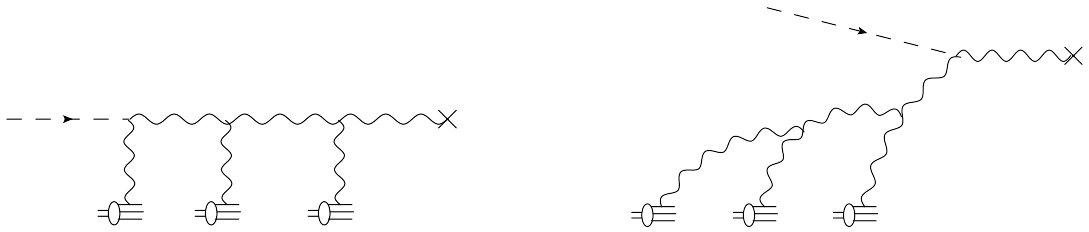

Figure 5.1: Left: colorless current on nucleus in covariant gauge. Right: same process in light cone gauge.

nucleus. Nevertheless, there is a way in which this multiple scattering interpretation makes sense and relates the WW distribution to a (unrealistic) scattering process. It was shown in [59] that if a colorless current coupled to gluons is considered, a DIS process using this current as a probe would measure exactly the WW unintegrated distribution. When considered in a covariant gauge, this process looks like a colorless current penetrating in the nucleus where it creates a gluon which undergoes subsequent multiple scatterings as depicted in the left part of Fig. 5.1. On the other hand, when considered in light-cone gauge (with an appropriate boundary condition) final state interactions can be turned off and the colorless current is seen as only freeing one of the gluons living inside the nucleus (right side of Fig. 5.1). By measuring the spectrum of produced gluons in this process it is possible to measure the WW distribution of the nucleus.

The description of the process above has the problem that it is a rather unrealistic one. The colorless current is only a theoretical device that does not have an analog in any collision experiment. A way to get around this problem and formulate the scattering process in terms of quarks and gluons only is presented in chapter 7.

5.3 Dipole distribution

After considering the difficulties to relate the Weizsäcker-Williams distribution to simple scattering processes it becomes unclear how it would be possible to have any k_t- factorized formulas for realistic processes involving gluons in the small-x regime, where multiple scatterings play a fundamental role. The complication seems to come from the fact that, in order to be able to have a partonic interpretation, it is desirable to not have either initial state or final state interactions. This would typically require a colorless probe which would only be able to interact with gluons coming from the nucleus if there is production of colored objects inside the nucleus, a process that is typically suppressed by powers of the center of mass energy of the collision.

Nevertheless, different calculations have shown that it is possible to obtain single particle production cross sections which can be written in a k_t-factorized way for different processes not necessarily involving colorless objects. The ability to factorize all the nuclear effects in a single gluon distribution comes at the price of this distribution not having a straightforward partonic interpretation.

The second unintegrated gluon distribution to be considered, the Fourier transform of the dipole cross section, is defined in the fundamental representation[1]

$$xG^{(2)}(x,k_\perp) = 2\int \frac{d\xi^- d\xi_\perp}{(2\pi)^3 P^+} e^{ixP^+\xi^- - ik_\perp\cdot\xi_\perp} \langle P|\mathrm{Tr}\left[F^{+i}(\xi^-,\xi_\perp)\mathcal{U}^{[-]\dagger}F^{+i}(0)\mathcal{U}^{[+]}\right]|P\rangle \ , \tag{5.9}$$

where the gauge link $\mathcal{U}^{[-]}$ was defined in Eq. (3.7) and stands for initial state interactions. Thus, the dipole gluon distribution contains both initial and final state interactions in the definition.

Even though this particular combination of the gauge links is very suggestive of a direct relation with a dipole scattering amplitude, in the sense that it has two Wilson

[1]The Fourier transform of the dipole cross section in the adjoint representation is also commonly used, as it enters single gluon production in pA collisions [76; 77; 78]. In the large-N_c limit, it is related to the convolution of two $xG^{(2)}$.

lines from minus infinity to plus infinity with two different transverse coordinates, it is not straightforward to go from one formulation to the other. The derivation is more clear when worked out backwards. Consider first the combination $k_\perp^2 S_\perp F(k_\perp)$ where $F(k_\perp)$ is the two-dimensional Fourier transform or the dipole-nucleus scattering S-matrix.

$$\begin{aligned} k_\perp^2 S_\perp F(k_\perp) &= k_\perp^2 S_\perp \int \frac{d^2 r_\perp}{(2\pi)^2} e^{-ik_\perp \cdot r_\perp} \frac{1}{N_c} \left\langle \mathrm{Tr} U(r_\perp) U^\dagger(0) \right\rangle \\ &= (2\pi)^2 k_\perp^2 \int \frac{d^2 v_\perp}{(2\pi)^2} \frac{d^2 v'_\perp}{(2\pi)^2} e^{-ik_\perp \cdot (v_\perp - v'_\perp)} \frac{1}{N_c} \left\langle \mathrm{Tr} U(v_\perp) U^\dagger(v'_\perp) \right\rangle \\ &= \frac{(2\pi)^2}{N_c} \int \frac{d^2 v_\perp}{(2\pi)^2} \frac{d^2 v'_\perp}{(2\pi)^2} e^{-ik_\perp \cdot (v_\perp - v'_\perp)} \partial_{v_i} \partial_{v'_i} \left\langle \mathrm{Tr} U(v_\perp) U^\dagger(v'_\perp) \right\rangle . \end{aligned} \tag{5.10}$$

Clearly, the transverse derivatives of the Wilson lines are given by

$$\partial_i U(v_\perp) = ig \int_{-\infty}^{\infty} \mathrm{d}v^+ \, U[-\infty, v^+; v_\perp] \left(\partial_i A^-(v^+, v_\perp) \right) U[v^+, \infty; v_\perp], \tag{5.11}$$

where $U[a, b; x_\perp] = \mathcal{P} \exp\{ig \int_a^b \mathrm{d}x^+ \, T^c A_c^-(x^+, x_\perp)\}$. Taking into account that the Wilson lines above represent the multiple scattering in a gauge where the only non-trivial component is A^-, it is easy to see that the correlator in (5.10) will take the desire form of (5.9) when the appropriate replacements due to the reversal of the direction of motion of the nucleus are taken into account. Introducing the proper normalization factors, it can be easily shown that the distribution in Eq. (5.9) can be written as

$$xG^{(2)}(x, k_\perp) = \frac{k_\perp^2 N_c}{2\pi^2 \alpha_s} S_\perp \int \frac{d^2 r_\perp}{(2\pi)^2} e^{-iq_\perp \cdot r_\perp} \frac{1}{N_c} \left\langle \mathrm{Tr} U(r_\perp) U^\dagger(0) \right\rangle . \tag{5.12}$$

When the dipole-nucleus amplitude is evaluated in the MV model, it can be shown [73] that for large transverse momentum, $k_\perp \gg Q_s$, this distribution has the same asymptotic limit as the WW distribution $xG^{(2)}(x, k_\perp) \propto \frac{Q_{s0}^2}{k_\perp^2}$.

Chapter 6

Single Particle Measurements

One of the motivations to consider transverse momentum dependent distributions is the limited scope of collinear factorization when it comes to less inclusive measurements. Collinear factorization works well when it comes to calculating total cross sections or when the measured transverse momentum of an outgoing particle is of the same order of the other large kinematical invariants of the process. The natural place where TMD distributions are supposed to provide a more complete formalism is single-particle measurements at low transverse momentum of the measured particle. The first processes that were successfully addressed by TMD factorization fall into this category, those are semi-inclusive deep inelastic scattering and Drell-Yan boson production. Now, formal proofs exist for these and some other slightly more complicated cases (see [6]).

If something was learned from the first attempts to use collinear factorization to extract parton distribution functions is that the simpler cases are of no use when it comes to determining the gluon distributions (to first approximation). The same is going to happen here, the simpler processes for which formal theorems have been stablished deal only with the quark distributions. The main reason is the same as for the integrated distributions, the simpler processes involve colorless objects either in the initial (DIS) or final state (Drell-Yan) which do not interact directly with gluons

and therefore the contributions from the gluon distributions are subdominant. As a first guess there are two possible ways of solving this problem, one is to consider more complicated processes possibly with more particles in the final state, the other is to move to the small-x regime where gluons are supposed to be dominant. The first approach is the subject of chapter 7, the second approach will be addressed in this chapter with partial success.

This chapter is intended as a review of existing results in the literature and therefore will not include details of the derivations. Emphasis will be made in relations between the different distributions and features of the calculations which will be useful for the development of chapter 7.

6.1 SIDIS

SIDIS in the small-x regime is better understood, as has been done here so far with most of the processes, when it is considered in a nuclear target. In that setup, the process is viewed as a virtual photon splitting into a quark-antiquark pair which subsequently multiply interacts with the nuclear target by gluon exchange. Precise calculations for this process are available either from a dipole approach [79] or from the MV model with classical Yang-Mills fields [80].

For instance, consider the dipole approach where the process can be seen as the convolution of the photon splitting wave function with the dipole-nucleus scattering amplitude. Since only the quark or the antiquark, but not both, will be detected in the final state, integration over the momentum of one of the two fermions have to be performed at the level of the cross section. The integrated particle then drops out of the multiple scattering terms because of real-virtual cancelations, therefore leaving only the scattering of one particle in the amplitude and in the conjugate amplitude with different transverse coordinates. The effect of these multiple scatterings can then be expressed in term of dipole amplitudes involving only the remaining unintegrated

particle. This particular cancelation between real and virtual contributions takes a simple form when the scattering is expressed in terms of Wilson lines. Integrating over transverse momentum means putting the particle at the same transverse coordinate in the amplitude and the conjugate amplitude, since the Wilson line is a unitary matrix its contribution times its conjugate drops out.

The result of this calculation is often rightfully quoted as the explicit calculation of the unintegrated quark distribution of the nucleus. In particular it was used in [79] to show that quark densities saturate at small-x. It can be confusing at first to consider this a calculation of the quark distribution of the nucleus since the nucleus only enters the calculation through gluon exchanges, but it is important to remember that this multiple scattering picture makes sense in a covariant gauge which is not well suited for a partonic interpretation. When light-cone gauge is used with the appropriate boundary condition, this process looks like a photon hitting a quark coming from the nucleus with no final state interactions. When translated to this picture, the assumption that the nucleus takes part on the scattering process only through gluon exchanges takes the form of assuming that the small-x quarks come only from small-x gluons splitting into quark-antiquark pairs.

The relation between quark and gluon distributions at small-x implied by these assumptions was studied to some extent in [81] where the expressions found in [79; 80] where written in terms of the Fourier transform of one dipole-nucleus amplitude. This clearly suggests a relation with the unintegrated gluon distribution function described in section 5.3. Nevertheless, it was also shown that the expressions found for the cross section within a CGC framework correspond exactly to the small-x limit of the factorized expression obtained from applying directly the TMD formalism.

This analysis shows that it is possible to obtain some information about the unintegrated gluon distribution when a process, that typically would depend only on the quark distributions, is considered in the small-x regime. One problem with this approach is that the gluon distribution enters through an integral over transverse

momentum and therefore would not be straightforward to extract it from data. The only way to fix the transverse momentum of the corresponding gluon distribution is by not integrating out the other particle in the original dipole, this possibility will be considered in chapter 7 where two-particle measurements are studied in detail.

Unintegrated quark distributions at small-x and their universality properties where thoroughly studied in [82; 83] and will not be considered here from now on.

6.2 Photon production and Drell-Yan in pA collisions

This process is strikingly similar to the one considered in the previous section when considered in the small-x region. First it is important to note that, in order to be able to access the small-x degrees of freedom in the nuclear target, it is necessary to look for particles emitted in the forward direction of the incident proton. When that is the case, the nuclear target can be considered to be in the dense saturated regime while the incident proton is in a dilute state where only valence quarks will contribute to the scattering process. Motivated by this observation, it is convenient to treat the proton in the parton model, described by an integrated quark distribution, and perform the rest of the calculation with an incoming quark with no transverse momentum.

If the transverse momentum dependence of the distributions of only one of the participants is going to be taken into account, it is not surprising that the photon emission process resembles the SIDIS process of the previous section. In principle, the SIDIS process should be sensitive to the quark distribution while the Drell-Yan process should be sensitive to the antiquark distribution. Since the nuclear target is included in the calculation only through gluon exchanges in the small-x regime, quark and antiquark distributions are going to look the same since both are coming from low-x gluons splitting into quark-antiquark pairs.

This process was first calculated in a CGC framework in [84; 85]. In this approach a quark emits a photon and interacts coherently with the target nucleus either before or after the emission. The aforementioned quark is not measured in the final state, so its momentum has to be integrated over (the same way that one of the particles was integrated over in SIDIS). Details of the calculation will be revisited in chapter 7 where it is shown explicitly how the dipole distribution of section 5.3 shows up in the final result.

The main reason to postpone the analysis of this process to chapter 7 is that the two particle measurement is, from a theoretical point of view, a much better place to look for the effects of the gluon distribution. This is the case because in the two-particle case the distribution can be isolated completely with the x value and the transverse momentum fixed by the kinematics of the final state particles. That is clearly not the case for the one-particle measurements where only one of the moments of the distribution could be measured and an additional integration over the longitudinal momentum fraction would be necessary. In general that will be the case when considering processes with more than one hadron (nucleus) in the initial state, the values of x of the partons involved in the process are not fixed by the kinematics and an integration over an extended range of longitudinal momentum fractions is always present in expressions for cross sections.

6.3 Single hadron production in pA collisions

When studying hadronic collisions, processes involving photons are suppressed as compared to processes which involve only strong interactions due to the smallness of the electromagnetic coupling. Because of this it is necessary to address particle production by strong mechanisms only and in particular hadron production due to emission of gluons. The main problem with this kind of process is that the nontrivial color flow makes resummation of multiple interactions not straightforward and even

in some cases it is not possible to obtain closed expressions unless the large-N_c limit is taken.

The first attempts to calculate the gluon production cross section in proton-ion collisions where performed under the soft gluon approximation where the produced gluon does not take a big fraction of the longitudinal momentum of the parent quark and therefore recoil effects can be safely ignored [86; 59; 87]. The fact that the result is nontrivial in this particular limit shows a fundamental difference between emissions of photons as compared to gluons, without a recoil of the charged particle there cannot be photon emission. This approximation makes the calculation suitable for production of hadrons at mid rapidities where this is clearly the dominant mechanism but runs into problems when forward rapidities are considered. As was already mentioned in the last section, the forward rapidity region is where the small-x component of the nucleus distributions become accessible and the small-x evolution effects become sizable.

Gluon production in the soft gluon approximation is nevertheless very interesting as it shows many of the aspects that are fundamental for this type of calculation in a simplified setup. The approach followed in [59] is particularly illuminating in the sense that allows for a clear interpretation of different contributions in terms of specific diagrams. As anticipated the resummation of multiple interactions is not straightforward, in particular the interference terms between initial and final state interactions when considered at the cross section level, which conveniently exponentiates due to the fact that the transverse coordinate of the quark does not change after the gluon emission. These simplifications allow to write the cross section in terms of a gluon dipole-nucleus scattering amplitude and therefore it is possible to write the cross section in a factorized form using a gluon distribution as the dipole distribution of section 5.3 but with a gluon dipole instead of a quark dipole (in the language of Wilson lines this is accounted for by taken the adjoint Wilson line instead of the fundamental). It was already noted in [74] that the gluon distribution describing the

nucleus is not the one with the straightforward partonic interpretation. The reason why this particular distribution is not studied separately from the two mentioned in the previous chapter is that in the large-N_c limit it can be related to the square of the quark dipole distribution. In the next chapter it will be seen that more complicated processes can be described in terms of the two aforementioned distributions only in the large-N_c limit, in that spirit the gluon dipole distribution is not considered as one the basic ones.

The cross section obtained in the soft gluon approximation is widely used for phenomenological applications where the main interest is in the central rapidity region. It has also been used to propose an ansatz for particle production in nucleus-nucleus collisions where two nuclear gluon distributions enter the process instead of just one [77; 88]. This approach will not be addressed here since the focus is on asymmetric collisions where the use of TMD factorization is well stablished.

Moving to the more general case where the recoil of the initial quark is taken into account, one runs into a similar situation as in the processes described in previous sections. The correct way to account for the recoil of the initial quark is to consider the two-particle process with a quark and a gluon in the final state and then integrate over the momentum of one of them. This problem was first approached in a momentum space representation in [89] where the two particles are kept in the final state, the integration over one of the particle momenta is performed in [90] where it is shown that the final form indeed shows a factorized form by also noticing that the collinear divergences are properly regulated by renormalizing the corresponding parton distributions of the incoming proton and the fragmentation functions for the final hadron. The result from this program is indeed very similar to the result from the soft gluon approximation with the main difference that there is another term accounting for the possibility that the detected particle comes from the fragmentation of the quark instead of the gluon. These formulas obtained by this approach have been successfully used in phenomenological applications which account for the

small-x evolution to explain the single hadron measurements at forward rapidities in deuteron-gold collisions [91].

The problem with the approach described above when it comes to generalize the procedure to the two-particle case is that the momentum space description yields very complicated formulas that obscure the dynamics of the interaction with the nucleus. In chapter 7 this process is revisited by considering the calculation in transverse coordinate space and much simpler formulas are found.

Chapter 7

Two Particle Measurements

After analyzing single particle production, the most natural path to follow would be to consider two-particle production processes and try to write the obtained cross sections in a factorized way. It is not difficult to foresee that this approach is doomed to fail, except for very specific cases, for a very simple reason: when more than one particle is detected in the final state the transverse momentum transferred to the particle transversing the nucleus has to be split in two (or more) parts. In that case the picture of an effective one-gluon interactions completely breaks and there is no hope of finding k_t-factorized expressions for the most general cases.

This problem was already observed in [92] where quark-antiquark pair production in pA collisions was considered. The other case that has been previously studied, and will be addressed in this chapter also, is the case of two-particle production in pA from a valence quark and an emitted gluon [93; 89] where it was also observed that the general case can not be written in a k_t-factorized form.

Despite those discouraging results, this chapter is devoted to the study of some of these two-particle processes and ways of obtaining k_t-factorized expressions. The goal is not to contradict results from the previous works cited above, but rather find kinematic regimes where an effective k_t-factorization is recovered. It turns out that putting constraints on the momenta of the outgoing particles allows for a separation

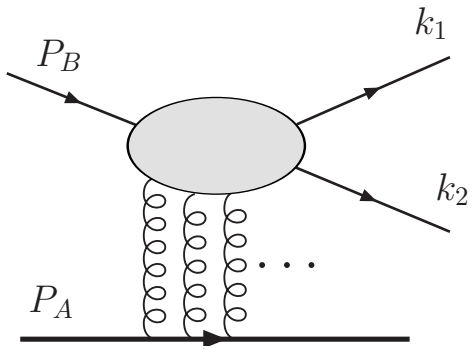

Figure 7.1: Schematic diagrams for two-particle production in a dilute system scattering on a dense target with multiple scattering. The imbalance between the two-particle in transverse momentum can be used to probe the unintegrated gluon distribution of the dense target.

of scales that naturally leads to k_t-factorized cross sections.

Consider a generic two-particle production process as illustrated in Fig. 7.1,

$$B + A \to H_1(k_1) + H_2(k_2) + X \ , \tag{7.1}$$

where A represents the dense target, B stands for the dilute projectile (such as a photon or a high-x parton in a hadron), H_1 and H_2 are the final state two particles with momenta k_1 and k_2, respectively. The kinematic region of interest is where the transverse momentum imbalance between the outgoing particles is much smaller than their individual momenta: $q_\perp = |\vec{k}_{1\perp} + \vec{k}_{2\perp}| \ll k_1 \simeq k_2 \simeq P_\perp$ where $\vec{P}_\perp$ is defined as $(\vec{k}_{1\perp} - \vec{k}_{2\perp})/2$. This is referred to as the back-to-back correlation limit (the correlation limit) in the discussion below. An important advantage of taking this limit is that it is possible to apply a power counting method to obtain the leading order contribution in $q_\perp/P_\perp$ where the differential cross section directly depends on the unintegrated gluon distribution of the nucleus.

The calculations in this chapter are set on a CGC framework. When the correlation limit described above is taken, it is possible to compare the resulting cross

section with a direct application of the TMD formalism of chapter 3. It is remarkable that both approaches agree within the regime where both are applicable.

7.1 Dijet production in DIS

The process of nuclear DIS has been widely studied in the literature and it is often used to introduce many of the relevant concepts for processes in the small-x regime. Most of these studies have focus either on the total cross section or in single inclusive gluon production but, except for isolated attempts, very little has been done regarding two-particle production. The particular process considered here, two-particle (jet) production from the initial quark-antiquark pair in which the photon splits, has a very particular and interesting color structure which will be crucial to include the WW distribution in the general picture.

7.1.1 CGC approach to the DIS dijet production

The appropriate to visualize this process in the CGC formalism is to consider the photon splitting into a quark-antiquark pair which then multiply interacts with the nucleus (see Fig. 7.2). As usual for this kind of high-energy process, the coherence time of the produced quark-antiquark pair is much longer than the length of the nucleus and therefore the splitting should occur much earlier than the scattering.

At the amplitude level the process can be divided into two parts: the splitting wave function of the incoming photon and the multiple scattering factor. It is convenient to write these quantities in transverse coordinate space since in this basis, and in the eikonal approximation, the multiple interaction factor is diagonal.

To be consistent with previous CGC calculations in the literature, a frame is chosen such that the photon is moving along the positive z direction whereas the nuclear target moves in the negative z direction. Note that even though the presentation in chapter 4 was given in this same kinematics, the formalism of chapter 3 differs

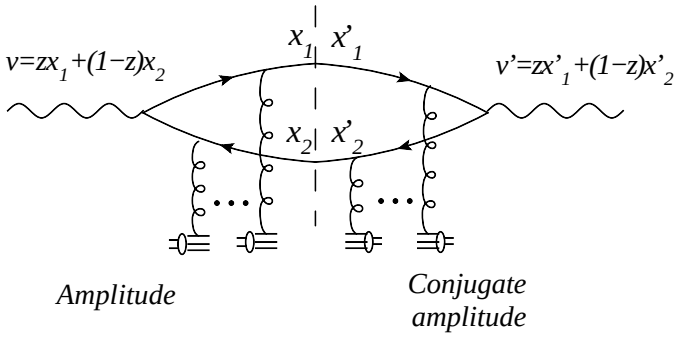

Figure 7.2: Typical diagrams contributing to the cross section in the deep inelastic process.

from this choice and therefore care should be taken when the result obtained here is compared to the TMD formalism.

For a right-moving photon with longitudinal momentum p^+, no transverse momentum, and virtuality Q^2, the splitting wave function in transverse coordinate space takes the form,

$$\psi^{T\lambda}_{\alpha\beta}(p^+,z,r)=2\pi\sqrt{\frac{2}{p^+}}\begin{cases} i\epsilon_f K_1(\epsilon_f|r|)\frac{r\cdot\epsilon^{(1)}_\perp}{|r|}[\delta_{\alpha+}\delta_{\beta+}(1-z)+\delta_{\alpha-}\delta_{\beta-}z], & \lambda=1,\\ i\epsilon_f K_1(\epsilon_f|r|)\frac{r\cdot\epsilon^{(2)}_\perp}{|r|}[\delta_{\alpha-}\delta_{\beta-}(1-z)+\delta_{\alpha+}\delta_{\beta+}z], & \lambda=2,\end{cases} \tag{7.2}$$

$$\psi^{L}_{\alpha\beta}(p^+,z,r)=2\pi\sqrt{\frac{4}{p^+}}z(1-z)QK_0(\epsilon_f|r|)\delta_{\alpha\beta}. \tag{7.3}$$

where z is the momentum fraction of the photon carried by the quark, λ is the photon polarization, α and β are the quark and antiquark helicities, r the transverse separation of the pair, $\epsilon_f^2=z(1-z)Q^2$, and the quarks are assumed to be massless. The heavy quark case will be considered in the next subsection.

Following section 4.4.3, the multiple scattering factor is written in terms of Wilson lines. Here it is very important to note that no assumption is made about the pair in the final state and therefore it is not appropriate to put the two Wilson lines inside a trace. It can be shown rigorously [94] that this interaction term takes the form

$\left[U^\dagger(x_2)U(x_1)-1\right]_{ji}$ where x_1 and x_2 are the transverse positions of the quark and the antiquark, i and j are their color indices, and the Wilson line is given in terms of the background field as usual by

$$U(x)=\mathcal{P}\exp\left\{ig_S\int_{-\infty}^{+\infty}\mathrm{d}x^+\,T^cA_c^-(x^+,x)\right\}\ . \tag{7.4}$$

The subtraction (the -1 term) performed in the multiple scattering factor requires an additional explanation. It represents the subtraction of the no interaction term in order to include the T-matrix instead of the S-matrix in the calculation of the cross section. In other words, the term without interaction has to be subtracted since without interaction a space-like photon can not decay into a quark-antiquark pair. This should be done in the amplitude and the conjugate amplitude separately. More details on this subtraction can be found in [76].

With the pieces described above it is possible to write down an explicit formula for the differential cross section for dijet production. After averaging over the photon's polarization and summing over the quark and antiquark helicities and colors the cross section takes the form

$$\begin{aligned}\frac{d\sigma^{\gamma^*_{T,L}A\to q\bar{q}X}}{d^3k_1d^3k_2} &= N_c\alpha_{em}e_q^2\delta(p^+-k_1^+-k_2^+)\int\frac{\mathrm{d}^2x_1}{(2\pi)^2}\frac{\mathrm{d}^2x_1'}{(2\pi)^2}\frac{\mathrm{d}^2x_2}{(2\pi)^2}\frac{\mathrm{d}^2x_2'}{(2\pi)^2}\\ &\quad\times e^{-ik_{1\perp}\cdot(x_1-x_1')}e^{-ik_{2\perp}\cdot(x_2-x_2')}\sum_{\lambda\alpha\beta}\psi^{T,L\lambda}_{\alpha\beta}(x_1-x_2)\psi^{T,L\lambda *}_{\alpha\beta}(x_1'-x_2')\\ &\quad\times\left[1+Q_{x_g}(x_1,x_2;x_2',x_1')-S^{(2)}_{x_g}(x_1,x_2)-S^{(2)}_{x_g}(x_2',x_1')\right]\ ,\end{aligned} \tag{7.5}$$

where the two- and four-point functions are defined as

$$S^{(2)}_{x_g}(x_1,x_2)=\frac{1}{N_c}\left\langle\mathrm{Tr}U(x_1)U^\dagger(x_2)\right\rangle_{x_g}\ , \tag{7.6}$$

$$Q_{x_g}(x_1,x_2;x_2',x_1')=\frac{1}{N_c}\left\langle\mathrm{Tr}U(x_1)U^\dagger(x_1')U(x_2')U^\dagger(x_2)\right\rangle_{x_g}\ . \tag{7.7}$$

The notation $\langle\ldots\rangle_{x_g}$ is used for the CGC average of the color charges over the nuclear wave function where x_g is the smallest fraction of longitudinal momentum probed, and is determined by the kinematics.

Notice that the transverse coordinates of the quark and antiquark in the amplitude (unprimed coordinates) are different from the coordinates in the complex conjugate amplitude (primed coordinates) since the two final momenta are not integrated over. This is a very important feature of this calculation that does not appear in previous CGC calculations of DIS in nuclei. It allows for a different color structure and in particular it is responsible for the appearance of the 4-point function Q_{x_g} which cannot be expressed in terms of 2-point functions, even in the large N_c limit.

This 4-point function is now referred to in the small-x community as a color quadrupole [89]. It can be evaluated explicitly with a Gaussian distribution of charges which as usual is associated to computing the multiple scattering in the two-gluon approximation with independent scattering centers. Even though this evaluation is restricted, it sheds some light on the dynamics of the color structure. In particular, it is seen that the final state of the pair is most likely found in an octet state. In order to go beyond the Gaussian distribution of charges, it is important to understand the evolution in rapidity of this correlator. This is a topic of current research and some comment will be made in the subject in chapter 8.

Eq. (7.5) is as far as one can go without assuming a model for the calculation of the medium averages or imposing kinematic constraints. As explained at the beginning of the chapter, it is necessary to take the correlation limit to get factorized cross sections. For convenience, new transverse coordinate variables are introduced: $u = x_1 - x_2$ and $v = zx_1 + (1-z)x_2$, and similarly for the primed coordinates. The respective conjugate momenta are $\tilde{P}_\perp = (1-z)k_{1\perp} - zk_{2\perp} \approx P_\perp$ and $q_\perp$, and therefore the correlation limit can be taken by assuming u and u' are small and then expanding the integrand with respect to these two variables before performing the Fourier transform.

First consider the multiple scattering factor. By using the following identities,

$$Q_{x_g}(x_1, x_2; v', v') = S^{(2)}_{x_g}(x_1, x_2) \ , \tag{7.8}$$

$$Q_{x_g}(v, v; x_2', x_1') = S^{(2)}_{x_g}(x_2', x_1') \ , \tag{7.9}$$

it is easy to see that terms from the expansion of Q_{x_g} cancel the other terms in (7.5). After applying

$$U^\dagger(v)\left(\partial_i U(v)\right) = -\left(\partial_i U^\dagger(v)\right) U(v)\ ,$$

it is straightforward that the lowest order contribution in u and u' to the scattering factor can be written as

$$-u_i u'_j \frac{1}{N_c}\langle \mathrm{Tr}\left[\partial_i U(v)\right] U^\dagger(v')\left[\partial_j U(v')\right] U^\dagger(v)\rangle_{x_g}\ . \tag{7.10}$$

Taking into account the path ordering of the Wilson lines, their derivatives can be written as

$$\partial_i U(v) = ig_S \int_{-\infty}^{\infty} \mathrm{d}v^+\, U[-\infty, v^+; v]\ \left(\partial_i A^-(v^+, v)\right)\ U[v^+, \infty; v], \tag{7.11}$$

where $U[a, b; x] = \mathcal{P}\exp\{ig_S \int_a^b \mathrm{d}x^+\, T^c A_c^-(x^+, x)\}$. Note that $(\partial_i A^-(v^+, v))$ is part of the gauge invariant field strength tensor $F^{i-}(\vec{v})$[1]. Therefore, the above correlator can be written in terms of a gauge invariant matrix element,

$$-\langle \mathrm{Tr}\left[\partial_i U(v)\right] U^\dagger(v')\left[\partial_j U(v')\right] U^\dagger(v)\rangle_{x_g} = g_S^2 \int_{-\infty}^{\infty} \mathrm{d}v^+ \mathrm{d}v'^+ \left\langle \mathrm{Tr}\left[F^{i-}(\vec{v})\mathcal{U}^{[+]\dagger} F^{j-}(\vec{v}')\mathcal{U}^{[+]}\right]\right\rangle_{x_g}\ . \tag{7.12}$$

Performing the u and u' integration in (7.5) after the expansion of the multiple scattering term, an explicit formula for the differential cross section in the desired kinematic region is found,

$$\begin{aligned}
\frac{d\sigma^{\gamma_T^* A\to q\bar{q}X}}{dy_1 dy_2 d^2P_\perp d^2q_\perp} &= \alpha_{em} e_q^2 \alpha_s \delta\left(x_{\gamma^*} - 1\right) z(1-z)\left(z^2 + (1-z)^2\right)\frac{P_\perp^4 + \epsilon_f^4}{(P_\perp^2 + \epsilon_f^2)^4} \\
&\quad \times (16\pi^3)\int \frac{d^3v d^3v'}{(2\pi)^6} e^{-iq_\perp\cdot(v-v')} 2\left\langle \mathrm{Tr}\left[F^{i-}(v)\mathcal{U}^{[+]\dagger} F^{i-}(v')\mathcal{U}^{[+]}\right]\right\rangle_{x_g} \qquad (7.13)\\
\frac{d\sigma^{\gamma_L^* A\to q\bar{q}X}}{dy_1 dy_2 d^2P_\perp d^2q_\perp} &= \alpha_{em} e_q^2 \alpha_s \delta\left(x_{\gamma^*} - 1\right) z^2(1-z)^2 \frac{8P_\perp^2\epsilon_f^2}{(P_\perp^2 + \epsilon_f^2)^4} \\
&\quad \times (16\pi^3)\int \frac{d^3v d^3v'}{(2\pi)^6} e^{-iq_\perp\cdot(v-v')} 2\left\langle \mathrm{Tr}\left[F^{i-}(v)\mathcal{U}^{[+]\dagger} F^{i-}(v')\mathcal{U}^{[+]}\right]\right\rangle_{x_g} \qquad (7.14)
\end{aligned}$$

[1]The other part of the the field strength tensor shall come from the transverse component of the Wilson lines as the gauge invariance of QCD requires. When the $A^+ = 0$ gauge is used the only non-zero component of the gauge field is A^- [95] and the transverse parts drop out of the equations, giving a simpler form of the equations.

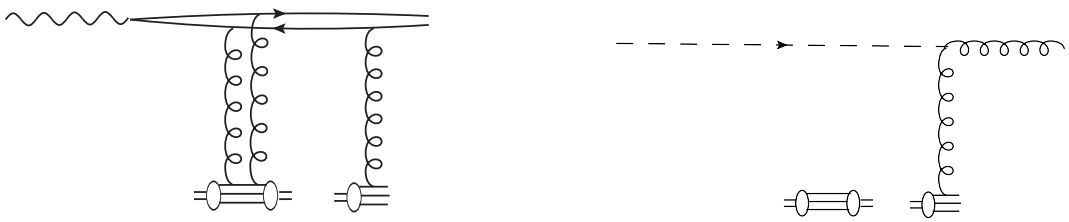

Figure 7.3: Left: interaction of quark-antiquark pair with a small distance. Right: effective picture of first order expansion.

Comparing with the definition for the WW distribution of section 5.2, it is clear that these results can be written in a factorized form as

$$\frac{d\sigma^{\gamma_T^* A\to q\bar{q}+X}_{\rm TMD}}{dy_1 dy_2 d^2P_\perp d^2q_\perp} = \delta(x_{\gamma^*}-1)x_g G^{(1)}(x_g,q_\perp)H_{\gamma_T^* g\to q\bar{q}}, \tag{7.15}$$

$$\frac{d\sigma^{\gamma_L^* A\to q\bar{q}+X}_{\rm TMD}}{dy_1 dy_2 d^2P_\perp d^2q_\perp} = \delta(x_{\gamma^*}-1)x_g G^{(1)}(x_g,q_\perp)H_{\gamma_L^* g\to q\bar{q}}, \tag{7.16}$$

with

$$H_{\gamma_T^* g\to q\bar{q}} = \alpha_s\alpha_{em}e_q^2 z(1-z)\left(z^2+(1-z)^2\right)\frac{P_\perp^4+\epsilon_f^4}{(P_\perp^2+\epsilon_f^2)^4}, \tag{7.17}$$

$$H_{\gamma_L^* g\to q\bar{q}} = \alpha_s\alpha_{em}e_q^2 z^2(1-z)^2\frac{8P_\perp^2\epsilon_f^2}{(P_\perp^2+\epsilon_f^2)^4}. \tag{7.18}$$

The fact that the WW distribution appears in the factorized version of this process is very important since it is the first time that that particular distribution has been related to an observable in terms of only quarks and gluons and no fictitious currents as in the approach described in chapter 5 and in [59]. How this distribution comes in is not very clear in the formal derivation, but there is a way to relate this process to the fictitious process of section 5.2. When the 4-point function is expanded to first order in the separation of the quark-antiquark pairs in the amplitude and the conjugate amplitude it is implied that only one of the scattering can resolve the separation of the quark-antiquark system. This particular interaction induces a transition in the pair from the singlet state to the octet state, when the separation is set to zero for

the rest of the interactions the singlet pair is effectively a colorless current while the octet pair behaves effectively as a gluon (see Fig. 7.3). This picture agrees exactly with the description of the DIS process with a colorless current as seen in covariant gauge.

In the spirit of the previous chapter, it is useful to compare the dijet production process in DIS to the inclusive and semi-inclusive DIS. As shown above, the dijet production cross section in DIS is proportional to the WW gluon distribution in the correlation limit. On the other hand, it is well-known that inclusive and semi-inclusive DIS involves the dipole cross section instead [81], which can be related to the second gluon distribution. This might look confusing at first sight, so it is useful to take a closer look at Eq. (7.5). If one integrates over one of the outgoing momenta, say k_1, one can easily see that the corresponding coordinates in the amplitude and conjugate amplitude are identified ($x_1 = x_1'$) and, therefore, the four-point function $Q_{x_g}(x_1, x_2; x_2', x_1')$ collapses to a two-point function $S^{(2)}_{x_g}(x_2, x_2')$. As a result, The SIDIS and inclusive DIS cross section only depend on two-point functions, thus they only involve the dipole gluon distribution. Now it is possible to see the unique feature of the dijet production process in DIS. By keeping the momenta of the quark and antiquark unintegrated, one keeps the full color structure of the four-point function which eventually leads to the WW gluon distribution in the correlation limit. Therefore, measuring the dijet production cross sections or dihadron correlations in DIS at future experimental facilities like EIC or LHeC would give a first direct and unique opportunity to probe and understand the Weizsäcker-Williams gluon distribution.

7.1.2 TMD-factorization approach to the DIS dijet production

Now it is time to turn to the TMD formalism described in chapter 3. The calculations are performed for Q^2 in the same order of $P_\perp^2$. As was discussed above, only the leading order contribution in the correlation limit is kept and all higher

order corrections are neglected. The typical Feynman diagram for the process is plotted in Fig. 7.4, where the bubble in the partonic part represents the hard interaction vertex including gluon attachments to both quark and antiquark lines. Fig. 7.4 (a) is the leading Born diagram whose contributions can be associated with the hard partonic cross section times the gluon distribution from Eq. (5.1) [96; 97]. In high energy scattering with the nucleus target, additional gluon attachments are important and their contributions should be resummed in the large nuclear number limit. Figs. 1(b,c) represent the diagrams contributing at two-gluon exchange order, where the second gluon can attach to either the quark line or the antiquark line. By applying the power counting method in the correlation limit ($q_\perp \ll P_\perp$), it is possible to simplify the scattering amplitudes within the Eikonal approximation [96; 97]. For example, Fig. 7.4 (b) can be reduced to:

$$\frac{g}{-q_2^+ + i\epsilon} T^b \Gamma^a \ , \tag{7.19}$$

where q_2 is the gluon momentum and Γ^a represents the rest of the partonic scattering amplitude with color indices for the two gluons a and b. Similarly, Fig. 7.4(c) can be reduced to:

$$-\frac{g}{-q_2^+ + i\epsilon} \Gamma^a T^b \ . \tag{7.20}$$

The sum of these two diagrams will be $g/(-q_2^+ + i\epsilon)\left[T^b\Gamma^a - \Gamma^a T^b\right]$. Because of the unique color index in Γ_a, the effective vertex is found to be

$$\text{Fig. 7.4(b, c)} \sim \frac{i}{-q_2^+ + i\epsilon}(-ig)(-if_{bca})T^c \ , \tag{7.21}$$

which corresponds to the first order expansion of the gauge link contribution in the gluon distribution defined in Eq. (5.1). For all high order contributions, one can follow the procedure outlined in Ref. [29; 28] to derive the gluon distribution.

Of course, to build a rigorous TMD factorization theorem for this process, it is needed to go beyond the diagrams shown in Fig. 7.4, and include the real gluon radiation contributions [25; 75]. These diagrams will introduce the large logarithms

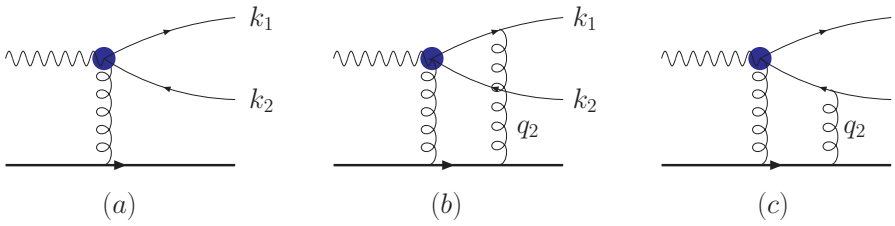

Figure 7.4: Typical Feynman diagrams contributing to the quark-antiquark jet correlation in deep inelastic scattering: (a) leading order, where the bubble represents the gluon attachments to both quark lines; (b,c) two-gluon exchange diagrams.

of $\ln(P_\perp^2/q_\perp^2)$, in addition to the small-x logarithms $\ln(1/x)$. The combination of both effects has not yet been systematically studied in the literature. Moreover, there have been discussions on the power counting method to factorize the gluon distribution from any generic Feynman diagrams, where one has to be extra cautions about the "super-leading-power" contributions (see, for example, Ref. [98]).

By putting in the hard partonic cross section $H_{\gamma^* g\to q\bar{q}}$ and especially the correct gluon distribution, namely the WW gluon distribution, which resums all the final state interactions between the $q\bar{q}$ pair and the target nucleus, one obtains the transverse and longitudinal differential cross sections for the quark-antiquark jet correlation in the DIS process of Eqs. (7.15) and (7.16) with the following leading order partonic cross sections

$$H_{\gamma_T^* g\to q\bar{q}} = \alpha_s\alpha_{em}e_q^2\frac{\hat{s}^2+Q^4}{(\hat{s}+Q^2)^4}\left(\frac{\hat{u}}{\hat{t}}+\frac{\hat{t}}{\hat{u}}\right) \tag{7.22}$$

$$H_{\gamma_L^* g\to q\bar{q}} = \alpha_s\alpha_{em}e_q^2\frac{8\hat{s}Q^2}{(\hat{s}+Q^2)^4} \tag{7.23}$$

with the usually defined partonic Mandelstam variables $\hat{s}=(k_1+k_2)^2=P_\perp^2/(z(1-z))$, $\hat{t}=(k_2-k_{\gamma^*})^2=-(P_\perp^2+\epsilon_f^2)/(1-z)$, and $\hat{u}=(k_1-k_{\gamma^*})^2=-(P_\perp^2+\epsilon_f^2)/z$ with $\epsilon_f^2=z(1-z)Q^2$ and $z=z_q$.

7.1.3 Heavy quark production in DIS dijet

In order to expand our calculation and include the possibility of charm and bottom production, we now consider the finite quark mass case. From the TMD point of view, having massive quarks modifies the hard cross sections while the parton distributions remain the same. The new leading order hard partonic cross sections read

$$H_{\gamma_T^* g\to q\bar{q}} = \alpha_s\alpha_{em}e_q^2 z^2(1-z)^2\left[\frac{P_\perp^4+\epsilon_f'^4}{(P_\perp^2+\epsilon_f'^2)^4}\left(\frac{\tilde{u}}{\tilde{t}}+\frac{\tilde{t}}{\tilde{u}}\right)+\frac{2m_q^2P_\perp^2}{z(1-z)(P_\perp^2+\epsilon_f'^2)^4}\right], \quad (7.24)$$

$$H_{\gamma_L^* g\to q\bar{q}} = \alpha_s\alpha_{em}e_q^2\frac{8Q^2}{(\tilde{s}+Q^2)^4}\left(\tilde{s}-\frac{m_q^2}{z(1-z)}\right), \quad (7.25)$$

where $\tilde{s}=(k_1+k_2)^2=(P_\perp^2+m_q^2)/(z(1-z))$, $\tilde{t}=(k_2-k_{\gamma^*})^2-m_q^2=-(P_\perp^2+\epsilon_f'^2)/(1-z)$, and $\tilde{u}=(k_1-k_{\gamma^*})^2-m_q^2=-(P_\perp^2+\epsilon_f'^2)/z$ with $\epsilon_f'^2=z(1-z)Q^2+m_q^2$ and $z=z_q$.

In terms of the CGC approach, one needs to modify the dipole splitting wave functions as follows:

$$\psi_{\alpha\beta}^{T\,\lambda}(p^+,z,r)=2\pi\sqrt{\frac{2}{p^+}}\begin{cases} i\epsilon_f' K_1(\epsilon_f'|r|)\frac{r\cdot\epsilon_\perp^{(1)}}{|r|}[\delta_{\alpha+}\delta_{\beta+}(1-z)+\delta_{\alpha-}\delta_{\beta-}z] & \\ \quad +\delta_{\alpha-}\delta_{\beta+}m_qK_0(\epsilon_f'|r|), & \lambda=1, \\ i\epsilon_f' K_1(\epsilon_f'|r|)\frac{r\cdot\epsilon_\perp^{(2)}}{|r|}[\delta_{\alpha-}\delta_{\beta-}(1-z)+\delta_{\alpha+}\delta_{\beta+}z] & \\ \quad +\delta_{\alpha+}\delta_{\beta-}m_qK_0(\epsilon_f'|r|), & \lambda=2, \end{cases} \quad (7.26)$$

$$\psi_{\alpha\beta}^{L}(p^+,z,r)=2\pi\sqrt{\frac{4}{p^+}}z(1-z)QK_0(\epsilon_f'|r|)\delta_{\alpha\beta}\,. \quad (7.27)$$

Following the same procedure, it is easy to show that again both approaches agree in the correlation limit for heavy quark production. By setting $Q^2=0$, one can get the results for the heavy quark production in real photon-nucleus scattering.

7.2 Direct-photon jet in pA collisions

In this context, the simplest process where the dipole distribution can be accessed is the direct photon-quark jet correlation in pA collisions,

$$pA \to \gamma(k_1) + q(k_2) + X \ , \tag{7.28}$$

where the incoming quark carries momentum p, and nucleus target with momentum P_A, and outgoing photon and quark with momenta k_1 and k_2, respectively.

7.2.1 CGC approach to the direct photon-jet production in pA collisions

This process was already considered in the CGC framework in [84] where the calculation was performed entirely in momentum space. In order to compare with the result from the previous section and illustrate why a different distribution should be used, the corresponding cross section will be derived following the same procedure as the previous section by showing the splitting wave function and the multiple scattering factor in transverse coordinate space. The obtained result is consistent with [84].

Consider the partonic level process $q \to q\gamma$. For a right-moving massless quark, with initial longitudinal momentum p^+ and no transverse momentum, the splitting wave function in transverse coordinate space is given by

$$\psi^{\lambda}_{\alpha\beta}(p^+, k_1^+, r) = 2\pi i \sqrt{\frac{2}{k_1^+}} \begin{cases} \frac{r\cdot\epsilon_\perp^{(1)}}{r^2}(\delta_{\alpha-}\delta_{\beta-} + (1-z)\delta_{\alpha+}\delta_{\beta+}), & \lambda = 1, \\ \frac{r\cdot\epsilon_\perp^{(2)}}{r^2}(\delta_{\alpha+}\delta_{\beta+} + (1-z)\delta_{\alpha-}\delta_{\beta-}), & \lambda = 2. \end{cases} \ , \tag{7.29}$$

where again λ is the photon polarization, α, β are helicities for the incoming and outgoing quarks, and z is the momentum fraction of the incoming quark carried by the photon. To account for the multiple scatterings in this process it is necessary to consider interactions both before and after the splitting. If the transverse coordinates of the quark and photon in the final state are b and x respectively, then the multiple

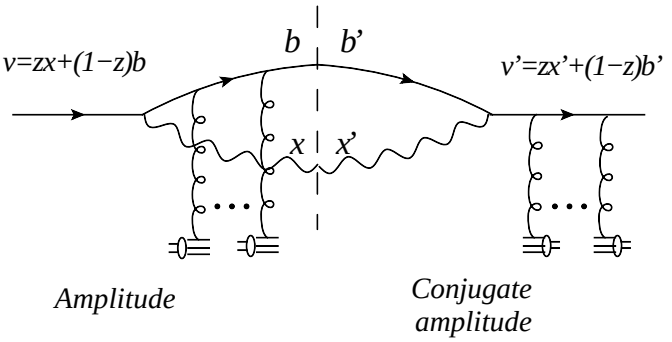

Figure 7.5: Interactions before and after the splitting have to be taken into account for both amplitude and conjugate amplitude. Here is a typical diagram representing the third interaction term in Eq. (7.30).

scattering factor in the amplitude takes the form $U(b) - U(zx + (1-z)b)$. Where the coordinate assigned to the quark before the scattering is a direct consequence of momentum conservation as expressed in this mixed formalism where only the transverse part is Fourier transformed.

After summing over final polarization, helicity and color, and averaging over initial helicity and color, we find the following expression for the partonic level cross section (see Fig. 7.5).

$$\begin{aligned}\frac{d\sigma^{qA\to q\gamma X}}{d^3k_1 d^3k_2} &= \alpha_{em} e_q^2 \delta(p^+ - k_1^+ - k_2^+) \int \frac{\mathrm{d}^2x}{(2\pi)^2}\frac{\mathrm{d}^2x'}{(2\pi)^2}\frac{\mathrm{d}^2b}{(2\pi)^2}\frac{\mathrm{d}^2b'}{(2\pi)^2} \\ &\quad \times e^{-ik_{1\perp}\cdot(x-x')} e^{-ik_{2\perp}\cdot(b-b')} \sum_{\lambda\alpha\beta} \psi^{\lambda *}_{\alpha\beta}(x'-b')\psi^{\lambda}_{\alpha\beta}(x-b) \\ &\quad \times \Big[S^{(2)}_{x_g}(b,b') + S^{(2)}_{x_g}(zx+(1-z)b, zx'+(1-z)b') \\ &\quad - S^{(2)}_{x_g}(b, zx'+(1-z)b') - S^{(2)}_{x_g}(zx+(1-z)b, b') \Big] . \end{aligned} \tag{7.30}$$

Notice that the color structure is simpler than in the DIS case. There is no four-point function and all the terms in the multiple scattering factor can be expressed in terms of the color dipole cross section $S^{(2)}_{x_g}$. By changing the variables on each of the terms of the scattering factor to $u = x - b$ and either $v = b$ or $v = zx + (1-z)b$, and

similarly for the primed coordinates, the cross section above can be written as

$$\begin{aligned}\frac{d\sigma^{qA\to q\gamma X}}{d^3k_1 d^3k_2} &= \alpha_{em}e_q^2\delta(p^+-k_1^+-k_2^+)\int\frac{\mathrm{d}^2u}{(2\pi)^2}\frac{\mathrm{d}^2u'}{(2\pi)^2}\frac{\mathrm{d}^2v}{(2\pi)^2}\frac{\mathrm{d}^2v'}{(2\pi)^2}\\ &\times e^{-iq_\perp\cdot(v-v')}S_{x_g}^{(2)}(v,v')\sum_{\lambda\alpha\beta}\psi^{\lambda *}_{\alpha\beta}(u')\psi^{\lambda}_{\alpha\beta}(u)\\ &\times\Big[e^{-iu\cdot(\tilde{P}_\perp+zq_\perp)}e^{iu'\cdot(\tilde{P}_\perp+zq_\perp)}+e^{-iu\cdot\tilde{P}_\perp}e^{iu'\cdot\tilde{P}_\perp}\\ &-e^{-iu\cdot(\tilde{P}_\perp+zq_\perp)}e^{iu'\cdot\tilde{P}_\perp}-e^{-iu\cdot\tilde{P}_\perp}e^{iu'\cdot(\tilde{P}_\perp+zq_\perp)}\Big]\ ,\end{aligned}\tag{7.31}$$

where $\tilde{P}_\perp=(1-z)k_{1\perp}-zk_{2\perp}\approx P_\perp$.

From the above expression it is easy to see that performing the u and u' integrations reduces to taking the Fourier transform of the splitting wave function with different values of the momentum variable for each term. Clearly, the Fourier transform of the dipole cross section factors out. Using collinear approximation for the proton projectile one finds the final result for the cross section of the desired process.

$$\begin{aligned}\frac{d\sigma^{pA\to\gamma q+X}}{d\mathcal{P}.\mathcal{S}.} &= \sum_f x_p q_f(x_p)\alpha_{em}e_f^2N_c\left[1+(1-z)^2\right]z^2(1-z)\frac{2q_\perp^2}{\tilde{P}_\perp^2(\tilde{P}_\perp+zq_\perp)^2}\\ &\times\int\frac{\mathrm{d}^2v}{(2\pi)^2}\frac{\mathrm{d}^2v'}{(2\pi)^2}e^{-iq_\perp\cdot(v-v')}S_{x_g}^{(2)}(v,v').\end{aligned}\tag{7.32}$$

Notice that this result already seems to be in a factorized form in the sense that all the nuclear effects are confined to the last factor with the Fourier transform of the dipole amplitude. Clearly, the distribution that will appear here is the dipole distribution of section 5.3 which was observed to be proportional to the dipole-nucleus scattering amplitude. Nevertheless, this expression is not in the desired factorized form yet. The problem lies in the denominator of the "hard" part of the expression where the two momentum variables appear through the combination $\tilde{P}_\perp+zq_\perp$ instead of factored out separately as would be desired for a true factorized expression where all the $q_\perp$ dependence is on the the gluon unintegrated distribution.

When the correlation limit $P_\perp\approx\tilde{P}_\perp\gg q_\perp$ is taken, the $q_\perp$ dependence of the hard part can be dropped yielding the result that will be shown in next subsection

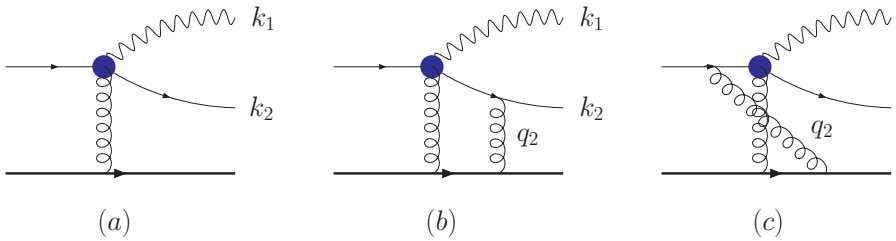

Figure 7.6: Same as Fig. (7.4) for direct photon-jet correlation in pA collisions.

to agree with the TMD factorization approach.

$$\frac{d\sigma^{(pA\to\gamma q+X)}}{dy_1 dy_2 d^2P_\perp d^2q_\perp} = \sum_f x_p q_f(x_p) x_g G^{(2)}(x_g, q_\perp) H_{qg\to\gamma q} \ , \tag{7.33}$$

with

$$H_{qg\to\gamma q} = \frac{\alpha_s \alpha_{em} e_q^2}{N_c} \frac{[1+(1-z)^2]\, z^2(1-z)}{P_\perp^4}. \tag{7.34}$$

7.2.2 TMD factorization approach to the direct photon-jet production in pA collisions

The analysis of this process follows that for the quark-antiquark jet correlation in DIS process in the previous section.

The relevant diagrams are plotted in Fig. 7.6(a,b,c), again for the leading one gluon exchange and two gluon exchanges. Similarly, the two gluon exchange contributions can be summarized as

$$\text{Fig. 7.6(b, c)} \sim (-ig)\left(\frac{i}{-q_2^+ + i\epsilon} T^b \Gamma^a + \frac{i}{q_2^+ + i\epsilon} \Gamma^a T^b\right) \ , \tag{7.35}$$

where the plus sign comes from the fact that the second gluon attaches to the quark line in the initial and final states. Since there is no color structure corresponding to Eq. (7.35), it can only be expressed in the fundamental representation. Following Ref. [28], one finds that the gluon distribution in this process can be written as

$$xG^{(2)}(x, k_\perp) = 2\int \frac{d\xi^- d\xi_\perp}{(2\pi)^3 P^+} e^{ixP^+\xi^- - ik_\perp\cdot\xi_\perp} \langle P|\mathrm{Tr}\left[F^{+i}(\xi^-, \xi_\perp)\mathcal{U}^{[-]\dagger} F^{+i}(0)\mathcal{U}^{[+]}\right]|P\rangle \ , \tag{7.36}$$

where the gauge link $\mathcal{U}_{\xi}^{[-]} = U^n\left[0,-\infty;0\right]U^n\left[-\infty,\xi^-;\xi_\perp\right]$ resums the initial state interactions between the incoming quark and the target nucleus. On the other hand, the gauge link $\mathcal{U}^{[+]}$ represents the final state interactions between the outgoing quark and the target nucleus.

Therefore, by plugging in the appropriate gluon distribution, namely the dipole gluon distribution, which resums both the initial and final state interactions, one can write the differential cross section of (7.28) as was done in Eq. (7.33 where x_p is the momentum fraction of the projectile nucleon carried by the quark, $q_f(x_p)$ is the integrated quark distribution. Because we are taking large nuclear number limit, the intrinsic transverse momentum associated with it can be neglected compared to that from the gluon distribution of nucleus. The hard partonic cross section is calculated perturbatively and found to be

$$H_{qg\to\gamma q} = \frac{\alpha_s\alpha_{em}e_q^2}{N_c\hat{s}^2}\left(-\frac{\hat{s}}{\hat{u}}-\frac{\hat{u}}{\hat{s}}\right). \tag{7.37}$$

where the Mandelstam variables can be expressed in terms of $P_\perp$ and z: $\hat{s} = (k_1 + k_2)^2 = \frac{P_\perp^2}{z(1-z)}$, $\hat{u} = (k_1 - p)^2 = -\frac{P_\perp^2}{z}$ and $\hat{t} = (k_2 - p)^2 = -\frac{P_\perp^2}{1-z}$.

7.3 Dijet production in pA collisions

Dijet production in pA collisions receive contributions from several channels such as $qg \to qg$, $gg \to q\bar{q}$ and $gg \to gg$. For convenience, the following common variables are defined as in the last two sections,

$$z = \frac{|k_{1\perp}|e^{y_1}}{|k_{1\perp}|e^{y_1}+|k_{2\perp}|e^{y_2}}, \quad x_p = \frac{|k_{1\perp}|e^{y_1}+|k_{2\perp}|e^{y_2}}{\sqrt{s}}, \quad x_g = \frac{|k_{1\perp}|e^{-y_1}+|k_{2\perp}|e^{-y_2}}{\sqrt{s}}\ , \tag{7.38}$$

where k_1 and k_2 are momenta, and y_1 and y_2 are rapidities for the two outgoing particles, x_p is the momentum fraction of the projectile nucleon carried by the incoming parton, x_g is the momentum fraction of the target nucleus carried by the gluon, respectively. Taking into account that the quark distribution functions are dominant

at large-x and the gluon distribution functions are dominant at low-x, it comes as no surprise the fact that different channels are relevant in different kinematic regions. At RHIC energies, the low -x region is only accessible in events where the two jets are produced in the forward rapidity region of the projectile. Under those conditions $x_p \sim 0.1$ and $x_g \ll 0.1$, and therefore quark initiated processes dominate ($qg \to qg$ channel).

The higher energies available at LHC will allow to explore more thoroughly the low-x regime in the target nucleus as well as in the projectile(see e.g., in a recent study [99]). Under these circumstances, and in particular at central rapidities at the LHC, it is possible to have processes with both x_p and x_g small where the dominant channels are $gg \to q\bar{q}$ and $gg \to gg$.

This process has attracted a lot of interest in the last few years due to the recent data from STAR and PHENIX on di-hadron measurements in the forward region in dAu collisions [100; 101]. When measuring two-particle azimuthal correlations in pA collisions it is common to find a near side peak due mostly to collinear pion production, and an away side peak due to the parent partons balancing exactly their transverse momentum. It was originally predicted in [93] (where only the quark initiated process was considered) that, as a consequence of small-x evolution, the away side peak should be present when considering particles at mid rapidity but suppressed when considering both particles at forward rapidities (in the direction of the proton). The data confirms the predictions, and since more complete studies of the process have been developed [102]. Even though it has been argued, and will also be explained here, that some of the approximations performed in [93; 102] are not well justified, this particular measurement stands as the most clear evidence of saturation physics.

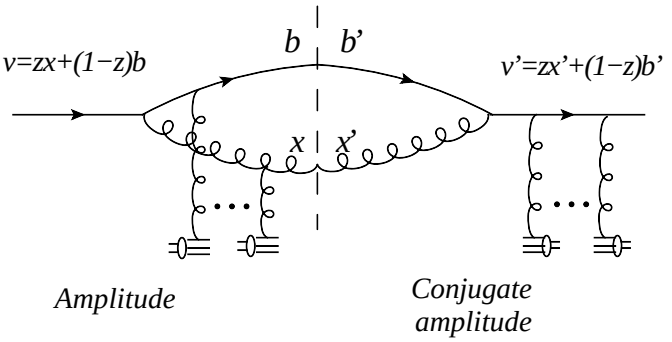

Figure 7.7: Interactions before and after the splitting have to be taken into account for both amplitude and conjugate amplitude. After the splitting the nucleus interacts coherently with the quark-gluon system. Here is a typical diagram representing the second interaction term in Eq. (7.39).

7.3.1 CGC Calculations

7.3.1.1 $q \to qg$

This process is studied in detail in Refs. [89; 93], and in particular Ref. [93] is close to the approach followed here, where an explicit formula analogous to the ones cited here for DIS and photon emission is given. As a starting point and in analogy with the previous cases, the cross section for this case can be taken as (see Fig. 7.7)

$$\begin{aligned}\frac{d\sigma^{qA\to qgX}}{d^3k_1 d^3k_2} &= \alpha_S C_F \delta(p^+ - k_1^+ - k_2^+) \int \frac{\mathrm{d}^2x}{(2\pi)^2}\frac{\mathrm{d}^2x'}{(2\pi)^2}\frac{\mathrm{d}^2b}{(2\pi)^2}\frac{\mathrm{d}^2b'}{(2\pi)^2} \\ &\times e^{-ik_{1\perp}\cdot(x-x')} e^{-ik_{2\perp}\cdot(b-b')} \sum_{\lambda\alpha\beta} \psi^{\lambda *}_{\alpha\beta}(x'-b')\psi^{\lambda}_{\alpha\beta}(x-b) \\ &\times \Big[S^{(6)}_{x_g}(b,x,b',x') - S^{(3)}_{x_g}(b,x,zx'+(1-z)b') \\ &\quad - S^{(3)}_{x_g}(zx+(1-z)b,x',b') + S^{(2)}_{x_g}(zx+(1-z)b,zx'+(1-z)b') \Big] \end{aligned} \tag{7.39}$$

where

$$S^{(6)}_{x_g}(b,x,b',x') = \frac{1}{C_F N_c}\left\langle \mathrm{Tr}\left(U(b)U^\dagger(b')T^dT^c\right)\left[W(x)W^\dagger(x')\right]^{cd}\right\rangle_{x_g}, \tag{7.40}$$

$$S^{(3)}_{x_g}(b,x,v') = \frac{1}{C_F N_c}\left\langle \mathrm{Tr}\left(U(b)T^dU^\dagger(v')T^c\right)W^{cd}(x)\right\rangle_{x_g}, \tag{7.41}$$

and $W(x)$ is a Wilson line in the adjoint representation. In the correlators above, Wilson lines in the fundamental representation appear when considering the multiple interaction of a quark with the nucleus and Wilson lines in the adjoint representation appear when considering multiple interactions of a gluon with the nucleus. Clearly, the $S_{x_g}^{(6)}$ term represents the case where interactions occur after the splitting both in the amplitude and in the conjugate amplitude, the $S_{x_g}^{(3)}$ terms represent the interference terms, and the $S_{x_g}^{(2)}$ term represent interactions before the splitting only.

This formula for the cross section has the same structure as Eqs. (7.5) and (7.31). The splitting wave function is the same as in the photon emission case (Eq. (7.29)). The only difference in the emission vertex is a color matrix which is included as part of the multiple scattering factor (therefore confining the color algebra to just the multiple scattering factor). Using Fierz identities, the terms appearing in the multiple scattering factor above can be written in terms of fundamental Wilson lines only as

$$S_{x_g}^{(6)}(b,x,b',x') = \frac{1}{2C_F N_c}\left\langle \mathrm{Tr}\left(U(b)U^\dagger(b')U(x')U^\dagger(x)\right)\mathrm{Tr}U(x)U^\dagger(x') - \frac{1}{N_c}\mathrm{Tr}U(b)U^\dagger(b')\right\rangle_{x_g}, \tag{7.42}$$

$$S_{x_g}^{(3)}(b,x,v') = \frac{1}{2C_F N_c}\left\langle \mathrm{Tr}U(b)U^\dagger(x)\mathrm{Tr}U(x)U^\dagger(v') - \frac{1}{N_c}\mathrm{Tr}U(b)U^\dagger(v')\right\rangle_{x_g}, \tag{7.43}$$

Some of the correlators appearing in the expressions above are familiar or have been calculated in the literature before. The 4-point function in $S_{x_g}^{(3)}$ is different from the one appearing in the DIS case but it has been studied and calculated in a model with Gaussian distribution of sources in [103]. The 6-point function appearing in $S_{x_g}^{(6)}$ presents a more difficult challenge even with only four independent coordinates. In order to deal with this difficulty, it is convenient to address the problem in the large-N_c limit where correlators of products of traces are evaluated as product of

correlators of traces. Specifically, for the correlators above

$$S^{(6)}_{x_g}(b,x,b',x') \simeq \frac{1}{N_c^2}\left\langle \mathrm{Tr}U(b)U^\dagger(b')U(x')U^\dagger(x)\right\rangle_{x_g}\left\langle \mathrm{Tr}U(x)U^\dagger(x')\right\rangle_{x_g}, \tag{7.44}$$

$$= Q_{x_g}(b,x,b',x')S^{(2)}_{x_g}(x,x'), \tag{7.45}$$

$$S^{(3)}_{x_g}(b,x,v') \simeq \frac{1}{N_c^2}\left\langle \mathrm{Tr}U(b)U^\dagger(x)\right\rangle_{x_g}\left\langle \mathrm{Tr}U(x)U^\dagger(v')\right\rangle_{x_g}, \tag{7.46}$$

$$= S^{(2)}_{x_g}(b,x)S^{(2)}_{x_g}(x,v'). \tag{7.47}$$

Note that in the large-N_c limit, the 6-point function is related to the 4-point function that appeared in the DIS dijet case.

The procedure to follow to enforce the correlation limit it the same used in the DIS case. From the structure of the terms in the multiple scattering factor, it is easy to see that the same kind of cancellations will occur and the final result will be the sum of the lowest order non-vanishing terms from the expansion of $S^{(6)}_{x_g}$. Moreover, since there is no linear term in the expansion of Q_{x_g}, the lowest non-vanishing terms come separately from the Q_{x_g} factor and the $S^{(2)}_{x_g}$ in the same fashion as in the previous calculations for DIS and photon emission. With the previous considerations in mind, it is easy to see that the final result takes the form

$$\begin{aligned}\frac{d\sigma^{pA\to qgX}}{d^2q_\perp d^2P_\perp dy_1dy_2} = & \sum_f x_p q_f(x_p) 16\pi^3 \frac{\alpha_S^2}{P_\perp^4}(1-z)\left[1+(1-z)^2\right] \\ & \times \int \frac{d^3v}{(2\pi)^3}\frac{d^3v'}{(2\pi)^3}e^{-iq_\perp\cdot(v-v')}\Big[(1-z)^2\left\langle \mathrm{Tr}\left[F^{i-}(\vec{v})\mathcal{U}^{[-]\dagger}F^{i-}(\vec{v}')\mathcal{U}^{[+]}\right]\right\rangle_{x_g} \\ & + \frac{1}{N_c}\left\langle \mathrm{Tr}U(v)U^\dagger(v')\right\rangle_{x_g}\left\langle \mathrm{Tr}\left[F^{i-}(\vec{v})\mathcal{U}^{[+]\dagger}F^{i-}(\vec{v}')\mathcal{U}^{[+]}\right]\right\rangle_{x_g}\Big].\end{aligned} \tag{7.48}$$

Taking into account the difference between the normalizations, it is straightforward to see that the result above agrees with the factorized formula (7.77).

In order to bring some insight to the relation between the processes considered so far, and how the different distributions come in for this particular channel, it is useful to consider the graphical representation of the large-N_c limit used to factorize

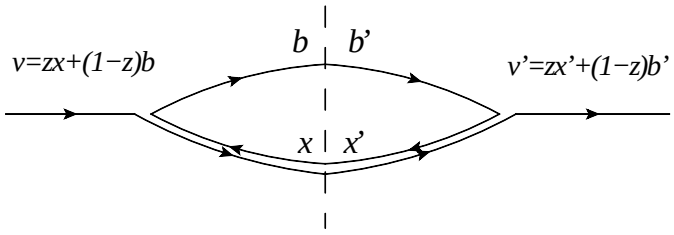

Figure 7.8: Graphical representation of the splitting $q \to qg$ in the large-N_c limit, in the amplitude and the conjugate amplitude.

the correlators of Wilson lines. In the large-N_c limit, a gluon line can be effectively considered as a quark-antiquark pair. Forgetting about the multiple interactions for the moment, and focusing primarily in the color flow of the process, one sees that in the large-N_c limit the process takes the form depicted in Fig. 7.8. The system splits into two separate pieces, a quark line in the lower part of the diagram which resembles the photon emission process, and a loop in the upper part of the diagram which has the same color structure as the DIS dijet case. Interactions involving both parts of the process are N_c-suppressed, so it comes as no surprise that the final result can be written as two separate pieces each involving the respective distributions found for DIS and photon emission.

The fact that one of the terms in the final result involves only one of the distributions while the other involves a convolution of two factors can also be understood in a simple way from the previous considerations. The enforcement of the correlation limit is schematically the same as singling out one hard scattering in the process and then taking $u = u' = 0$ for the rest of the interactions. When the hard scattering occurs on the lower part of the diagram in Fig. 7.8, the quark-antiquark pair in the upper part does not interact by color transparency ($Q_{x_g}(b, b; b', b') = 1$) and therefore there is no trace of it in the first term of the factorized expression. When the hard scattering occurs in the upper part of the diagram in Fig. 7.8, the quark in the lower part still interacts with the nucleus (and exchanges transverse momentum) and therefore has

to be included in the form of a dipole cross section.

7.3.1.2 $g \to q\bar{q}$

Following the same strategy from previous sections, start with the partonic level formula for the cross section built from the splitting wave function and the multiple scattering factor. In this particular case it takes the following form,

$$\begin{aligned}\frac{d\sigma^{gA\to q\bar{q}X}}{d^3k_1 d^3k_2} &= \alpha_S\delta(p^+-k_1^+-k_2^+)\frac{1}{2}\int\frac{\mathrm{d}^2x_1}{(2\pi)^2}\frac{\mathrm{d}^2x_1'}{(2\pi)^2}\frac{\mathrm{d}^2x_2}{(2\pi)^2}\frac{\mathrm{d}^2x_2'}{(2\pi)^2}\\ &\times e^{-ik_{1\perp}\cdot(x_1-x_1')}e^{-ik_{2\perp}\cdot(x_2-x_2')}\sum_{\lambda\alpha\beta}\psi^{T\lambda}_{\alpha\beta}(x_1-x_2)\psi^{T\lambda *}_{\alpha\beta}(x_1'-x_2')\\ &\times\Big[C_{x_g}(x_1,x_2,x_1',x_2')+S^A_{x_g}(zx_1+(1-z)x_2,zx_1'+(1-z)x_2')\\ &\quad -S^{(3)}_{x_g}(x_1,zx_1'+(1-z)x_2',x_2)-S^{(3)}_{x_g}(x_2',zx_1+(1-z)x_2,x_1')\Big]\end{aligned} \tag{7.49}$$

where $S^{(3)}_{x_g}$ is given by (7.43) and

$$C_{x_g}(x_1,x_2,x_1',x_2')=\frac{1}{C_F N_c}\left\langle \mathrm{Tr}\left(U^\dagger(x_2)T^cU(x_1)U^\dagger(x_1')T^cU(x_2')\right)\right\rangle_{x_g}, \tag{7.50}$$

$$S^A_{x_g}(v,v')=\frac{1}{N_c^2-1}\left\langle \mathrm{Tr}W(v)W^\dagger(v')\right\rangle, \tag{7.51}$$

and the splitting wave function is the same as in the DIS case with $Q^2=0$. Notice this cross section is down by a factor of N_c as compared to the $q\to qg$ case. This is due to the averaging over the incoming particle which amounts for a factor of $\frac{1}{N_c^2-1}$ for gluons instead of the factor of $\frac{1}{N_c}$ for quarks.

All the correlators above have been previously studied in the literature and explicit expressions for a Gaussian distribution of charges have been found. The only new ingredient that has not been considered in previous sections is C_{x_g} which was thoroughly studied in [92]. Following the procedure from the previous section, express the correlators defined above in terms of fundamental Wilson lines only by means of

Fierz identities.

$$C_{x_g}(x_1,x_2,x_1',x_2') = \frac{1}{2C_F N_c}\left\langle \mathrm{Tr}U(x_1)U^\dagger(x_1')\mathrm{Tr}U(x_2')U^\dagger(x_2) - \frac{1}{N_c}\mathrm{Tr}U(x_1)U^\dagger(x_1')U(x_2')U^\dagger(x_2)\right\rangle_{x_g}, \tag{7.52}$$

$$S^A_{x_g}(v,v') = \frac{1}{N_c^2-1}\left\langle \mathrm{Tr}U(v)U^\dagger(v')\mathrm{Tr}U(v')U^\dagger(v)-1\right\rangle_{x_g}. \tag{7.53}$$

Take the large-N_c limit in order to be able to compare with the results from the previous section and relate the cross section to the gluon distributions defined before. Under this approximation, the correlators above can be expressed entirely in terms of 2-point functions.

$$C_{x_g}(x_1,x_2,x_1',x_2') \simeq S^{(2)}_{x_g}(x_1,x_1')S^{(2)}_{x_g}(x_2',x_2), \tag{7.54}$$

$$S^A_{x_g}(v,v') \simeq S^{(2)}_{x_g}(v,v')S^{(2)}_{x_g}(v',v). \tag{7.55}$$

This way of factorizing the correlators and the fact that the 4-point function is absent suggests that this process is related to the distribution given by the Fourier transform of the dipole cross section only. With this consideration in mind, we Fourier transform all the $S^{(2)}_{x_g}$ factors and perform the usual change of variables $u = x_1 - x_2$ and $v = zx_1 + (1-z)x_2$ (and similarly for the primed coordinates) and obtain

$$\begin{aligned}\frac{d\sigma^{gA\to q\bar{q}X}}{d^3k_1 d^3k_2} &= \alpha_S\delta(p^+-k_1^+-k_2^+)\frac{1}{2}\int\frac{\mathrm{d}^2u}{(2\pi)^2}\frac{\mathrm{d}^2u'}{(2\pi)^2}\frac{\mathrm{d}^2v}{(2\pi)^2}\frac{\mathrm{d}^2v'}{(2\pi)^2}\mathrm{d}^2q_1\mathrm{d}^2q_2F_{x_g}(q_1)F_{x_g}(q_2)\\ &\times e^{-i(q_\perp-q_1-q_2)\cdot(v-v')}e^{-i\tilde{P}_\perp\cdot(u-u')}\sum_{\lambda\alpha\beta}\psi^{\lambda *}_{\alpha\beta}(u')\psi^{\lambda}_{\alpha\beta}(u)\\ &\times\left[e^{i((1-z)q_2-zq_1)\cdot(u-u')}-e^{i((1-z)q_2-zq_1)\cdot u}-e^{-i((1-z)q_2-zq_1)\cdot u'}+1\right].\end{aligned} \tag{7.56}$$

As in the photon emission case, the u and u' integrations reduce to calculate the Fourier transform of the splitting wave function with different momentum variables for each of the terms. The v and v' integrations give a δ-function relating the momentum variables of the two distributions and a factor of the total transverse area. As in previous cases, collinear factorization is used for the incoming parton from the proton

projectile and obtain

$$\frac{d\sigma^{pA\to q\bar{q}X}}{d\mathcal{P}.\mathcal{S}.} = x_p g_f(x_p)\alpha_S\left[z^2+(1-z)^2\right]z(1-z)\frac{S_\perp}{(2\pi)^2} \times \int \mathrm{d}^2q_1\mathrm{d}^2q_2\delta^{(2)}(q_\perp-q_1-q_2)F_{x_g}(q_1)F_{x_g}(q_2)\frac{(zq_1-(1-z)q_2)^2}{\tilde{P}_\perp^2(\tilde{P}_\perp+zq_1-(1-z)q_2)^2}. \tag{7.57}$$

In the correlation limit, the denominator of the last fraction above becomes just $P_\perp^4$. From this expression it is clear that the distributions involved will be written as a convolution of two factors involving the Fourier transform of the dipole cross section. To notice how this equation above agrees with the factorized form in (7.81), expand the numerator and write the momentum factors as derivatives with respect to transverse coordinates of the dipole cross sections inside the definition of F_{x_g} as was explained for the case of photon emission. There is a subtlety concerning the relative signs of the different terms when this identification is made. In order to find a complete agreement between the formula above and the factorized formula from the TMD formalism, it is necessary to write the two F_{x_g} factors as Fourier transforms of Wilson loops in opposite directions (one of them in terms of $\mathcal{U}^{[\square]}$ and the other in terms of $\mathcal{U}^{[\square]\dagger}$). Because of this, q_1 and q_2 enter with opposite signs when expressed as derivatives of the Wilson loops. This sign is not visible in the terms with q_1^2 or q_2^2 but it changes the sign of the cross term, giving complete agreement with the factorized expression.

As done for the previous channel, consider the graphical representation of this channel in the large-N_c limit in Fig. 7.9. After replacing the gluon line with a quark-antiquark pair we are left with two independent fermion lines which scatter separately with the nucleus. Each of them resembles the photon emission case and therefore we expect, even before performing the calculation, to obtain a convolution of two Fourier transforms of the dipole cross section. In the correlation limit, the two terms in (7.81) have a simple explanation in terms of a hard scattering. The first term accounts for the cases where the hard scattering involves only one of the two quark lines, while

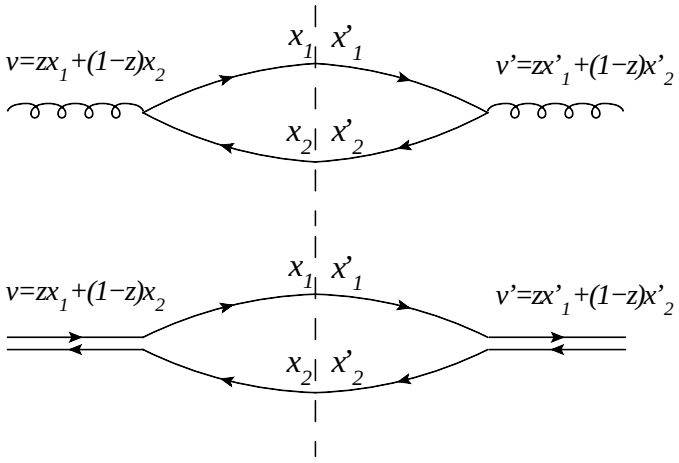

Figure 7.9: Above: graphical representation of the splitting in the amplitude and conjugate amplitude. Below: splitting in the large-N_c limit.

the second term is an interference term when the large momentum transfer involves the two participants.

This channel had already been considered in [92] where, due to the choice of gauge, the separation of the amplitude in terms of splitting function and multiple scattering terms is not visible. It is possible to show the expressions above are consistent with their results when expressed in the same set of coordinates and momentum variables.

7.3.1.3 $g \to gg$

In order to study the partonic process $g \to gg$, it is necessry to derive the splitting function first. It can be written in momentum space as

$$\Psi_{g\to gg}(z, p_\perp) = \frac{1}{\sqrt{8p^+k_1^+k_2^+}} \frac{V_{g\to gg}}{k_1^- + k_2^- - p^-}, \tag{7.58}$$

where $V_{g\to gg}$ is just the three-gluon vertex with the coupling and color factor factorized out. This can be written as

$$V_{g\to gg} = \epsilon_a^\alpha \epsilon_b^\beta \epsilon_c^\gamma \left[g_{\alpha\beta} \left(p_a - p_b\right)_\gamma + g_{\beta\gamma} \left(p_b - p_c\right)_\alpha + g_{\gamma\alpha} \left(p_c - p_a\right)_\beta \right]. \tag{7.59}$$

Here ϵ_i^μ represents the polarization vector for gluon i with four momentum p_i. It is straightforward to find that

$$\sum_{\text{spin}} |V_{g\to gg}|^2 = \frac{8p_\perp^2}{z(1-z)}\left[\frac{z}{1-z}+\frac{1-z}{z}+z(1-z)\right]. \tag{7.60}$$

After summing over all polarizations, the squared splitting function in transverse coordinate space reads

$$\sum \Psi^*_{g\to gg}(z,u')\Psi_{g\to gg}(z,u) = (2\pi)^2\frac{4}{p^+}\left[\frac{z}{1-z}+\frac{1-z}{z}+z(1-z)\right]\frac{u'\cdot u}{u'^2u^2}. \tag{7.61}$$

Now focus on the multiple scattering terms. Since all the particles involved in the process are gluons, all terms contain only Wilson lines in the adjoint representation. In the following explicit forms of the scattering terms are given with their respective large-N_c expressions in terms of fundamental Wilson lines.

$$\left\langle f_{ade}\left[W(x_1)W^\dagger(x_1')\right]^{db}\left[W(x_2)W^\dagger(x_2')\right]^{ec}f_{abc}\right\rangle_{x_g} \simeq \left\langle \mathrm{Tr}U^\dagger(x_1)U(x_1')\right\rangle_{x_g}\left\langle \mathrm{Tr}U(x_2)U^\dagger(x_2')\right\rangle_{x_g} \times \left\langle \mathrm{Tr}U(x_1)U^\dagger(x_1')U(x_2')U^\dagger(x_2)\right\rangle_{x_g}, \tag{7.62}$$

$$\left\langle f_{ade}W^{db}(x_1)W^{ec}(x_2)f_{fbc}W^{fa}(v')\right\rangle_{x_g} \simeq \left\langle \mathrm{Tr}U^\dagger(x_1)U(v')\right\rangle_{x_g}\left\langle \mathrm{Tr}U(x_2)U^\dagger(v')\right\rangle_{x_g} \times \left\langle \mathrm{Tr}U(x_1)U^\dagger(x_2)\right\rangle_{x_g}, \tag{7.63}$$

$$\left\langle f_{ade}W^{db}(x_1')W^{ec}(x_2')f_{fbc}W^{fa}(v)\right\rangle_{x_g} \simeq \left\langle \mathrm{Tr}U^\dagger(v)U(x_1')\right\rangle_{x_g}\left\langle \mathrm{Tr}U(v)U^\dagger(x_2')\right\rangle_{x_g} \times \left\langle \mathrm{Tr}U(x_2')U^\dagger(x_1')\right\rangle_{x_g}, \tag{7.64}$$

$$N_c\left\langle \mathrm{Tr}W(v)W^\dagger(v')\right\rangle_{x_g} \simeq N_c\left\langle \mathrm{Tr}U^\dagger(v)U(v')\right\rangle_{x_g}\left\langle \mathrm{Tr}U(v)U^\dagger(v')\right\rangle_{x_g} \tag{7.65}$$

The correlation limit is applied by following the procedure developed in the DIS case and reproduced in the $q\to qg$ channel. By inspection of the multiple scattering terms above, it is easy to see that the same kind of cancelations occur for this channel. Since the lowest order terms left after the various cancelations come from the first of the scattering terms, it is easy to see that the final result will involve combinations

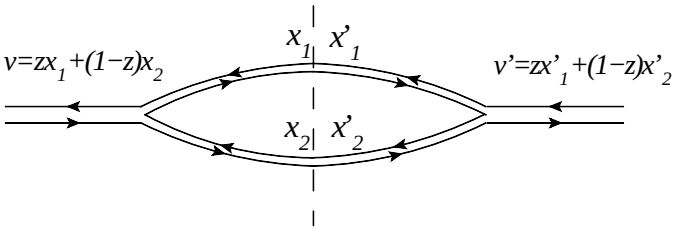

Figure 7.10: Graphical representation of the splitting $g \to gg$ in the large-N_c limit, in the amplitude and the conjugate amplitude.

of one WW distribution and two Fourier transforms of the dipole cross section.

$$\begin{aligned}\frac{d\sigma^{pA\to ggX}}{d\mathcal{P}.\mathcal{S}.} &= x_p g(x_p) 64\pi^3 \frac{\alpha_S^2}{P_\perp^4} z(1-z)\left[\frac{1-z}{z}+\frac{z}{1-z}+z(1-z)\right]\int \frac{d^3v}{(2\pi)^3}\frac{d^3v'}{(2\pi)^3}e^{-iq_\perp\cdot(v-v')} \\ &\times\left[\left(z^2+(1-z)^2\right)\frac{1}{N_c}\left\langle \mathrm{Tr}U(v)U^\dagger(v')\right\rangle_{x_g}\left\langle \mathrm{Tr}\left[F^{i-}(\vec{v})\mathcal{U}^{[+]\dagger}F^{i-}(\vec{v}')\mathcal{U}^{[-]}\right]\right\rangle_{x_g}\right. \\ &+\frac{1}{N_c}\left\langle \mathrm{Tr}U(v)U^\dagger(v')\right\rangle_{x_g}\frac{1}{N_c}\left\langle \mathrm{Tr}U(v')U^\dagger(v)\right\rangle_{x_g}\left\langle \mathrm{Tr}\left[F^{i-}(\vec{v})\mathcal{U}^{[+]\dagger}F^{i-}(\vec{v}')\mathcal{U}^{[+]}\right]\right\rangle_{x_g} \\ &\left.+2z(1-z)\frac{1}{N_c}\left\langle \mathrm{Tr}F^{i-}(\vec{v})U(v)U^\dagger(v')\right\rangle_{x_g}\frac{1}{N_c}\left\langle \mathrm{Tr}F^{i-}(\vec{v}')U(v')U^\dagger(v)\right\rangle_{x_g}\right], \quad (7.66)\end{aligned}$$

which is straightforward to compare to the factorized expression in (7.89).

This structure could have been anticipated by looking at the graphical representation of this process in the large-N_c limit shown in Fig. 7.10. In terms of the hard scattering picture used in previous sections the structure of the expression above is consistent with previous results. The first and third term look exactly the same as the two terms in the $g \to q\bar{q}$ case and they correspond to the case in which the hard scattering does not involve the inner loop in Fig. 7.10. The second term corresponds to the case where the hard scattering occurs in the inner loop. It has the same structure as one of the terms found in the $q \to qg$ case with an additional convolution associated to the extra quark line in the top of the diagram.

Table 7.1: The color and hard factors for the $qg \to qg$ scattering channels in Fig. 7.11, where $C_F = (N_c^2 - 1)/2N_c$.

	(1)	(2)	(3)	(4)	(5)	(6)
h	$-\frac{4(\hat{t}^2-\hat{s}\hat{u})^2}{\hat{t}^2\hat{s}\hat{u}}$	$-\frac{2(\hat{u}^2+\hat{t}^2)}{\hat{s}\hat{u}}$	$\frac{2(\hat{t}^2-\hat{s}\hat{u})(\hat{u}-\hat{t})}{\hat{s}\hat{t}\hat{u}}$	$-\frac{2(\hat{s}^2+\hat{t}^2)}{\hat{s}\hat{u}}$	$-\frac{2(\hat{t}^2-\hat{s}\hat{u})(\hat{s}-\hat{t})}{\hat{s}\hat{t}\hat{u}}$	$\frac{2\hat{t}^2}{\hat{s}\hat{u}}$
C_u	$\frac{1}{2}$	$\frac{C_F}{2N_c}$	$-\frac{1}{4}$	$\frac{C_F}{2N_c}$	$\frac{1}{4}$	$-\frac{1}{4N_c^2}$

7.3.2 TMD-factorization approach

7.3.2.1 The $qg \to qg$ channel

The calculations follow the previous examples. However, there are several different Feynman graphs contributing to the production of qg in the final state, as shown in Fig. 7.11. In addition, they have different color structures. Therefore, we need to compute the hard factors and the associated initial/final state interaction phases separately. In the end, we will sum their contributions together to obtain the final result.

It is straightforward to obtain the hard cross section contributions from each diagram in Fig. 7.11 for the $qg \to qg$ process, and have been calculated in Ref. [96; 97]. These results are listed in Table 7.1 with the same notations, where $h^{(i)}$ is the partonic hard factor and $C_u^{(i)}$ is the associated color factor. In the calculations, in order to apply the eikonal approximation when multiple gluon interactions are formulated, physical polarizations have been chosen for the outgoing gluon. However, the final result for the differential cross section does not depend on this choice.

As a consistency check, the known results for the total hard cross section are easily reproduced by summing all the graphs in Fig. 7.11 and explicitly taking $N_c = 3$,

$$\begin{aligned}\frac{\mathrm{d}\hat{\sigma}}{\mathrm{d}\hat{t}}(gq \to gq) &= \frac{g^4}{16\pi\hat{s}^2}\left\{\sum_{i=1,2,4} C_u^{(i)}h^{(i)} + 2\sum_{i=3,5,6} C_u^{(i)}h^{(i)}\right\} \\ &= \frac{g^4}{16\pi\hat{s}^2}\left(\frac{4}{9}\frac{\hat{s}^2+\hat{u}^2}{-\hat{s}\hat{u}} + \frac{\hat{s}^2+\hat{u}^2}{\hat{t}^2}\right) . \end{aligned} \tag{7.67}$$

Since the graphs in Fig. 7.11 have different color structure, the gluon distributions

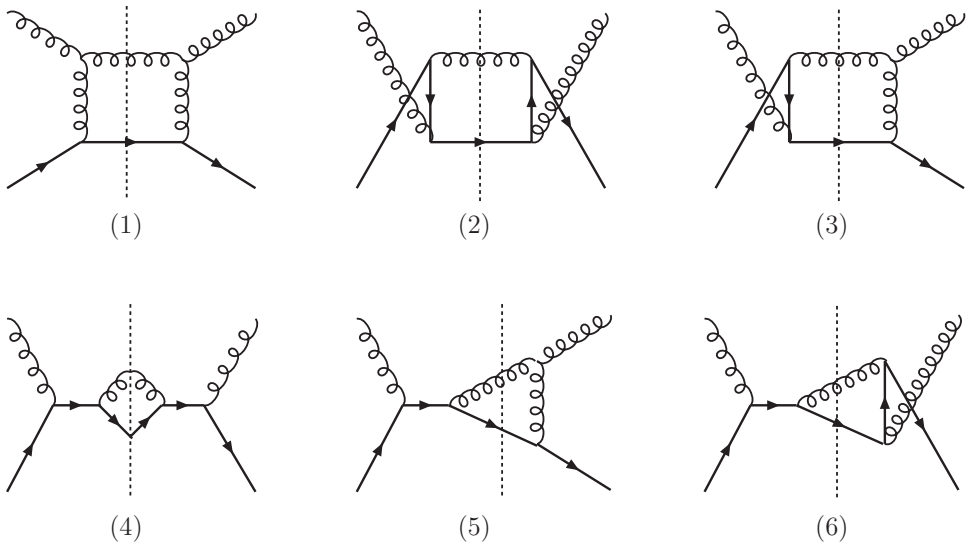

Figure 7.11: Quark-gluon scattering diagrams. The mirror diagrams of (3), (5) and (6) give identical contributions.

associated with those graphs have different gauge links according to Ref. [28]. Therefore, the corresponding gluon distributions in coordinate space are found as follows:

$$\Phi_g^{(1)} = \left\langle \mathrm{Tr}\left[F(\xi)\left\{\frac{1}{2}\frac{\mathrm{Tr}\left[\mathcal{U}^{[\square]}\right]}{N_c}\mathcal{U}^{[+]\dagger}+\frac{1}{2}\mathcal{U}^{[-]\dagger}\right\}F(0)\mathcal{U}^{[+]}\right]\right\rangle, \tag{7.68}$$

$$\Phi_g^{(2)} = \left\langle \mathrm{Tr}\left[F(\xi)\left\{\frac{N_c^2}{N_c^2-1}\frac{\mathrm{Tr}\left[\mathcal{U}^{[\square]}\right]}{N_c}\mathcal{U}^{[+]\dagger}-\frac{1}{N_c^2-1}\mathcal{U}^{[-]\dagger}\right\}F(0)\mathcal{U}^{[+]}\right]\right\rangle, \tag{7.69}$$

$$\Phi_g^{(3)} = \left\langle \mathrm{Tr}\left[F(\xi)\frac{\mathrm{Tr}\left[\mathcal{U}^{[\square]}\right]}{N_c}\mathcal{U}^{[+]\dagger}F(0)\mathcal{U}^{[+]}\right]\right\rangle, \tag{7.70}$$

$$\Phi_g^{(4),(5),(6)} = \left\langle \mathrm{Tr}\left[F(\xi)\mathcal{U}^{[-]\dagger}F(0)\mathcal{U}^{[+]}\right]\right\rangle, \tag{7.71}$$

where $\mathcal{U}^{[\square]} = \mathcal{U}^{[+]}\mathcal{U}^{[-]\dagger} = \mathcal{U}^{[-]\dagger}\mathcal{U}^{[+]}$ emerges as a Wilson loop. Now it is possible to combine all the channels together. The distributions above will be factorizable in terms of convolutions of the two basic distributions from the previous sections. Anticipating this result, only the leading contribution in N_c is considered. Noting that graph (6) in Fig 7.11 does not contribute in the large-N_c limit, one can find

$$\frac{d\sigma_{\mathrm{TMD}}^{qA\to qgX}}{d^2P_\perp d^2q_\perp dy_1 dy_2} = \sum_f x_p q(x_p)\frac{\alpha_s^2}{\hat{s}^2}\left[\mathcal{F}_{qg}^{(1)}H_{qg\to qg}^{(1)}+\mathcal{F}_{qg}^{(2)}H_{qg\to qg}^{(2)}\right], \tag{7.72}$$

with

$$\mathcal{F}_{qg}^{(1)} = xG^{(2)}(x,q_\perp) = 2\int \frac{d\xi^- d\xi_\perp}{(2\pi)^3 P^+} e^{ixP^+\xi^- - iq_\perp\cdot\xi_\perp} \left\langle \mathrm{Tr}\left[F(\xi)\mathcal{U}^{[-]\dagger}F(0)\mathcal{U}^{[+]}\right]\right\rangle, \quad (7.73)$$

$$\mathcal{F}_{qg}^{(2)} = 2\int \frac{d\xi^- d\xi_\perp}{(2\pi)^3 P^+} e^{ixP^+\xi^- - iq_\perp\cdot\xi_\perp} \left\langle \mathrm{Tr}\left[F(\xi)\frac{\mathrm{Tr}\left[\mathcal{U}^{[\square]}\right]}{N_c}\mathcal{U}^{[+]\dagger}F(0)\mathcal{U}^{[+]}\right]\right\rangle. \quad (7.74)$$

In the large-N_c limit, it is straightforward to find that only graphs (1), (2) and (3) in Fig. 7.11 (t and u channels together with their cross diagrams) contribute to $H_{qg\to qg}^{(2)}$ and only graphs (1), (4) and (5) (t and s channels together with their cross diagrams) contribute to $H_{qg\to qg}^{(1)}$. By using $\frac{C_F}{2N_c} = \frac{1}{4}$ in the large-N_c limit, one obtains

$$H_{qg\to qg}^{(1)} = -\frac{\left(\hat{t}^2-\hat{s}\hat{u}\right)^2}{\hat{s}\hat{u}\hat{t}^2} - \frac{1}{2}\frac{\hat{t}^2+\hat{s}^2}{\hat{s}\hat{u}} - \frac{\left(\hat{t}^2-\hat{s}\hat{u}\right)\left(\hat{s}-\hat{t}\right)}{\hat{s}\hat{u}\hat{t}} = -\frac{\hat{u}^2\left(\hat{s}^2+\hat{u}^2\right)}{2\hat{s}\hat{u}\hat{t}^2}, \quad (7.75)$$

$$H_{qg\to qg}^{(2)} = -\frac{\left(\hat{t}^2-\hat{s}\hat{u}\right)^2}{\hat{s}\hat{u}\hat{t}^2} - \frac{1}{2}\frac{\hat{t}^2+\hat{u}^2}{\hat{s}\hat{u}} - \frac{\left(\hat{t}^2-\hat{s}\hat{u}\right)\left(\hat{u}-\hat{t}\right)}{\hat{s}\hat{u}\hat{t}} = -\frac{\hat{s}^2\left(\hat{s}^2+\hat{u}^2\right)}{2\hat{s}\hat{u}\hat{t}^2} \quad (7.76)$$

Note that although the individual diagram's contribution to the above two hard factors depends on the polarization chosen for the outgoing gluon, the final results for the hard factors do not depend on this choice. This means the combination of Feynman graphs according to the relevant color structure is gauge invariant. Similar conclusion has also been obtained for the spin related observables calculated in Refs. [28; 96; 97].

Since one has $\hat{s} = \frac{P_\perp^2}{z(1-z)}$, $\hat{u} = -\frac{P_\perp^2}{z}$ and $\hat{t} = -\frac{P_\perp^2}{1-z}$ in the correlation limit, Eq. (7.72) leads to the following cross section for qg dijet production in pA collisions

$$\frac{d\sigma_{\mathrm{TMD}}^{pA\to qgX}}{d^2P_\perp d^2q_\perp dy_1 dy_2} = \sum_f x_p q_f(x_p)\frac{\alpha_s^2}{2P_\perp^4}\left[1+(1-z)^2\right](1-z)\left[(1-z)^2 xG^{(2)}(x,q_\perp)+\mathcal{F}_{qg}^{(2)}\right] \quad (7.77)$$

where $x_p q_f(x_p)$ is the integrated quark distribution for the proton projectile.

7.3.2.2 The $gg \to q\bar{q}$ channel

Following the same procedure illustrated in the $qg \to qg$ channel, the dijet production cross section can be calculated from the $gg \to q\bar{q}$ channel. First of all, the color factors

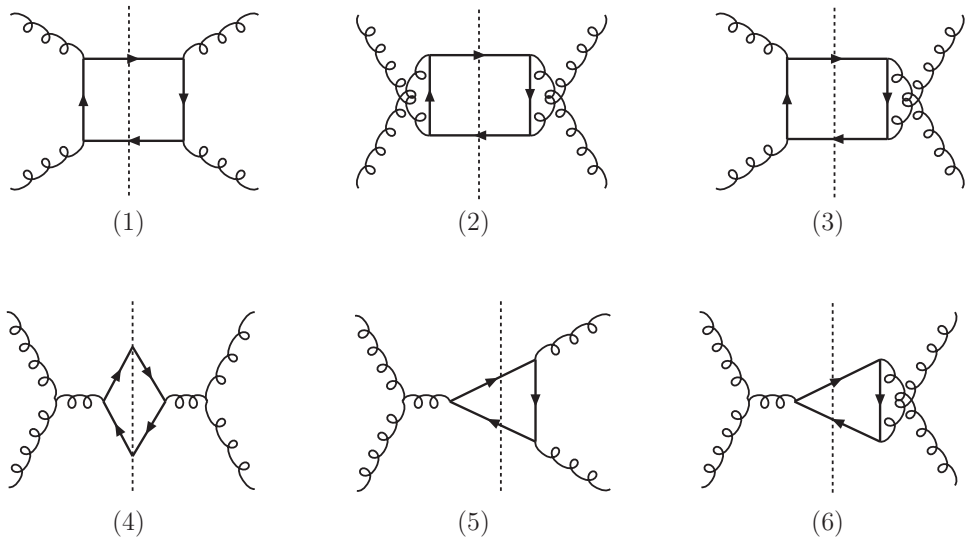

Figure 7.12: $gg \to q\bar{q}$ scattering diagrams. The mirror diagrams of (3), (5) and (6) give identical contributions.

Table 7.2: The color and hard factors for the $gg \to q\bar{q}$ scattering channels in Fig. 7.12.

	(1)	(2)	(3)	(4)	(5)	(6)
h	$\frac{2(3\hat{t}^2+\hat{u}^2)\hat{u}}{(\hat{t}+\hat{u})^2\hat{t}}$	$\frac{2(\hat{t}^2+3\hat{u}^2)\hat{t}}{(\hat{t}+\hat{u})^2\hat{u}}$	$\frac{2(\hat{t}-\hat{u})^2}{(\hat{t}+\hat{u})^2}$	$\frac{4\hat{t}\hat{u}}{(\hat{t}+\hat{u})^2}$	$-\frac{4\hat{t}\hat{u}}{(\hat{t}+\hat{u})^2}$	$\frac{4\hat{t}\hat{u}}{(\hat{t}+\hat{u})^2}$
C_u	$\frac{1}{4N_c}$	$\frac{1}{4N_c}$	$-\frac{1}{4N_c(N_c^2-1)}$	$\frac{N_c}{2(N_c^2-1)}$	$\frac{N_c}{4(N_c^2-1)}$	$-\frac{N_c}{4(N_c^2-1)}$

and hard factors are computed for each graph in Fig. 7.12 and listed in Table 7.2. Then, the appropriate gluon distributions[2] as found in Ref. [28] are plugged in.

$$\Phi_g^{(1),(2)} = \left\langle \mathrm{Tr}\left[F(\xi)\left\{\frac{\mathrm{Tr}\left[\mathcal{U}^{[\square]}\right]}{N_c}\mathcal{U}^{[-]\dagger}\right\}F(0)\,\mathcal{U}^{[+]}\right]\right\rangle, \tag{7.78}$$

$$\Phi_g^{(3)} = -N_c\left\langle \mathrm{Tr}\left[F(\xi)\,\mathcal{U}^{[\square]}\right]\mathrm{Tr}\left[F(0)\,\mathcal{U}^{[\square]\dagger}\right]\right\rangle, \tag{7.79}$$

$$\begin{aligned}\Phi_g^{(4),(5),(6)} = &\left\langle \mathrm{Tr}\left[F(\xi)\,\mathcal{U}^{[-]\dagger}F(0)\,\mathcal{U}^{[+]}\right]\frac{\mathrm{Tr}\left[\mathcal{U}^{[\square]}\right]}{N_c}\right\rangle \\ &-\frac{1}{N_c}\left\langle \mathrm{Tr}\left[F(\xi)\,\mathcal{U}^{[\square]}\right]\mathrm{Tr}\left[F(0)\,\mathcal{U}^{[\square]\dagger}\right]\right\rangle.\end{aligned} \tag{7.80}$$

[2]These gluon distributions have been simplified by using large-N_c limit and the fact that they are real in the CGC formalism.

Table 7.3: The color and hard factors for the $gg \to gg$ scattering channels in Fig. 7.13.

	h	C_u
(1)	$\frac{2(\hat{s}^4+4\hat{s}^3\hat{t}+11\hat{s}^2\hat{t}^2+10\hat{s}\hat{t}^3+4\hat{t}^4)}{(\hat{s}+\hat{t})^2\hat{s}^2}$	$\frac{N_c^2}{N_c^2-1}$
(2)	$\frac{2(2\hat{s}^6+6\hat{s}^5\hat{t}+14\hat{s}^4\hat{t}^2+20\hat{s}^3\hat{t}^3+21\hat{s}^2\hat{t}^4+14\hat{s}\hat{t}^5+4\hat{t}^6)}{(\hat{s}+\hat{t})^2\hat{s}^2\hat{t}^2}$	$\frac{N_c^2}{N_c^2-1}$
(3)	$-\frac{(2\hat{s}^4+5\hat{s}^3\hat{t}+10\hat{s}^2\hat{t}^2+10\hat{s}\hat{t}^3+4\hat{t}^4)(\hat{s}+2\hat{t})}{(\hat{s}+\hat{t})^2\hat{s}^2\hat{t}}$	$\frac{N_c^2}{2(N_c^2-1)}$
(4)	$\frac{2(\hat{s}^4+\hat{s}^3\hat{t}+5\hat{s}^2\hat{t}^2+6\hat{s}\hat{t}^3+2\hat{t}^4)}{(\hat{s}+\hat{t})^2\hat{s}^2}$	$\frac{N_c^2}{N_c^2-1}$
(5)	$\frac{2\hat{s}^5+\hat{s}^4\hat{t}-\hat{s}^3\hat{t}^2-10\hat{s}^2\hat{t}^3-12\hat{s}\hat{t}^4-4\hat{t}^5}{(\hat{s}+\hat{t})^2\hat{s}^2\hat{t}}$	$\frac{N_c^2}{2(N_c^2-1)}$
(6)	$\frac{(\hat{s}^3+10\hat{s}^2\hat{t}+12\hat{s}\hat{t}^2+4\hat{t}^3)t}{(\hat{s}+\hat{t})^2\hat{s}^2}$	$-\frac{N_c^2}{2(N_c^2-1)}$

Combining all the channels in the large N_c limit, one finds

$$\frac{d\sigma_{\rm TMD}^{gA\to q\bar{q}X}}{d^2P_\perp d^2q_\perp dy_1 dy_2} = \sum_f x_p g(x_p) \frac{\alpha_s^2}{\hat{s}^2} \left[\mathcal{F}_{gg}^{(1)} H_{gg\to q\bar{q}}^{(1)} + \mathcal{F}_{gg}^{(2)} H_{gg\to q\bar{q}}^{(2)}\right], \tag{7.81}$$

with

$$\mathcal{F}_{gg}^{(1)} = 2\int \frac{d\xi^- d\xi_\perp}{(2\pi)^3 P^+} e^{ixP^+\xi^- - iq_\perp\cdot\xi_\perp} \left\langle \mathrm{Tr}\left[F(\xi)\frac{\mathrm{Tr}\left[\mathcal{U}^{[\square]}\right]}{N_c}\mathcal{U}^{[-]\dagger}F(0)\mathcal{U}^{[+]}\right]\right\rangle \tag{7.82}$$

$$\mathcal{F}_{gg}^{(2)} = 2\int \frac{d\xi^- d\xi_\perp}{(2\pi)^3 P^+} e^{ixP^+\xi^- - iq_\perp\cdot\xi_\perp} \frac{1}{N_c} \left\langle \mathrm{Tr}\left[F(\xi)\mathcal{U}^{[\square]\dagger}\right]\mathrm{Tr}\left[F(0)\mathcal{U}^{[\square]}\right]\right\rangle , \tag{7.83}$$

and

$$H_{gg\to q\bar{q}}^{(1)} = \frac{1}{4N_c}\frac{2\left(\hat{t}^2+\hat{u}^2\right)^2}{\hat{s}^2\hat{u}\hat{t}} , \tag{7.84}$$

$$H_{gg\to q\bar{q}}^{(2)} = \frac{1}{4N_c}\frac{4\left(\hat{t}^2+\hat{u}^2\right)}{\hat{s}^2}, \tag{7.85}$$

where $x_p g(x_p)$ is the integrated gluon distribution in the proton projectile.

7.3.2.3 The $gg \to gg$ channel

Similarly, the color factors and hard factors for all the graphs plotted in Fig. 7.13 have been calculated and listed in Table 7.3. Combining these factors with the corresponding gluon distributions, taking into account the appropriate gauge links [28],

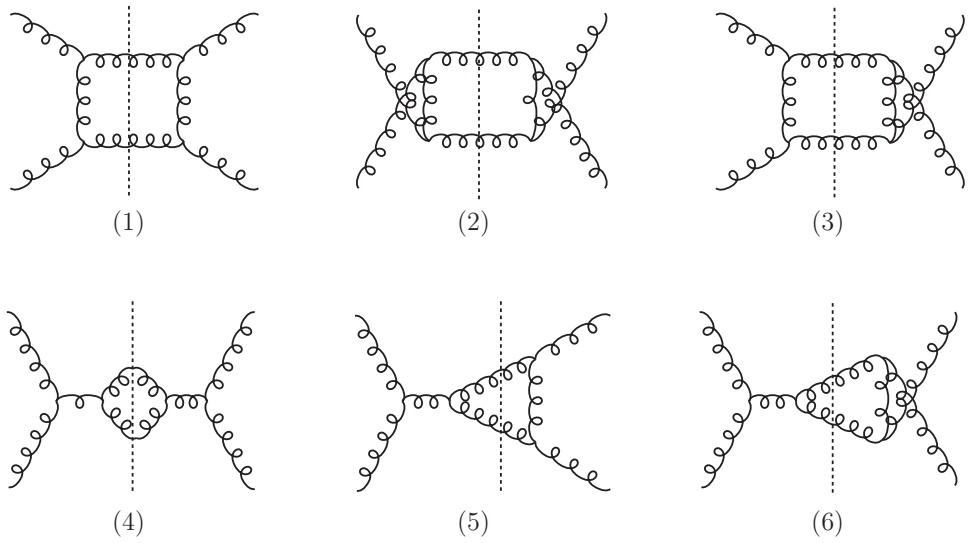

Figure 7.13: $gg \to gg$ scattering diagrams. The mirror diagrams of (3), (5) and (6) give identical contributions.

one arrives at

$$\begin{aligned}
\Phi_g^{(1),(2)} &= \frac{1}{2}\left\langle \mathrm{Tr}\left[F(\xi)\mathcal{U}^{[+]\dagger}F(0)\mathcal{U}^{[+]}\right]\frac{\mathrm{Tr}\left[\mathcal{U}^{[\square]}\right]}{N_c}\frac{\mathrm{Tr}\left[\mathcal{U}^{[\square]}\right]}{N_c}\right\rangle \\
&\quad + \left\langle \mathrm{Tr}\left[F(\xi)\mathcal{U}^{[-]\dagger}F(0)\mathcal{U}^{[+]}\right]\frac{\mathrm{Tr}\left[\mathcal{U}^{[\square]}\right]}{N_c}\right\rangle, \qquad (7.86)\\
\Phi_g^{(3)} &= \left\langle \mathrm{Tr}\left[F(\xi)\mathcal{U}^{[+]\dagger}F(0)\mathcal{U}^{[+]}\right]\frac{\mathrm{Tr}\left[\mathcal{U}^{[\square]}\right]}{N_c}\frac{\mathrm{Tr}\left[\mathcal{U}^{[\square]}\right]}{N_c}\right\rangle \\
&\quad + \frac{1}{N_c}\left\langle \mathrm{Tr}\left[F(\xi)\mathcal{U}^{[\square]}\right]\mathrm{Tr}\left[F(0)\mathcal{U}^{[\square]\dagger}\right]\right\rangle, \qquad (7.87)\\
\Phi_g^{(4),(5),(6)} &= \left\langle \mathrm{Tr}\left[F(\xi)\mathcal{U}^{[-]\dagger}F(0)\mathcal{U}^{[+]}\right]\frac{\mathrm{Tr}\left[\mathcal{U}^{[\square]}\right]}{N_c}\right\rangle \\
&\quad - \frac{1}{N_c}\left\langle \mathrm{Tr}\left[F(\xi)\mathcal{U}^{[\square]}\right]\mathrm{Tr}\left[F(0)\mathcal{U}^{[\square]\dagger}\right]\right\rangle. \qquad (7.88)
\end{aligned}$$

Summing over all the channels in the large-N_c limit, one obtains

$$\frac{d\sigma_{\mathrm{TMD}}^{gA\to ggX}}{d^2P_\perp d^2q_\perp dy_1 dy_2} = \sum_f x_p g(x_p)\frac{\alpha_s^2}{\hat{s}^2}\left[\mathcal{F}_{gg}^{(1)}H_{gg\to gg}^{(1)} + \mathcal{F}_{gg}^{(2)}H_{gg\to gg}^{(2)} + \mathcal{F}_{gg}^{(3)}H_{gg\to gg}^{(3)}\right], \quad (7.89)$$

where $\mathcal{F}_{gg}^{(1,2)}$ have been defined in Eqs. (7.82,7.83) and $\mathcal{F}_{gg}^{(3)}$ is defined as

$$\mathcal{F}_{gg}^{(3)} = 2\int \frac{d\xi^- d\xi_\perp}{(2\pi)^3 P^+} e^{ixP^+\xi^- - iq_\perp\cdot\xi_\perp} \left\langle \mathrm{Tr}\left[F\left(\xi\right)\mathcal{U}^{[-]\dagger}F\left(0\right)\mathcal{U}^{[+]}\right]\frac{\mathrm{Tr}\left[\mathcal{U}^{[\square]}\right]}{N_c}\frac{\mathrm{Tr}\left[\mathcal{U}^{[\square]}\right]}{N_c}\right\rangle \quad (7.90)$$

The hard factors are found as

$$\begin{aligned} H_{gg\to gg}^{(1)} &= \frac{2\left(\hat{t}^2+\hat{u}^2\right)\left(\hat{s}^2-\hat{t}\hat{u}\right)^2}{\hat{u}^2\hat{t}^2\hat{s}^2}, \quad H_{gg\to gg}^{(2)} = \frac{4\left(\hat{s}^2-\hat{t}\hat{u}\right)^2}{\hat{u}\hat{t}\hat{s}^2}\ , \\ H_{gg\to gg}^{(3)} &= \frac{2\left(\hat{s}^2-\hat{t}\hat{u}\right)^2}{\hat{u}^2\hat{t}^2}. \end{aligned} \quad (7.91)$$

Using the mean field approximation [82], one can simplify the gluon distributions and find the total dijet production cross section which includes the $qg \to qg$, $gg \to q\bar{q}$ and $gg \to gg$ channels as follows

$$\begin{aligned} \frac{d\sigma^{(pA\to\mathrm{Dijet}+X)}}{d\mathcal{P}.\mathcal{S}.} &= \sum_q x_1 q(x_1)\frac{\alpha_s^2}{\hat{s}^2}\left[\mathcal{F}_{qg}^{(1)}H_{qg\to qg}^{(1)} + \mathcal{F}_{qg}^{(2)}H_{qg\to qg}^{(2)}\right] \\ &\quad + x_1 g(x_1)\frac{\alpha_s^2}{\hat{s}^2}\left[\mathcal{F}_{gg}^{(1)}\left(H_{gg\to q\bar{q}}^{(1)} + \frac{1}{2}H_{gg\to gg}^{(1)}\right)\right. \\ &\quad \left. + \mathcal{F}_{gg}^{(2)}\left(H_{gg\to q\bar{q}}^{(2)} + \frac{1}{2}H_{gg\to gg}^{(2)}\right) + \frac{1}{2}\mathcal{F}_{gg}^{(3)}H_{gg\to gg}^{(3)}\right]\ , \end{aligned} \quad (7.92)$$

where again $q(x_1)$ and $g(x_1)$ are integrated quark and gluon distributions from the projectile nucleon. A statistical factor of $\frac{1}{2}$ has been included in Eq. (7.92) for the $gg \to gg$ channel due to the identical final state. The various gluon distributions of nucleus A are defined as

$$\begin{aligned} \mathcal{F}_{qg}^{(1)} &= xG^{(2)}(x,q_\perp), \quad \mathcal{F}_{qg}^{(2)} = \int xG^{(1)}(q_1)\otimes F(q_2)\ , \\ \mathcal{F}_{gg}^{(1)} &= \int xG^{(2)}(q_1)\otimes F(q_2), \quad \mathcal{F}_{gg}^{(2)} = -\int \frac{q_{1\perp}\cdot q_{2\perp}}{q_{1\perp}^2} xG^{(2)}(q_1)\otimes F(q_2)\ , \\ \mathcal{F}_{gg}^{(3)} &= \int xG^{(1)}(q_1)\otimes F(q_2)\otimes F(q_3)\ , \end{aligned} \quad (7.93)$$

where $\otimes$ represents the convolution in momentum space: $\int\otimes = \int d^2q_1 d^2q_2 \delta^{(2)}(q_\perp - q_1 - q_2)$. These expressions follow directly from Eqs. (7.73), (7.74), (7.82), (7.83), (7.90) and the assumption that in the large-N_c limit the expectation values involved

in these equations can be factored as products of expectation values of the traces within. Clearly, this process depends on both UGDs in a complicated way, and the naive TMD-factorization does not hold.

Chapter 8

Evolution

This chapter gives a first attempt to understand the small-x evolution of the distributions mentioned in the previous chapters. This is still work in progress and more detailed analysis are necessary to be able to use this formalism for specific phenomenological applications.

The way that all the calculations have been set in the CGC framework, all the evolution is put in the correlators which are calculated with a particular weight function at a certain value of x determined by the kinematics of the process. In the spirit of the always present large-N_c limit taken all over the presentation of the previous chapters this correlators, and their respective evolution, can be evaluated independently. Therefore all that is needed to understand the small-x evolution of the different distributions quoted before is to study the evolution of the basic distributions of chapter 5.

First consider the dipole distribution. Since it is expressed in terms of a correlator of two Wilson lines, its evolution can be determined entirely by the BK equation, at least in the large-N_c approximation in which it is valid and has been used throughout this work. Since this equation has been widely studied in the literature and its behavior is already known even including part of the next to leading order terms, it will not be discussed here.

On the other hand, not much has been said about the full small-x evolution of the WW distribution including nonlinear effects. In very specific cases, it has been shown that, to leading order in the sources (the linear regime), a BFKL-like equation can be recovered when considering occupation numbers of gluons in light-cone gauge. A more systematic study using the techniques provided by the CGC framework is therefore necessary. The way to proceed is to take advantage of the specific operator definition shown for the WW distribution in chapter 5 to put to use the JIMWLK equation.

8.1 Quadrupole evolution

As it is seen directly from the derivation of the factorized version of the dijet process in DIS, the correlator involved in the operator definition of the WW distribution is directly related to the quadrupole term defined as the average of the trace of four Wilson lines at different coordinates. Applying the JIMWLK equation to such operator one obtains:

$$
\begin{aligned}
&\frac{\partial}{\partial Y}\left\langle \mathrm{Tr}\left[U(x_1)U^\dagger(x_1')U(x_2)U^\dagger(x_2')\right]\right\rangle_Y \\
= \;& -\frac{\alpha_s N_c}{(2\pi)^2}\int d^2z_\perp \mathcal{K}_1(x_1,x_1',x_2,x_2';z)\left\langle \mathrm{Tr}\left[U(x_1)U^\dagger(x_1')U(x_2)U^\dagger(x_2')\right]\right\rangle_Y \\
&+\frac{\alpha_s N_c}{(2\pi)^2}\int d^2z_\perp \mathcal{A}(x_1,x_1',x_2,x_2';z)\frac{1}{N_c}\left\langle \mathrm{Tr}\left[U^\dagger(x_1')U(x_2)\right]\mathrm{Tr}\left[U^\dagger(x_2')U(x_1)\right]\right\rangle_Y \\
&+\frac{\alpha_s N_c}{(2\pi)^2}\int d^2z_\perp \mathcal{B}(x_1,x_1',x_2,x_2';z)\frac{1}{N_c}\left\langle \mathrm{Tr}\left[U(x_1)U^\dagger(x_1')\right]\mathrm{Tr}\left[U(x_2)U^\dagger(x_2')\right]\right\rangle_Y \\
&+\frac{\alpha_s N_c}{(2\pi)^2}\int d^2z_\perp \mathcal{K}_2(x_1;x_1',x_2';z)\frac{1}{N_c}\left\langle \mathrm{Tr}\left[U(x_1)U^\dagger(z)\right]\mathrm{Tr}\left[U(z)U^\dagger(x_1')U(x_2)U^\dagger(x_2')\right]\right\rangle_Y \\
&+\frac{\alpha_s N_c}{(2\pi)^2}\int d^2z_\perp \mathcal{K}_2(x_1';x_1,x_2;z)\frac{1}{N_c}\left\langle \mathrm{Tr}\left[U(z)U^\dagger(x_1')\right]\mathrm{Tr}\left[U(x_1)U^\dagger(z)U(x_2)U^\dagger(x_2')\right]\right\rangle_Y \\
&+\frac{\alpha_s N_c}{(2\pi)^2}\int d^2z_\perp \mathcal{K}_2(x_2;x_1',x_2';z)\frac{1}{N_c}\left\langle \mathrm{Tr}\left[U(x_2)U^\dagger(z)\right]\mathrm{Tr}\left[U(x_1)U^\dagger(x_1')U(z)U^\dagger(x_2')\right]\right\rangle_Y \\
&+\frac{\alpha_s N_c}{(2\pi)^2}\int d^2z_\perp \mathcal{K}_2(x_2';x_1,x_2;z)\frac{1}{N_c}\left\langle \mathrm{Tr}\left[U(z)U^\dagger(x_2')\right]\mathrm{Tr}\left[U(x_1)U^\dagger(x_1')U(x_2)U^\dagger(z)\right]\right\rangle_Y
\end{aligned}
\tag{8.1}
$$

where

$$\mathcal{K}_1(x_1,x_1',x_2,x_2';z) = \frac{(x_1'-x_1)^2}{(x_1'-z)^2(z-x_1)^2}+\frac{(x_2'-x_2)^2}{(x_2'-z)^2(z-x_2)^2}+\frac{(x_1'-x_2)^2}{(x_1'-z)^2(z-x_2)^2} + \frac{(x_2'-x_1)^2}{(x_2'-z)^2(z-x_1)^2}, \tag{8.2}$$

$$\mathcal{A}(x_1,x_1',x_2,x_2';z) = \frac{(x_1'-x_2')^2}{(x_1'-z)^2(z-x_2')^2}+\frac{(x_1-x_2)^2}{(x_1-z)^2(z-x_2)^2}-\frac{(x_1'-x_2)^2}{(x_1'-z)^2(z-x_2)^2} - \frac{(x_2'-x_1)^2}{(x_2'-z)^2(z-x_1)^2}, \tag{8.3}$$

$$\mathcal{B}(x_1,x_1',x_2,x_2';z) = \frac{(x_1'-x_2')^2}{(x_1'-z)^2(z-x_2')^2}+\frac{(x_1-x_2)^2}{(x_1-z)^2(z-x_2)^2}-\frac{(x_2'-x_2)^2}{(x_2'-z)^2(z-x_2)^2} - \frac{(x_1'-x_1)^2}{(x_1'-z)^2(z-x_1)^2}, \tag{8.4}$$

$$\mathcal{K}_2(x_1;x_1',x_2';z) = \frac{(x_1-x_1')^2}{(x_1-z)^2(z-x_1')^2}+\frac{(x_1-x_2')^2}{(x_1-z)^2(z-x_2')^2}-\frac{(x_1'-x_2')^2}{(x_1'-z)^2(z-x_2')^2} \tag{8.5}$$

Eq. (8.1) suffers the same problem as Eq. (4.32) in the sense that it is not a closed equation because the right hand side includes higher-point correlations. The way to deal with this difficulty is the same as for the BK equation assuming that, for a large nucleus, these correlators can be factored as products of correlators involving only one trace at a time when the large-N_c limit is taken. The resulting equation is equivalent to the quadrupole evolution equation found in Ref. [89] which was derived considering only the leading N_c contributions from the beginning. In other words, the full evolution equation has no terms which are explicitly suppressed by powers of $1/N_c$ and taking the large-N_c limit only has the effect of allowing the aforementioned factorization of the correlators. This was also the case for the BK equation [47].

8.2 WW distribution evolution

The operator definition of the WW gluon distribution is given by a slightly different operator which can be obtained from the quadrupole correlator. As seen in chapter

5, the WW gluon distribution can be written as

$$xG^{(1)}(x,k_\perp) = -\frac{2}{\alpha_s}\int \frac{d^2v}{(2\pi)^2}\frac{d^2v'}{(2\pi)^2}\, e^{-ik_\perp\cdot(v-v')}\left\langle \mathrm{Tr}\left[\partial_i U(v)\right] U^\dagger(v')\left[\partial_i U(v')\right] U^\dagger(v)\right\rangle_Y . \tag{8.6}$$

The evolution equation for the correlator $\left\langle \mathrm{Tr}\left[\partial_i U(v)\right] U^\dagger(v')\left[\partial_i U(v')\right] U^\dagger(v)\right\rangle_Y$ can be obtained from Eq. (8.1) by differentiating with respect to x_1 and x_2, and then setting $x_1 = x_2' = v$ and $x_2 = x_1' = v'$. Then the resulting evolution equation becomes

$$\begin{aligned}
&\frac{\partial}{\partial Y}\left\langle \mathrm{Tr}\left[\partial_i U(v)\right] U^\dagger(v')\left[\partial_i U(v')\right] U^\dagger(v)\right\rangle_Y \\
= \;& -\frac{\alpha_s N_c}{2\pi^2}\int d^2z_\perp \frac{(v-v')^2}{(v-z)^2(z-v')^2}\left\langle \mathrm{Tr}\left[\partial_i U(v)\right] U^\dagger(v')\left[\partial_i U(v')\right] U^\dagger(v)\right\rangle_Y \\
& -\frac{\alpha_s N_c}{2\pi^2}\int d^2z_\perp \frac{1}{N_c}\frac{(v-v')^2}{(v-z)^2(z-v')^2}\left[\frac{(v-v')_i}{(v-v')^2}-\frac{(v-z)_i}{(v-z)^2}\right] \\
& \quad\times\Big\{\left\langle \mathrm{Tr}\left[U(v)U^\dagger(v')\left[\partial_i U(v')\right] U^\dagger(z)\right]\mathrm{Tr}\left[U(z)U^\dagger(v)\right]\right\rangle_Y \\
& \qquad -\left\langle \mathrm{Tr}\left[U(z)U^\dagger(v')\left[\partial_i U(v')\right] U^\dagger(v)\right]\mathrm{Tr}\left[U(v)U^\dagger(z)\right]\right\rangle_Y\Big\} \\
& -\frac{\alpha_s N_c}{2\pi^2}\int d^2z_\perp \frac{1}{N_c}\frac{(v-v')^2}{(v-z)^2(z-v')^2}\left[\frac{(v'-v)_i}{(v'-v)^2}-\frac{(v'-z)_i}{(v'-z)^2}\right] \\
& \quad\times\Big\{\left\langle \mathrm{Tr}\left[\left[\partial_i U(v)\right] U^\dagger(z)U(v')U^\dagger(v)\right]\mathrm{Tr}\left[U(z)U^\dagger(v')\right]\right\rangle_Y \\
& \qquad -\left\langle \mathrm{Tr}\left[\left[\partial_i U(v)\right] U^\dagger(v')U(z)U^\dagger(v)\right]\mathrm{Tr}\left[U(v')U^\dagger(z)\right]\right\rangle_Y\Big\} \\
& -\frac{\alpha_s N_c}{\pi^2}\int d^2z_\perp \frac{1}{N_c}\frac{1}{(v-z)^2(z-v')^2}\left[1-\frac{2\left((v-z)\cdot(z-v')\right)^2}{(v-z)^2(z-v')^2}\right] \\
& \quad\times\Big\{\left\langle \mathrm{Tr}\left[U(v')U^\dagger(z)\right]\mathrm{Tr}\left[U(z)U^\dagger(v')\right]\right\rangle_Y + \left\langle \mathrm{Tr}\left[U(v)U^\dagger(z)\right]\mathrm{Tr}\left[U(z)U^\dagger(v)\right]\right\rangle_Y \\
& \qquad -\left\langle \mathrm{Tr}\left[U(v')U^\dagger(v)\right]\mathrm{Tr}\left[U(v)U^\dagger(v')\right]\right\rangle_Y - N_c^2\Big\} .
\end{aligned} \tag{8.7}$$

Among these four terms in Eq. (8.7), the second and third terms are quite troublesome since they introduce new correlators involving three coordinates. The first term can be understood as the virtual correction as analogous to the first term in the BK equation. The last term is in agreement with the results obtained from the one-loop calculation in Ref. [79] in the setup where the WW distribution appear directly from a process with a fictitious colorless current.

In addition, it is found that one will inevitably run into the evolution of quadrupoles irrespective of the initial conditions when the WW gluon distribution appears in the

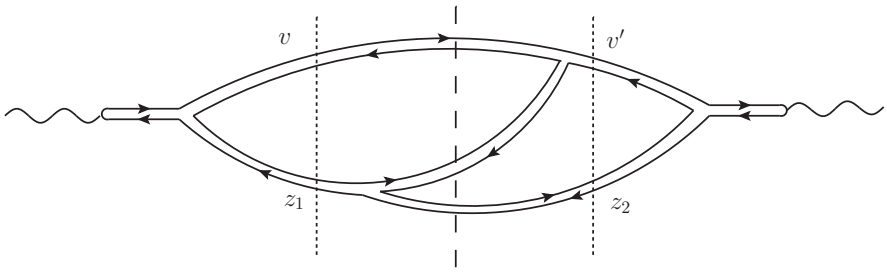

Figure 8.1: Illustration of two-step evolution which generates the quadruple amplitude. The dotted lines indicate the moments of the interaction with the target nucleus and the dashed line represents the cut. The two dipoles correspond to the two internal color lines, and are characterized by the coordinates (z_1, v) and (v', z_2) respectively at the time of the interaction. The single external color line interacts as a quadrupole defined by the coordinates (v, z_1, z_2, v').

process before small-x evolution is included. As far as the WW gluon distribution is concerned, one finds that after two steps of evolution, the contribution of quadrupoles appears as the following S-matrix amplitude

$$\frac{1}{N_c}\mathrm{Tr}\left[U(z_1)U^\dagger(z_2)U(v')U^\dagger(v)\right]\frac{1}{N_c}\mathrm{Tr}\left[U(v)U^\dagger(z_1)\right]\frac{1}{N_c}\mathrm{Tr}\left[U(z_2)U^\dagger(v')\right] \tag{8.8}$$

Starting from the correlator $\left\langle \mathrm{Tr}\left[\partial_i U(v)\right] U^\dagger(v')\left[\partial_i U(v')\right] U^\dagger(v)\right\rangle_Y$, the first step of evolution is given by Eq. (8.7) which generates terms like

$$\left\langle \mathrm{Tr}\left[U(z_1)U^\dagger(v')\left[\partial_i U(v')\right] U^\dagger(v)\right]\mathrm{Tr}\left[U(v)U^\dagger(z_1)\right]\right\rangle_Y . \tag{8.9}$$

One can further evolve such object and find that the second step of evolution yields a combination of a quadrupole plus two dipoles as in Eq. (8.8). In terms of the picture introduced to justify the presence of the WW distribution in the DIS dijet process, the above terms are illustrated in Fig. 8.1 where the double lines at v and v' have the highest longitudinal momentum, the double line at z_1 has the next highest longitudinal momentum and the double line at z_2 has the smallest longitudinal momentum. Fig. 8.1 and its radiative corrections are characterized by the

feature that the double line in the middle does not directly connect to the virtual photons. By squaring the production amplitude, one gets the basic color and spatial structure of a quadrupole $\frac{1}{N_c}\mathrm{Tr}\left[U(z_1)U^\dagger(z_2)U(v')U^\dagger(v)\right]$ together with two dipoles $\frac{1}{N_c}\mathrm{Tr}\left[U(v)U^\dagger(z_1)\right]$ and $\frac{1}{N_c}\mathrm{Tr}\left[U(z_2)U^\dagger(v')\right]$ before further evolution. This shows that the Weizsäcker-Williams distribution does not have a closed evolution equation on its own and, despite its apparently simpler structure in terms of only two coordinates, the full quadrupole evolution is needed to include small-x effects.

Bibliography

[1] A. D. Martin, W. J. Stirling, R. S. Thorne, and G. Watt, "Parton distributions for the LHC," *Eur. Phys. J.*, vol. C63, pp. 189–285, 2009.

[2] K. Nakamura *et al.*, "Review of particle physics," *J.Phys.G*, vol. G37, p. 075021, 2010.

[3] F. Dominguez, B.-W. Xiao, and F. Yuan, "k_t-factorization for Hard Processes in Nuclei," *Phys.Rev.Lett.*, vol. 106, p. 022301, 2011.

[4] F. Dominguez, C. Marquet, B.-W. Xiao, and F. Yuan, "Universality of Unintegrated Gluon Distributions at Small x," *Phys.Rev.*, vol. D83, p. 105005, 2011.

[5] F. Dominguez, A. H. Mueller, S. Munier, and B.-W. Xiao, "On the small-x evolution of the color quadrupole and the Weizsácker-Williams gluon distribution," 2011.

[6] J. Collins, *Foundations of Perturbative QCD*. Cambridge University Press, 2011.

[7] R. Brock *et al.*, "Handbook of perturbative QCD: Version 1.0," *Rev.Mod.Phys.*, vol. 67, pp. 157–248, 1995.

[8] A. H. Mueller, "Perturbative QCD at High-Energies," *Phys.Rept.*, vol. 73, p. 237, 1981.

[9] R. K. Ellis, W. J. Stirling, and B. R. Webber, *QCD and Collider Physics*. Cambridge University Press, 1996.

[10] W. Greiner, S. Schramm, and E. Stein, *Quantum Chromodynamics*. Springer, 2007.

[11] H. Politzer, "Reliable Perturbative Results for Strong Interactions?," *Phys.Rev.Lett.*, vol. 30, pp. 1346–1349, 1973.

[12] D. Gross and F. Wilczek, "Ultraviolet Behavior of Nonabelian Gauge Theories," *Phys.Rev.Lett.*, vol. 30, pp. 1343–1346, 1973.

[13] N. Nielsen, "ASYMPTOTIC FREEDOM AS A SPIN EFFECT," *Am.J.Phys.*, vol. 49, p. 1171, 1981.

[14] S. J. Brodsky, H.-C. Pauli, and S. S. Pinsky, "Quantum chromodynamics and other field theories on the light cone," *Phys.Rept.*, vol. 301, pp. 299–486, 1998.

[15] G. P. Lepage and S. J. Brodsky, "Exclusive processes in perturbative quantum chromodynamics," *Phys. Rev. D*, vol. 22, pp. 2157–2198, Nov 1980.

[16] L. Lipatov, "The parton model and perturbation theory," *Sov.J.Nucl.Phys.*, vol. 20, pp. 94–102, 1975.

[17] V. Gribov and L. Lipatov, "Deep inelastic e p scattering in perturbation theory," *Sov.J.Nucl.Phys.*, vol. 15, pp. 438–450, 1972.

[18] G. Altarelli and G. Parisi, "Asymptotic Freedom in Parton Language," *Nucl.Phys.*, vol. B126, p. 298, 1977.

[19] Y. L. Dokshitzer, "Calculation of the Structure Functions for Deep Inelastic Scattering and e+ e- Annihilation by Perturbation Theory in Quantum Chromodynamics.," *Sov.Phys.JETP*, vol. 46, pp. 641–653, 1977.

[20] E. Kuraev, L. Lipatov, and V. S. Fadin, "The Pomeranchuk Singularity in Nonabelian Gauge Theories," *Sov.Phys.JETP*, vol. 45, pp. 199–204, 1977.

[21] E. Kuraev, L. Lipatov, and V. S. Fadin, "Multi - Reggeon Processes in the Yang-Mills Theory," *Sov.Phys.JETP*, vol. 44, pp. 443–450, 1976.

[22] V. S. Fadin, E. Kuraev, and L. Lipatov, "On the Pomeranchuk Singularity in Asymptotically Free Theories," *Phys.Lett.*, vol. B60, pp. 50–52, 1975.

[23] I. Balitsky and L. Lipatov, "The Pomeranchuk Singularity in Quantum Chromodynamics," *Sov.J.Nucl.Phys.*, vol. 28, pp. 822–829, 1978.

[24] J. C. Collins, D. E. Soper, and G. F. Sterman, "Factorization of Hard Processes in QCD," *Adv.Ser.Direct.High Energy Phys.*, vol. 5, pp. 1–91, 1988. To be publ. in 'Perturbative QCD' (A.H. Mueller, ed.) (World Scientific Publ., 1989).

[25] J. C. Collins and D. E. Soper, "Parton Distribution and Decay Functions," *Nucl.Phys.*, vol. B194, p. 445, 1982.

[26] C. Bomhof, P. Mulders, and F. Pijlman, "Gauge link structure in quark-quark correlators in hard processes," *Phys.Lett.*, vol. B596, pp. 277–286, 2004.

[27] A. Bacchetta, C. Bomhof, P. Mulders, and F. Pijlman, "Single spin asymmetries in hadron-hadron collisions," *Phys.Rev.*, vol. D72, p. 034030, 2005.

[28] C. Bomhof, P. Mulders, and F. Pijlman, "The construction of gauge-links in arbitrary hard processes," *Eur.Phys.J.*, vol. C47, pp. 147–162, 2006.

[29] A. V. Belitsky, X. Ji, and F. Yuan, "Final state interactions and gauge invariant parton distributions," *Nucl.Phys.*, vol. B656, pp. 165–198, 2003.

[30] J. Collins and J.-W. Qiu, "k_T factorization is violated in production of high-transverse-momentum particles in hadron-hadron collisions," *Phys.Rev.*, vol. D75, p. 114014, 2007.

[31] T. C. Rogers and P. J. Mulders, "No generalized TMD-factorization in hadroproduction of high transverse momentum hadrons," *Phys.Rev.*, vol. D81, p. 094006, 2010.

[32] S. Catani, M. Ciafaloni, and F. Hautmann, "High-energy factorization and small x heavy flavor production," *Nucl.Phys.*, vol. B366, pp. 135–188, 1991.

[33] E. Iancu, A. Leonidov, and L. McLerran, "The Color glass condensate: An Introduction," pp. 73–145, 2002.

[34] E. Iancu and R. Venugopalan, "The Color glass condensate and high-energy scattering in QCD," 2003.

[35] F. Gelis, E. Iancu, J. Jalilian-Marian, and R. Venugopalan, "The Color Glass Condensate," *Ann.Rev.Nucl.Part.Sci.*, vol. 60, pp. 463–489, 2010.

[36] J. Jalilian-Marian and Y. V. Kovchegov, "Saturation physics and deuteron-Gold collisions at RHIC," *Prog.Part.Nucl.Phys.*, vol. 56, pp. 104–231, 2006.

[37] H. Weigert, "Evolution at small x(bj): The Color glass condensate," *Prog.Part.Nucl.Phys.*, vol. 55, pp. 461–565, 2005.

[38] L. Gribov, E. Levin, and M. Ryskin, "Semihard Processes in QCD," *Phys.Rept.*, vol. 100, pp. 1–150, 1983.

[39] A. H. Mueller and J.-w. Qiu, "Gluon Recombination and Shadowing at Small Values of x," *Nucl.Phys.*, vol. B268, p. 427, 1986.

[40] M. Froissart, "Asymptotic behavior and subtractions in the Mandelstam representation," *Phys.Rev.*, vol. 123, pp. 1053–1057, 1961.

[41] A. H. Mueller, "Soft gluons in the infinite momentum wave function and the BFKL pomeron," *Nucl.Phys.*, vol. B415, pp. 373–385, 1994.

[42] H. Navelet and S. Wallon, "Onium - onium scattering at fixed impact parameter: Exact equivalence between the color dipole model and the BFKL pomeron," *Nucl.Phys.*, vol. B522, pp. 237–281, 1998.

[43] M. Boonekamp, A. De Roeck, C. Royon, and S. Wallon, "Gamma* gamma* total cross-section in the dipole picture of BFKL dynamics," *Nucl.Phys.*, vol. B555, pp. 540–564, 1999.

[44] L. Lipatov, "The Bare Pomeron in Quantum Chromodynamics," *Sov.Phys.JETP*, vol. 63, pp. 904–912, 1986.

[45] I. Balitsky, "Operator expansion for high-energy scattering," *Nucl.Phys.*, vol. B463, pp. 99–160, 1996.

[46] I. Balitsky, "Factorization and high-energy effective action," *Phys.Rev.*, vol. D60, p. 014020, 1999.

[47] Y. V. Kovchegov, "Small x F(2) structure function of a nucleus including multiple pomeron exchanges," *Phys.Rev.*, vol. D60, p. 034008, 1999.

[48] Y. V. Kovchegov, "Unitarization of the BFKL pomeron on a nucleus," *Phys.Rev.*, vol. D61, p. 074018, 2000.

[49] E. Iancu, K. Itakura, and L. McLerran, "Geometric scaling above the saturation scale," *Nucl.Phys.*, vol. A708, pp. 327–352, 2002.

[50] A. Mueller and D. Triantafyllopoulos, "The Energy dependence of the saturation momentum," *Nucl.Phys.*, vol. B640, pp. 331–350, 2002.

[51] D. Triantafyllopoulos, "The Energy dependence of the saturation momentum from RG improved BFKL evolution," *Nucl.Phys.*, vol. B648, pp. 293–316, 2003.

[52] A. H. Mueller, "Nuclear A-dependence near the saturation boundary," *Nucl. Phys.*, vol. A724, pp. 223–232, 2003.

[53] E. Levin and K. Tuchin, "Solution to the evolution equation for high parton density QCD," *Nucl.Phys.*, vol. B573, pp. 833–852, 2000.

[54] K. Rummukainen and H. Weigert, "Universal features of JIMWLK and BK evolution at small x," *Nucl.Phys.*, vol. A739, pp. 183–226, 2004.

[55] K. J. Golec-Biernat and A. Stasto, "On solutions of the Balitsky-Kovchegov equation with impact parameter," *Nucl.Phys.*, vol. B668, pp. 345–363, 2003.

[56] E. Gotsman, E. Levin, M. Lublinsky, and U. Maor, "Towards a new global QCD analysis: Low x DIS data from nonlinear evolution," *Eur.Phys.J.*, vol. C27, pp. 411–425, 2003.

[57] A. H. Mueller, "Small x Behavior and Parton Saturation: A QCD Model," *Nucl.Phys.*, vol. B335, p. 115, 1990.

[58] R. Baier, Y. L. Dokshitzer, A. H. Mueller, S. Peigne, and D. Schiff, "Radiative energy loss and p(T) broadening of high-energy partons in nuclei," *Nucl.Phys.*, vol. B484, pp. 265–282, 1997.

[59] Y. V. Kovchegov and A. H. Mueller, "Gluon production in current nucleus and nucleon - nucleus collisions in a quasiclassical approximation," *Nucl.Phys.*, vol. B529, pp. 451–479, 1998.

[60] L. D. McLerran and R. Venugopalan, "Computing quark and gluon distribution functions for very large nuclei," *Phys.Rev.*, vol. D49, pp. 2233–2241, 1994.

[61] L. D. McLerran and R. Venugopalan, "Gluon distribution functions for very large nuclei at small transverse momentum," *Phys.Rev.*, vol. D49, pp. 3352–3355, 1994.

[62] J. Jalilian-Marian, A. Kovner, L. D. McLerran, and H. Weigert, "The Intrinsic glue distribution at very small x," *Phys.Rev.*, vol. D55, pp. 5414–5428, 1997.

[63] J. Jalilian-Marian, A. Kovner, A. Leonidov, and H. Weigert, "The BFKL equation from the Wilson renormalization group," *Nucl.Phys.*, vol. B504, pp. 415–431, 1997.

[64] J. Jalilian-Marian, A. Kovner, A. Leonidov, and H. Weigert, "The Wilson renormalization group for low x physics: Towards the high density regime," *Phys.Rev.*, vol. D59, p. 014014, 1999.

[65] J. Jalilian-Marian, A. Kovner, and H. Weigert, "The Wilson renormalization group for low x physics: Gluon evolution at finite parton density," *Phys.Rev.*, vol. D59, p. 014015, 1999.

[66] J. Jalilian-Marian, A. Kovner, A. Leonidov, and H. Weigert, "Unitarization of gluon distribution in the doubly logarithmic regime at high density," *Phys.Rev.*, vol. D59, p. 034007, 1999.

[67] A. Kovner, J. Milhano, and H. Weigert, "Relating different approaches to nonlinear QCD evolution at finite gluon density," *Phys.Rev.*, vol. D62, p. 114005, 2000.

[68] E. Iancu, A. Leonidov, and L. D. McLerran, "Nonlinear gluon evolution in the color glass condensate. 1.," *Nucl.Phys.*, vol. A692, pp. 583–645, 2001.

[69] E. Iancu, A. Leonidov, and L. D. McLerran, "The Renormalization group equation for the color glass condensate," *Phys.Lett.*, vol. B510, pp. 133–144, 2001.

[70] E. Ferreiro, E. Iancu, A. Leonidov, and L. McLerran, "Nonlinear gluon evolution in the color glass condensate. 2.," *Nucl.Phys.*, vol. A703, pp. 489–538, 2002.

[71] J. Casalderrey-Solana and C. A. Salgado, "Introductory lectures on jet quenching in heavy ion collisions," *Acta Phys.Polon.*, vol. B38, pp. 3731–3794, 2007.

[72] A. Dumitru and J. Jalilian-Marian, "Forward dijets in high-energy collisions: Evolution of QCD n-point functions beyond the dipole approximation," *Phys.Rev.*, vol. D82, p. 074023, 2010.

[73] F. Gelis and A. Peshier, "Probing colored glass via q anti-q photoproduction," *Nucl.Phys.*, vol. A697, pp. 879–901, 2002.

[74] D. Kharzeev, Y. V. Kovchegov, and K. Tuchin, "Cronin effect and high p(T) suppression in pA collisions," *Phys.Rev.*, vol. D68, p. 094013, 2003.

[75] X.-d. Ji, J.-P. Ma, and F. Yuan, "Transverse-momentum-dependent gluon distributions and semi-inclusive processes at hadron colliders," *JHEP*, vol. 0507, p. 020, 2005.

[76] A. Kovner and U. A. Wiedemann, "Eikonal evolution and gluon radiation," *Phys.Rev.*, vol. D64, p. 114002, 2001.

[77] Y. V. Kovchegov and K. Tuchin, "Inclusive gluon production in DIS at high parton density," *Phys.Rev.*, vol. D65, p. 074026, 2002.

[78] C. Marquet, "A QCD dipole formalism for forward-gluon production," *Nucl.Phys.*, vol. B705, pp. 319–338, 2005.

[79] A. H. Mueller, "Parton saturation at small x and in large nuclei," *Nucl.Phys.*, vol. B558, pp. 285–303, 1999.

[80] L. D. McLerran and R. Venugopalan, "Fock space distributions, structure functions, higher twists and small x," *Phys.Rev.*, vol. D59, p. 094002, 1999.

[81] C. Marquet, B.-W. Xiao, and F. Yuan, "Semi-inclusive Deep Inelastic Scattering at small x," *Phys.Lett.*, vol. B682, pp. 207–211, 2009.

[82] B.-W. Xiao and F. Yuan, "Non-Universality of Transverse Momentum Dependent Parton Distributions at Small-x," *Phys.Rev.Lett.*, vol. 105, p. 062001, 2010.

[83] B.-W. Xiao and F. Yuan, "Initial and final state interaction effects in small-x quark distributions," *Phys.Rev.*, vol. D82, p. 114009, 2010.

[84] F. Gelis and J. Jalilian-Marian, "Photon production in high-energy proton nucleus collisions," *Phys.Rev.*, vol. D66, p. 014021, 2002.

[85] F. Gelis and J. Jalilian-Marian, "Dilepton production from the color glass condensate," *Phys.Rev.*, vol. D66, p. 094014, 2002.

[86] A. Dumitru and L. D. McLerran, "How protons shatter colored glass," *Nucl.Phys.*, vol. A700, pp. 492–508, 2002.

[87] J. P. Blaizot, F. Gelis, and R. Venugopalan, "High-energy pA collisions in the color glass condensate approach. 1. Gluon production and the Cronin effect," *Nucl.Phys.*, vol. A743, pp. 13–56, 2004.

[88] J. L. Albacete and A. Dumitru, "A model for gluon production in heavy-ion collisions at the LHC with rcBK unintegrated gluon densities," 2010.

[89] J. Jalilian-Marian and Y. V. Kovchegov, "Inclusive two-gluon and valence quark-gluon production in DIS and pA," *Phys.Rev.*, vol. D70, p. 114017, 2004.

[90] A. Dumitru, A. Hayashigaki, and J. Jalilian-Marian, "The Color glass condensate and hadron production in the forward region," *Nucl.Phys.*, vol. A765, pp. 464–482, 2006.

[91] J. L. Albacete and C. Marquet, "Single Inclusive Hadron Production at RHIC and the LHC from the Color Glass Condensate," *Phys.Lett.*, vol. B687, pp. 174–179, 2010.

[92] J. P. Blaizot, F. Gelis, and R. Venugopalan, "High-energy pA collisions in the color glass condensate approach. 2. Quark production," *Nucl.Phys.*, vol. A743, pp. 57–91, 2004.

[93] C. Marquet, "Forward inclusive dijet production and azimuthal correlations in p(A) collisions," *Nucl.Phys.*, vol. A796, pp. 41–60, 2007.

[94] F. Gelis and J. Jalilian-Marian, "From DIS to proton nucleus collisions in the color glass condensate model," *Phys.Rev.*, vol. D67, p. 074019, 2003.

[95] F. Gelis and Y. Mehtar-Tani, "Gluon propagation inside a high-energy nucleus," *Phys.Rev.*, vol. D73, p. 034019, 2006.

[96] J.-W. Qiu, W. Vogelsang, and F. Yuan, "Asymmetric di-jet production in polarized hadronic collisions," *Phys.Lett.*, vol. B650, pp. 373–378, 2007.

[97] J.-W. Qiu, W. Vogelsang, and F. Yuan, "Single transverse-spin asymmetry in hadronic dijet production," *Phys.Rev.*, vol. D76, p. 074029, 2007.

[98] J. Collins and T. Rogers, "The Gluon Distribution Function and Factorization in Feynman Gauge," *Phys.Rev.*, vol. D78, p. 054012, 2008.

[99] M. Deak, F. Hautmann, H. Jung, and K. Kutak, "Forward-Central Jet Correlations at the Large Hadron Collider," 2010.

[100] E. Braidot, "Two Particle Correlations at Forward Rapidity in STAR," *Nucl.Phys.*, vol. A854, pp. 168–174, 2011.

[101] A. Adare *et al.*, "Suppression of back-to-back hadron pairs at forward rapidity in d+Au Collisions at $sqrt(s_N N) = 200$ GeV," 2011.

[102] J. L. Albacete and C. Marquet, "Azimuthal correlations of forward di-hadrons in d+Au collisions at RHIC in the Color Glass Condensate," *Phys.Rev.Lett.*, vol. 105, p. 162301, 2010.

[103] F. Dominguez, C. Marquet, and B. Wu, "On multiple scatterings of mesons in hot and cold QCD matter," *Nucl.Phys.*, vol. A823, pp. 99–119, 2009.